Resource Allocation and Secure Communication Design in Simultaneous Wireless Information and Power Transfer Systems

Yi Yuan

School of Computing and Communications
Lancaster University

This dissertation is submitted for the degree of
Doctor of Philosophy

February 2018

Declaration

I hereby declare that except where specific reference is made to the work of others, the contents of this thesis are original and have not been submitted in whole or in part for consideration for any other degree or qualification in this, or any other university.

Yi Yuan
February 2018

Acknowledgements

Foremost, I would like to express my sincere gratitude to my supervisor Prof. Zhiguo Ding for his tremendous guidance and continuous support during my Ph.D. study. This thesis would not be possible without his invaluable advices and intensive training. For the past four years, I have enormously benefited from his strong research enthusiasm, expertise knowledge and hard-working attitude. I feel extremely lucky to have a great opportunity to work with his. This experience will profoundly affect on my future carrier.

I would like to thank my collaborators Dr. Peng Xu, Dr. Gaofeng Pan, Dr. Wei Liang, and Dr. Kanapathippillai Cumanan for their valuable suggestions and comments on my research. I also would like to special thank Dr. Chee Yen Leow for hosting my visit in Universiti Teknologi Malaysia (UTM). In addition, I am also very grateful to current and past members, Dr. Zheng Chu, Dr. YuanweiLiu, Dr. Jia Shi, Jingjing Cui, Shi Yan, Kaidi Wang, and Al Basit Suhaib. I thank all my friends and all colleagues in communication group at Lancaster University.

Last but most importantly, I would like to express my deepest gratitude to my family: my parents, Tongsheng Yuan and Cuihua Wu, my wife, Xiaotong Zheng, and my dear sister, Lu Yuan for their unconditional love, support and encouragement.

Abstract

Radio frequency (RF) energy transfer techniques have been regarded as the key enabling solutions to supply continuous and stable energy for the energy-constrained wireless devices. Simultaneous wireless information and power transfer (SWIPT) has been developed as a more promising RF energy transfer technique since it enables wireless information and wireless energy to access users from a same transmitted signal. Therefore, SWIPT has received remarkable attention. This thesis provides an investigation on applications and security issues of this emerging technology in various wireless communication scenarios.

First, this thesis examines the application of SWIPT to a multi-user cooperative network in which the amplify-and-forward (AF) relay protocol is employed at the multi-antenna relay. A power splitting (PS) receiver architecture is utilized at each destination node to implement energy harvesting (EH) and information decoding (ID) simultaneously. The aim of this chapter is to minimize the relay transmit power by jointly designing relay beamforming vectors and PS ratios based on channel uncertainty models. The non-convex problem is converted into a semidefinite programming (SDP) problem by using the semidefinite relaxation (SDR) approach. In addition, a rank-one proof presents that the solution generated by the relaxed problem is optimal to the original problem.

Second, a security issue about the SWIPT system is investigated in a cooperative network in the presence of potential eavesdroppers. The AF relay protocol and a PS receiver architecture are adopted at the multi-antenna relay and the desired destination node, respectively. Based on the system setup and the assumption of perfect channel state information (CSI), a transmit power minimization problem combined with the secrecy rate and harvested energy constraints is proposed to jointly optimize the beamforming vector and the PS ratio. The proposed

optimization problem is non-convex and hard to tackle due to the issues of the quadratic terms and the coupled variables. To deal with this non-convex problem, two algorithms are proposed. In the first algorithm case, the proposed problem can be globally solved by using a two-level optimization approach which involves the SDR method and the one-dimensional (1-D) line search method. In addition, a rank reduction theorem is introduced to guarantee the tightness of the relaxation of the proposed scheme. In the second algorithm case, the proposed problem can be locally solved by exploiting a low complexity iterative algorithm which is embedded in the sequential parametric convex approximation (SPCA) method. Furthermore, the proposed optimization problem is extended to the imperfect CSI case.

Third, a secure communication case is studied in an underlay multiple-input multiple-output (MIMO) cognitive radio (CR) network where the secondary transmitter (ST) provides SWIPT to receivers. In this chapter, two uncertainty channel models are proposed. One is based on the assumption that the ST has the perfect channel knowledge of the secondary information receiver (SIR) and the imperfect channel knowledge of secondary energy receivers (SERs) and primary receivers (PUs). The other one assumes that the ST only has the imperfect channel knowledge of all receivers. In each uncertainty channel model, an outage-constrained secrecy rate maximization (OC-SRM) problem combined with probability constraints is proposed to jointly optimizing the transmit covariance matrix and the artificial noise (AN)-aided covariance matrix. The designed OC-SRM problem for both models is non-convex due to the unsolvable probabilistic constraints. To solve this non-convex problem, the log determinant functions are first approximated to the easy handle the functions that the channel error terms are included in the trace function. Then, the probability constraints are converted into the deterministic constraints by exploiting the Bernstein-type inequality (BTI) approach. Finally, the reformulated problem for both models is solvable by using the existing convex tools.

Last, a novel security issue is investigated in a MIMO-SWIPT downlink network where non-linear energy receivers (ERs) are considered as the potential eavesdroppers. In this chapter, two uncertainty channel models, namely partial channel uncertainty (PCU) and full channel uncertainty (FCU), are proposed. An OC-SRM problem of each model is proposed to design the transmit signal covariance matrix while satisfying probabilistic constraints of the secrecy rate and the harvested energy. To surmount the non-convexity of the proposed OC-SRM problem in each model, several transformations and approximations are utilized. In the PCU model, the OC-SRM problem is first converted into two subproblems by introducing auxiliary variables. Then, three conservative approaches are adopted to obtain the safe approximation expressions of the probabilistic constraints, which are deterministic constraints. Moreover, an alternating optimization (AO) algorithm is proposed to iteratively solve two convex conic subproblems. In the FCU model, log determinant functions are first approximated to the trace functions. Then, the three approaches aforementioned are employed to convert probabilistic constraints into deterministic ones. The bisection method is utilized to solve the reformulated problem. Finally, the computational complexity of the proposed three approaches based on the PCU and FCU model is analyzed.

Table of contents

List of figures

List of tables

List of Abbreviations

1-D	One-Dimensional
5G	The Fifth Generation
AC	Alternating Current
ADC	Analog-to-Digital Converter
AF	Amplify-and-Forward
AN	Artificial Noise
AO	Alternating Optimization
AWGN	Additive White Gaussian Noise
BER	Bit Error Rate
BS	Base Stations
BTI	Bernstein-Type Inequality
CDF	Cumulative Distribution Function
CR	Cognitive Radio
CSCG	Circularly Symmetric Complex Gaussian
CSI	Channel State Information
D2D	Device-to-Device
DC	Direct Current
DF	Decode-and-Forward
DPS	Dynamic Power Splitting
DR	Desired Receiver
DSA	Dynamic Spectrum Access
EH	Energy Harvesting

EM	Electromagnetic
ER	Energy Receiver
EVD	Eigenvalue Decomposition
FCU	Full Channel Uncertainty
FD	Full Duplex
HD	Half Duplex
ID	Information Decoding
IR	Information Receiver
JBPS	Joint Beamforming and Power Splitting
KKT	Karush-Kuhn-Tucker
LDI	Large Deviation Inequality
LHS	Left Hand Side
LMI	Linear Matrix Inequality
LP	Linear Program
LPF	Low-Pass Filter
mmWave	Millimetre Wave
MIMO	Multiple-Input Multiple-Output
MRT	Maximum Ratio Transmission
MISO	Multiple-Input Single-Output
OC-SRM	Outage-Constrained Secrecy Rate Maximization
OFDM	Orthogonal Frequency Division Multiplexing
OSTBC	Orthogonal Space-Time Block Code
PCU	Partial Channel Uncertainty
PHY	Physical Layer
PM	Power Minimization
PS	Power Splitting

PSD	Positive semidefinite
PU	Primary User
PSR	PS-based Relaying
QCQP	Quadratically Constrained Quadratic Program
QoS	Quality of Service
QP	Quadratic Program
R-E	Rate-Energy
RF	Radio Frequency
RHS	Right Hand Side
SDP	Semidefinite Program
SDR	Semidefinite Relaxation
SEE	Secrecy Energy Efficiency
SER	Secondary Energy Receiver
SINR	Signal-to-Interference-Plus-Noise Ratio
SIR	Secondary Information Receiver
SNR	Signal-to-Noise Ratio
SOC	Second-Order Cone
SOCP	Second-Order Cone Program
SPCA	Sequential Parametric Convex Approximation
SSE	Secrecy Spectral Efficiency
ST	Secondary Transmitter
SWIPT	Simultaneous Wireless Information and Power Transfer
TS	Time Switching
TSR	TS-based Relaying
WPT	Wireless Power Transfer
WIT	Wireless Information Transfer
ZF	Zero-Forcing

List of Mathematical Notations

$\mathbf{0}$	All-Zero matrix with appropriate dimension
$\mathbf{I}$	Identity matrix with appropriate dimension
$\mathbf{a}$	$\mathbf{a}$ is vector
$\mathbf{A}$	$\mathbf{A}$ is matrice
$(\cdot)^H$	Hermitian transpose
$(\cdot)^T$	Transpose
$(\cdot)^{-1}$	Inverse
$\mathrm{Tr}(\cdot)$	Trace operator
$\Re\{\cdot\}$	Real part
$\Im\{\cdot\}$	Imaginary part
$\mathrm{vec}(\cdot)$	Vectorization of matrix
$\mathscr{L}(\cdot)$	Lagrange dual function
$\lambda_{max}(\cdot)$	Maximum eigenvalue
$E\{\cdot\}$	Statistical expectation
$\lvert\cdot\rvert$	Magnitude of a complex number
$Diag(\cdot)$	Diagonal matrix
$\lvert\mathbf{A}\rvert$	Determinant of matrix $\mathbf{A}$
$\lVert\cdot\rVert_F$	Frobenius norm
$\lVert\cdot\rVert_2$	Euclidean norm
$[x]^+$	$\mathbf{max}(x,0)$
$\otimes$	Kronecker products
$\mathbf{A}\succeq\mathbf{0}$	$\mathbf{A}$ is a positive semidefinite matrix

$\Pr\{\cdot\}$	Probability functions
dom f	Domain of a function f
$\mathrm{CN}(\mu,\Sigma)$	Complex Gaussian distribution with mean μ and covariance Σ
$\mathbb{C}^{x\times y}$	Set of complex $x \times y$ matrices
$\mathbb{H}^n$	Set of $n \times n$ complex Hermitian matrices
$\mathbb{H}^n_+$	Set of $n \times n$ positive semidefinite matrices
$\mathbb{R}$	Set of real numbers
$\mathbb{R}^n$	Set of real n-vertors
$\mathbb{R}^{n\times m}$	Set of real $n \times m$ matrices
$\mathbb{S}^n$	Set of $n \times n$ real symmetric matrices

Chapter 1

Introduction

In the last decade, wireless communication technologies have grown dramatically to satisfy the escalating data rate and ubiquitous wireless services. The unprecedented increase of wireless devices leads to the sharp growth of energy consumption. However, the lifetime of the wireless devices is restricted by their finite battery capacity. Although battery replacement/recharging can prolong the lifetime of the wireless devices, this solution is inconvenient and costly in the practical implementation due to the unpredictable environmental change and a large number of devices. Hence, efficiently prolonging the operation time of the devices is significant for the design of next generation wireless communication networks.

Recently, energy harvesting (EH) has been considered as a promising technique to extend the lifetime of the devices since it provides an opportunity for energy-constrained devices to replenish their batteries by extracting energy from natural energy sources (e.g., solar, wind, thermal, etc.) [1, 2]. However, there exist limitations on these natural sources for supplying sustainable energy since they greatly depend on environmental conditions. Compared with natural energy sources, radio frequency (RF) cannot only provide controllable and constant energy but also suffer less effect by environment. Hence, EH from the RF source has attracted attention from scholars. Based on the advantages of the RF source, this thesis provides unified studies about the applications of the RF energy source in modern wireless communication scenarios.

1.1 Overview of Wireless Power Transfer

Wireless power transfer (WPT) is a advanced technology that enables to transmit electromagnetic energy from a power source to a device without interconnecting cords. The idea of this technology has been around since hundreds years ago. In the late 19th century, Nikola Tesla conducted several experiments to transfer electromagnetic (EM) power based on microwave technology. Although these experiments were failed due to the limitations of the devices and the technology, Tesla had profound influence on later development of WPT technology.

After a century researches and experiments, WPT technology has been implemented through three different physical mechanisms, namely, inductive coupling [3], magnetic resonant coupling [4], and RF/microwave [5]. The former two techniques, which work on near-field, use the non-radiative characteristic to transfer energy. Specifically, energy transfers happening in inductive coupling is based on the magnetic field change between the primary coil at the transmitter side and the secondary coil at the receiver side [3]. Different from the inductive coupling, the implementation of electrical energy transfer in magnetic resonance coupling is based on the magnetic field oscillation between two strongly coupled resonant coils [4]. Although two non-radiative technologies aforementioned are capable to provide high power conversion efficiency, the charging distance for them is limited within a few meters. Hence, the power transmission efficiency of the inductive coupling and the magnetic resonant coupling decreases along the cube of the reciprocal of the operation distance [6]. Therefore, these two techniques are not suitable for the long distance energy transfer. However, the WPT technique based on the RF can overcome such limitations since it works on far-field by exploiting the radiative characteristic of the EM wave. Therefore, RF energy transfer is a powerful technique to provide energy for a larger number of devices distributed in a wide area [6].

1.2 Motivations

Since RF signals are capable to carry not only energy but also information at the same time, simultaneous wireless information and power transfer (SWIPT) has been recognized as a promising candidate for future 5G systems. However, there exist three key challenges to apply SWIPT in practical communication scenarios. In the following, these challenges are discussed from the aspects of security issues, channel models, and structure of energy receivers (ERs).

- **Security Issue.** In SWIPT systems, the transmitted information is easily eavesdropped by malicious eavesdroppers due to the broadcast nature of the wireless medium. On the other hand, ERs are generally deployed closer to transmitters to receive higher power compared to information receivers (IRs) since IRs and ERs operate with different power sensitivities in practice. Due to the distribution of these two receivers, ERs might eavesdrop the information instead of harvesting energy based on better channel conditions. Therefore, designing a proper resource allocation strategy to enhance security in SWIPT systems need more research efforts in general.

- **Imperfect channel condition.** In practical wireless communication scenarios, it is difficult for a base station (BS) to obtain perfect channel state information (CSI) of the receivers because of the channel estimation errors and quantization errors, especially for SWIPT systems. Therefore, the practical channel model should be considered for the problem design. There are two types of channel error models. The first type uses a bounded set to model the CSI error. This model has an advantage for the implementation complexity but obtains the worst-case performance. The second type uses a statistic model to describe the CSI error. In contrast to the former one, the later one provides an good average performance but with the higher complexity. Since there exists the significant performance deterioration of the imperfect CSI model compared

to the perfect CSI model, it is more interesting to investigate the application of SWIPT under the imperfect CSI model.

- **Non-linear ER.** In a linear EH model, the RF-to-direct current (DC) power conversion efficiency is independent to the RF power available received at EH circuits. However, the use of the linear EH model in practice might cause resource allocation mismatches and performance degradations since the relationship between the inputs and the outputs of the EH circuits is highly non-linear. Therefore, it is more interesting to investigate system performance in non-linear EH model.

1.3 Contributions and Thesis Organization

1.3.1 Contributions

Motivated by the above discussions, this thesis focus on the applications of SWIPT in modern wireless communication networks to three aspects: channel estimations, security issues, and receiver designs. More particularly, SWIPT technique is first applied to a multiuser cooperative network to investigate the system performance. Then, security issue of SWIPT system is investigated in cooperative networks and cognitive radio (CR) networks. In the last, the impact of the non-linear EH model on the system security is investigated. The contributions of this dissertation are summarized in the following.

In chapter 2, the application of SWIPT is considered in a multi-antenna relay network in which the amplify-and-forward (AF) relaying protocol is employed at the relay, and a power splitting (PS) scheme is utilized at each destination node to decode information and harvest power from the same waveform. In this cooperative communication scenario, optimization problems are proposed based on two channel uncertainty models. In each channel model,

relay beamforming vectors and PS ratios are jointly designed to minimize the relay transmit power while satisfying the quality of service (QoS) and the EH constraint of each receiver. In order to solve the optimization problem, the semidefinite relaxation (SDR) method and the Lagrangian duality method are adopted to relax the original problem to the tractable convex problem. Besides, a rank-one proof presents that the solution generated by the relaxed problem is optimal to the original problem. Finally, the performances of the robust schemes are evaluated by simulations.

In chapter 3, a secure information transmission is investigated in a multi-antenna AF relay network in the presence of potential eavesdroppers based on the assumptions of perfect and imperfect CSI. In the considered scenario, a PS receiver architecture is employed at a desired receiver (DR) to harvest energy from the information bearing signal. A power minimization (PM) problem is designed by jointly optimizing the secure beamforming vector and the PS ratio to satisfy the constraint requirements of the secrecy rate and the harvested energy. Since the nonconvexity of the PM problem is arising from the quadratic terms and the coupled variables, the one-dimensional (1-D) linear search and the SDR method are employed to obtain the solutions. Furthermore, a rank reduction algorithm is proposed to guarantee that the optimal solution of the problem is achieved. On the other hand, a low complexity iterative algorithm based on the sequential parametric convex approximation (SPCA), is proposed to obtain the suboptimal solutions. In addition, the S-procedure method is employed to convert the semi-infinite constraints into linear matrix inequalities (LMIs) in the imperfect CSI case.

In chapter 4, the secure communication is considered in a multiple-input multiple-output (MIMO) underlay CR network with SWIPT. The artificial noise (AN) is adopted to improve security of the secondary system. A robust transmit design is proposed based on the assumption of Gaussian CSI errors for the ERs' channels and the primary receivers' (PUs) channels. The objective of this chapter is to design the covariance matrix of the transmit signal and the AN signal to satisfy the three outage probabilistic constraints: secrecy rate at

the secondary receiver, harvested energy at the secondary ER, and the maximum interference at the PU. Since there is no closed-form expression for the probabilistic constraint, the Bernstein-type inequality (BTI) approach is employed to convert the probabilistic constraints into the deterministic constraints. The tractable solution of the proposed problem can be obtained by alternately solving two convex conic subproblems. Furthermore, the same robust design is considered in the full Gaussian CSI uncertainty case. Finally, the effectiveness of the proposed algorithm is validated by simulations.

In chapter 5, a secure information transmission is studied in a downlink MIMO scenario where all ERs are considered as the potential eavesdroppers. In the considered system, non-linear EH model is employed in each ER. A robust transmit design for an outage-constrained secrecy rate maximization (OC-SRM) problem is proposed based on the assumption of Gaussian CSI errors for the ERs' channels in order to figure out a suitable transmit signal covariance matrix to satisfy the outage probability requirements. The proposed problem is challenging to be solved due to the nonsmooth secrecy rate function and the more complicated probabilistic constraints. To tackle the challenges, the original problem can be transferred to two subproblems based on the Fenchel conjugate arguments. Then, three approximated approaches are proposed to convert each subproblem to a safe approximation problem, conservative solutions of which automatically satisfy the outage requirements of the original OC-SRM problem. Finally, an alternating optimization (AO) method is employed to alternately solve these two subproblems. Furthermore, the robust transmit design for the OC-SRM problem is extended to a general case where the transmitter only has imperfect knowledge for the information receiver (IR) and the ERs channels.

1.3.2 Thesis Outline

The remainder of this thesis is organized as following. Chapter 2 introduces some fundamental concepts and reviews literature relevant to this thesis, e.g. basic principles of RF energy transfer, SWIPT, CR, cooperative communication, physical layer security, and convex optimization technique. Chapter 3 investigates beamforming and receiver design in SWIPT assisted cooperative networks. Chapter 4 studies the application of SWIPT in cooperative networks by considering security issue. Chapter 5 investigates the impact of security on SWIPT in underlay CR networks. Chapter 6 presents the secure communication in downlink MIMO-SWIPT networks with non-linear ERs. Chapter 7 draws the conclusions of this thesis and discusses the promising future research directions.

1.4 Publication List

- Journal Papers

  1. **Y. YUAN** and Z. Ding, "Robust Outage Constrained Design for Secrecy MIMO-SWIPT Systems Based on a Non-linear EH Model," *IEEE Transactions on Vehicular Technology (under preparation)* .

  2. **Y. YUAN**, Z. Ding, Mai Xu, and Ningning Qin, "Secure Beamforming and Power Splitting Designs in Multi-antenna AF Relay Networks," submitted to *IET Communications (In review)*.

  3. **Y. YUAN** and Z. Ding, "Outage Constraints Secrecy Rate Maximization Design with SWIPT in MIMO-CR System," *IEEE Transactions on Vehicular Technology 2017 (Accepted for Publication in the current format, 20th June 2017)*.

4. G Pan, H Lei, **Y Yuan**, and Z Ding, "Performance analysis and optimization for SWIPT wireless sensor networks," *IEEE Transactions on Communications*, vol. 65, no. 5, pp. 2291-2302, May 2017.

5. P Xu, **Y Yuan**, Z Ding, X Dai, and R Schober, "On the Outage Performance of Non-Orthogonal Multiple Access With 1-bit Feedback," *IEEE Transactions on Wireless Communications*, vol. 15, no. 10, pp. 6716-6730, Jul. 2016.

- Conference Papers

1. **Y Yuan** and Z. Ding, "Secrecy Outage Design in MIMO-SWIPT Systems Based on a Non-linear EH Model", in *Proc. IEEE Proc. IEEE Globecom Workshops*, Singapore, December 2017.

2. **Y Yuan** and Z. Ding, "The application of non-orthogonal multiple access in wireless powered communication networks", *in 17th IEEE International Workshop on Signal Processing Advances in Wireless Communications (SPAWC)*, Edinburgh, July 2016.

3. S. Hu, Z. Ding, Q. Ni, and Y. **Y. Yuan**, "Beamforming optimization for full-duplex cooperative cognitive radio networks", *in 17th IEEE International Workshop on Signal Processing Advances in Wireless Communications (SPAWC)*, Edinburgh, July 2016.

4. **Y. Yuan**, Z. Chu, Z. Ding, K. Cumanan, and M. Johnston, "Joint Relay Beamforming and Power Splitting Ratio Optimization in a Multi-Antenna Relay Network" *in Proc. IEEE Wireless Communications and Signal Processing (WCSP),*, pp. 1-5, Oct. 2014.

The analysis in Chapter 3 has been presented in conference paper 4. The analysis in Chapter 4 has been presented in journal paper 2. The analysis in Chapter 5 has been presented in journal paper 3. The analysis in Chapter 6 has been presented in journal paper 1.

Chapter 2

Fundamental Concepts and Literature Review

2.1 Fundamental Concepts

2.1.1 RF Energy Transfer

RF energy transfer is capable of powering the far-field devices by exploiting the radiative feature of the EM wave. Compared with other energy sources, RF sources are capable to provide controllable and constant energy for low energy consumption devices distributed in a wide area [5]. One of the most promising application areas of the RF energy transfer is wireless sensor networks since a sensor node can work with a small energy [7]. RF-powered sensors have been applied in the several areas, such as wireless body area networks for health-care monitoring [8, 9], Internet of Things [10, 11], machine-to-machine communication systems [12], and smart grid systems [13]. Some experiments have proved that the amount of harvested energy at the terminals significantly depends on the strength of the source power and the distance between the source and the terminals. In [14], an experimental study shows that the amount of harvested energy is 60 μW from the broadcasting signals of the KING-TV

tower, which is 4.1 km away and uses 960 kW transmission power. Typically, the amount of harvested energy is in order of micro-watts, which is sufficient for powering small devices [15].

In RF-WPT systems, RF signals is broadcasted to the distributed users from the BS or the energy transmitter. Generally, energy carried by RF signals cannot be harvested by the typical information receiver (shown in Figure 2.1). As shown in Figure 2.1 [16], the received

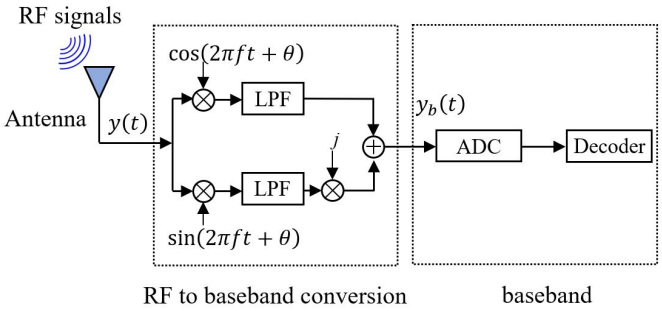

Fig. 2.1 Architecture for information receiver.

RF signal are first converted to a baseband signal through the processing at two low-pass filters (LPF). Then, the baseband signal is converted to a digital signal by analog-to-digital converter (ADC) before decoding.

In order to enable EH, typical ERs are added in distributed users. According to the design of the RF energy receiver in [5], the architecture of the typical RF energy receiver is depicted in Figure 2.2. As depicted in Figure 2.2, a typical ER includes a antenna system, an independent

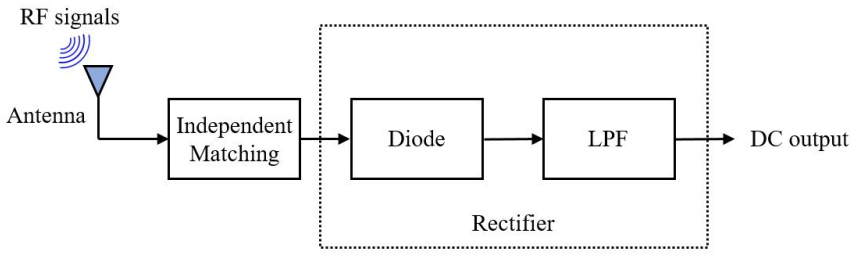

Fig. 2.2 Architecture for energy receiver.

matching system and a RF-to-direct current (DC) system [5]. In the antenna system, the

received antenna can be designed to work on a single or multiple frequency bands. The aim of the independence matching part is to maximize the power transfer between the antenna and the rectifier by using a resonator circuit. The designed frequency is capable to enhance the matching efficiency at the resonator. The rectifier including diodes and LPF is an important part for ERs, because the input RF signals (alternating current (AC) type) captured by the antenna can be converted into DC voltage by using diodes and LPF. Finally, the DC voltage can either power the load directly or charge energy storage. Note that the lower turn-on voltage at the diodes can provide higher conversion efficiency. The reason is that diodes will not work until the received power at the energy harvester is greater than its turn-on voltage. If the received power at the energy harvester cannot overcome this barrier, the conversion efficiency will be zero. In addition, the capacitor at the rectifying circuit not only smoothly delivers power to the load but also supplies energy for a short time when RF energy is unavailable. Typically, a RF signal with frequency rang between 3kHz to 300GHz can be utilized as a medium to carry energy. The RF-to-DC conversion efficiency is mainly dependent on three parts: the captured power density at the receiver antenna, the accuracy of the independence matching and the power efficiency of the rectifier [17]. Due to the benefits of the far-field RF propagation model, the energy transfer based RF signals has clearly advantages of powering a large number of terminals in a wide area [6, 15, 18]. Therefore, this thesis focus on RF energy transfer technique to enable EH.

At the physical layer, the mean signal strength for an arbitrary transmitter-receiver separation distance can be predicted by using large-scale fading propagation models. The free space propagation model is an ideal model used to compute the received signal strength based on the assumption of only line-of-sight path between the transmitter and receiver. Hence, when free space propagation model is considered in the RF energy transfer system, the received

signal power can be expressed as following by exploiting the Friis equation [19]

$$P_{EH} = P_T \frac{G_T G_R \lambda^2}{(4\pi d)^2 L}, \tag{2.1}$$

where P_{EH} denotes the received energy, P_T is the transmit power, G_T and G_R represent the transmit antenna gain and the receiver antenna gain, λ is the wavelength, d is the distance between the transmit antenna and the receiver antenna, and L denotes the path loss factor.

Equation (2.1) provides an ideal model for the received signal power based on the no reflection path assumption. However, in practical scenario, scattering and reflection exist between the transmitter and the receiver. The scattering and reflection may cause that the received signal at the receiver comes from multiple path. In this situation, the equation (2.1) cannot be used to compute the received signal power. Therefore, a more general two-ray ground reflection model, which includes a line-of-sight path and a ground reflection path, is considered to compute the received signal power [20]. The received signal power according to the two-ray ground model is given by [15]

$$P_{EH} = P_T \frac{G_T G_R h_t^2 h_r^2}{d^4 L}, \tag{2.2}$$

where h_t and h_r denote the heights of the transmit and receive antennas, respectively. Note that the wavelength is eliminated by calculation. More details can be found in [20].

2.1.2 Simultaneous Wireless Information and Power Transfer

Since the RF signal not only carries energy but also is used as a vehicle to transport information at the same time, harvesting energy and receiving information from the same RF signal input can be theoretically realized. An interesting application of the RF signal, namely SWIPT, has drawn significant attentions. SWIPT system can be divided into two

categories, integrated-SWIPT (shown in Figure 2.1 (a)) and decoupled-SWIPT (shown in Figure 2.1 (b)), based on whether the received signal at the receiver comes from the same BS. In integrated-SWIPT scenarios, the energy signal and the information signal are both carried

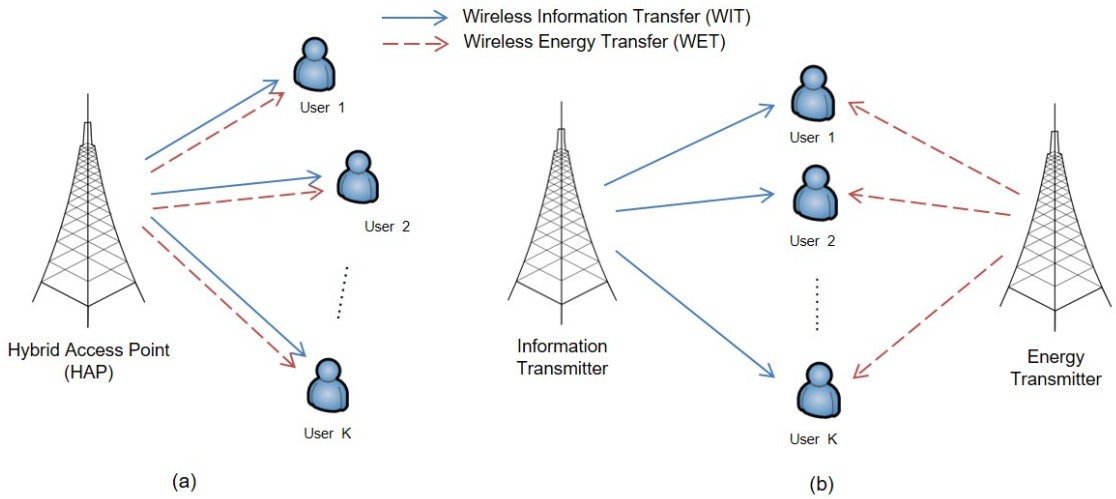

Fig. 2.3 Architecture for SWIPT systems.

in the same RF signal. In decoupled-SWIPT scenarios, the information signal and the energy signal, generated by the different BS, are received at the receiver at the same time. This model can overcome the limitation of integrated-SWIPT model, because of receivers can be deployed close to the energy transmitter. However, this model causes serious interference at the receiver side.

Since the information and energy transfer of the system cannot be maximized at the same time, there exists conflict between WPT and WIT in SWIPT systems. The question of how the trade-off between the information and energy transmission impacts the system performance has attracted the attention of the research community. Varshney first investigated the trade-off between the information and energy transmission by exploiting a rate-energy (R-E) function in a point-to-point additive white Gaussian noise (AWGN) channel [21]. Then, Grover et al. extended the work in [21] to frequency-selective channels with the AWGN model to study the trade-off between information and energy [22]. The studies in [21] and [22] were proposed

based on the assumption of the ideal receiver architecture, which means that receivers in both studies are capable to decode information and harvest energy from the same received signal at the same time. However, this assumption is difficult to implement in practical systems because practical circuits are totally different for ID and EH [23, 24]. In other words, the transmitted information cannot be decoded at the ideal receiver during the EH processing. Inspired by this challenge, three types of receiver architectures are designed to implement SWIPT in wireless communication networks in the current thesis. In the following parts, these practical receiver designs are introduced, namely separated receiver architecture, co-located receiver architecture and integrated receiver architecture.

2.1.2.1 Separated Receiver Architecture

Zhang et al. proposed a separated receiver architecture to simultaneously implement ID and EH at the receiver side. In this practical architecture, the EH circuit and the ID circuit are adopted in two independent receivers, respectively [23]. These two types of receivers can be easily built based on off-the-shelf information receivers and energy receivers. Moreover, the trade-off between the achievable information rate and the harvested energy can be obtained by using optimization techniques.

2.1.2.2 Co-located Receiver Architecture

Different from the separated receiver, the ER and the IR are capable to receive the same signal by sharing the same antenna in the co-located receiver. As the received signal at the EH circuit and the ID circuit comes from the same antenna, the system complexity of using the co-located receiver is smaller than that of the separated receiver. Similar to ideal receivers [21, 22], the question of how EH and ID are simultaneously implemented in the co-located receiver design is still an important issue. To answer this question, Zhang et al.

[23] proposed two practical receiver models, namely time switching (TS) receiver and power splitting (PS) receiver, to overcome the practical limitation of the co-located receiver design. In the following, these two practical receivers are introduced in orders.

1. **Time Switching Receiver**. An information receiver and a RF energy receiver are connected to the same antenna in the TS receiver. In this scheme, the transmission block is divided into two orthogonal time slots at the transmitter, i.e., one for information transmission and the other for energy transfer. Based on a time switching sequence, each antenna is capable to switch the received signal to the EH circuit or the ID circuit in two time slots [23]. The perfect time synchronization between the receiver and the transmitter is important to implement SWIPT in the TS receiver. The optimal R-E trade-off can be achieved by optimizing the time switching sequence.

2. **Power Splitting Receiver**. A passive power splitter is equipped at each antenna to distribute the received signal to the EH circuit and the ID circuit based on different power levels. In fact, the received signal is split into two signal streams with different power. One stream with $0 \leq \rho \leq 1$ portion signal power is used for ID, and the other stream is used for EH with $1-\rho$ power [23, 24]. The different trade-off between the achievable information rate and the harvested energy can be achieved by using different PS ratio ρ. When ratio $\rho = 0$ or $\rho = 1$, the PS receiver becomes as the TS receiver.

2.1.2.3 Integrated Receiver Architecture

An integrated information and energy receiver was proposed by Zhou et al. [24] to implement ID and EH operations by exploiting one-time RF-to-baseband conversion. In this receiver, the received RF signal is first converted to a DC signal by a rectifier at the ER. Then, the DC signal is distributed to the battery and the IR. Note that the DC signal can be considered as

the baseband signal for information decoding. Therefore, the IR at the integrated receiver does not need any RF band to baseband conversions.

2.1.3 Physical Layer Security

Information security has been considered as one of the most essential issues in wireless communication systems as broadcast characteristics of wireless medium cause that confidential messages are susceptible serious eavesdropping threats from unauthorized users. With continuous research of secure communications, cryptography has been considered as a traditional high-layer encryption technique to circumvent the occurrence of the information eavesdropping [25]. However, traditional cryptographic techniques may have defects since the operations of these techniques are based on the assumption of the limited computational capability of the eavesdroppers [26, 27]. Additionally, the perfect key distribution and management may not always be available when establish secure communication links by using cryptographic techniques [28].

Due to the limitation of cryptographic techniques, information-theoretical physical (PHY) layer security considered as a complement technique for cryptographic technique has been investigated by many scholars. Different from cryptography, PHY layer security exploits physical characteristics of wireless channels to guarantee information security [29]. In order to investigate the performance of PHY layer security, Wyner [29] proposed a model which includes a source, a destination and a malicious eavesdropper. The key concept of achieving perfect secrecy in the wiretap channel is to ensure that the quality of the channel between the source and the destination (main channel) is better than that of the channel between the source and the eavesdropper (eavesdropper's channel). The reason is that if the quality of the main channel is worse than the quality of the eavesdropper's channel, the capacity of the eavesdropper will greater than the capacity of the user. This will cause the zero secrecy

capacity. Therefore, the perfect secrecy capacity can be given by [30]

$$I_s = [I_M - I_E]^+, \tag{2.3}$$

where I_M and I_E denote the capacity of the main channel and the eavesdropper channel, respectively. The method to achieve the perfect secrecy communication in the wiretap channel has attracted more attention. Two approaches are considered to ensure the perfect secure communication. One is to improve the received signal power at the legitimate receiver, that is the legitimate receiver is distributed closer to the source than the eavesdropper. However, this approach is not easy to implement in practice due to the silent features of eavesdroppers. The other one is to impair the received signal quality at the eavesdropper. Jamming signals [31] and AN signals [32] can be utilized to impair the received signal at the eavesdroppers.

2.1.4 Cooperative Networks

The concept of cooperative communication was proposed from the information theoretical perspective by Cover and Gamal in their early work, which analyzed the system capacity of a three-node network [33]. Based on this fundamental concept, cooperative technique has a rapid development in the past decades. Cooperative communication has attracted an upsurge of interests of both academic research and industrial applications as it is capable to overcome the fading and attenuation characteristics of wireless transmission by exploiting the broadcast nature of wireless mediums [34–36]. Specifically, the aim of cooperative communication is to establish multi-path transmission to reduce the path loss impact by allowing terminals in networks to collaborate with each other for information transmission. Compared with other emerging techniques, cooperative communication is an alternative low-cost approach of achieving transmit diversity by cooperatively sharing antennas of terminals. In this way, a

virtual antenna array and a multi-path transmission can be constructed. As a consequence, the cooperative technique can offer important enhancement in terms of energy and spectrum efficiency, network connectivity, and communication reliability [37].

In cooperative communication networks, each terminal performs two roles-a source node to transmit information and a relay node to help information transmission. A classic three-node cooperative system is shown in Figure 2.4 to illustrate the communication procedure. In this system, there exist two different communication channels - a direct transmission

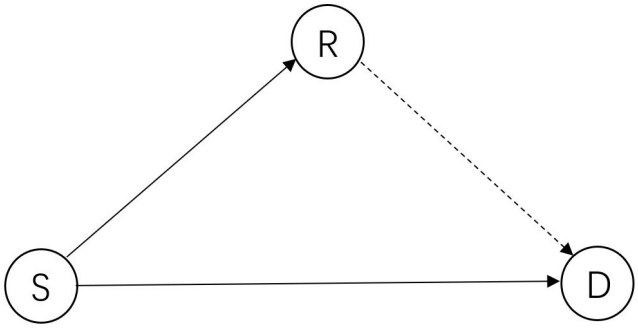

Fig. 2.4 A classic three-node cooperative system.

channel (connecting the source (S) to the destination (D)) and a cooperative transmission channel (connecting the source (S) through the relay (R) to the destination (D)). Therefore, a typical cooperative procedure consists of two phases. The information broadcasting from the source to the relay and to the destination are happened in the first phase (solid lines). Then, the relay forwards the received information to the destination in the second phase. After the two - phase transmissions, the destination node exploits combination techniques to process the received signals. The challenge to implement cooperative communication arises from the design of efficient cooperative protocols. With the development of cooperative communication technique, many protocols have been designed by researchers to process the received signal at the relay node. In the following, brief descriptions about the two most widely-used protocols, namely AF and decode-and-forward (DF), are introduced.

The AF protocol - the simplest relay protocols - was first proposed and analyzed by Laneman *et al.* [38]. In the AF relay system, the relay node forwards the amplified information and noise to the destination node. This protocol is suitable for the relay node with the limited power. The DF protocol is another simple cooperative signaling method, which was proposed in [39, 40]. In the DF relay system, the relay node decodes the received signals and re-encodes them before forwarding to the destination. The protocol may cause higher bit error rate (BER) compared with the AF protocol.

2.1.5 Cognitive Radio Networks

CR technology was first developed by Mitola to establish dynamic spectrum access (DSA) networks [41]. It has been considered as a promising technology to alleviate the spectrum scarcity issue, which is caused by the rapid explosion of wireless devices and the inefficient usage of the existing spectrum, by utilizing the network resources in a more efficient and intelligent way. Different from traditional communication paradigms, CR technology is capable for unlicensed users to access the licensed spectrum intelligently according to the variations of the surrounding environment [42].

Based on the three existing paradigms of the CR network, namely, interweave, overlay, and underlay, secondary users are capable to efficiently utilize the spectrum resources [43]. These three paradigms are categorized according to different interference management strategies. A brief description of these three paradigms is provided as follows.

1) Interweave Paradigm. The interweave paradigm was originally introduced by Mitola based on the idea of opportunistic communication [41]. The interweave technique requires activity information of all users in the spectrum. Secondary users are required to detect spectrum holes based on the activity information before accessing to the licensed spectrum [44, 45]. The key concept of the interweave technique is that the

communication of the secondary system does not interfere the existing communication of the primary system. In other words, the concurrent communications of the secondary system and the primary system are not allowed in the interweave CR network.

2) *Overlay Paradigm*. The overlay paradigm refers to an interference mitigating technique by exploiting sophisticated signal processing and coding. The key idea of enabling overlay CR is that the codebooks and the messages of the primary system are well known at the secondary transmitters. By exploiting this knowledge, the secondary transmitters not only completely cancel the interference of the primary system to the secondary receivers but also can be used as relays to assist the information transmission of primary system. Therefore, in overlay CR systems, the communication rate of the primary system is capable to remain unchanged while the secondary system is capable to obtain additional bandwidth for its own communication [43].

3) *Underlay Paradigm*. The underlay paradigm allows concurrent communications of the secondary system and the primary system by intelligently controlling the interference caused by the secondary system to the primary system. Specifically, the secondary system is permitted to transmit its information on the spectrum allocated to the primary system only if the interference generated by the secondary system is below the acceptable constraint [46]. The available transmission power of the secondary transmitter is limited due to the restrictive interference control in underlay CR systems. As the interference caused by the secondary system is rigorously controlled in underlay CR systems, the available transmission power of the secondary system is restricted. In other words, the secondary system is only suitable for short-range communication in underlay CR systems.

Since CR technology is capable to reconfigure operating features of networks to best match outside situations by sensing and detecting the environment surrounding RF, it can improve spectrum efficiency and support higher bandwidth service. As a consequence, CR technology

can be employed in many wireless communication scenarios to improve the usage efficiency of bandwidth.

2.2 A Brief Literature Review of SWIPT Application

Recently, SWIPT has been considered as a promising technology to solve the energy scarcity problem in energy-constrained wireless networks as RF signals not only carry information but also transfer energy. Motivated by this, SWIPT technique has been widely applied for academic research and industry applications. In the following subsections, the related works of this thesis surrounding SWIPT are discussed in different wireless communication networks.

2.2.1 SWIPT in Single-Hop Systems

SWIPT technique was applied in single antenna scenarios [24, 47–50] and multi-antenna scenarios [23, 51–59].

2.2.1.1 SWIPT in Single-Antenna Systems

Based on the motivations of the TS and static power splitting (SPS) scheme, a dynamic power splitting (DPS) scheme was proposed by Zhou et al [24] to dynamically split the received signals. The rate-energy tradeoffs of the separated receiver and the integrated receiver were investigated by exploiting the DPS scheme in a point-to-point system. The authors investigated the information and energy tradeoff based on the dynamic time switching operation policy in the co-channel interference system [47] and DPS operation policy in the flat fading channel system [48]. Specifically, the optimal rate-energy tradeoff for delay

tolerant scenarios and the optimal outage-energy tradeoff for delay-limited scenarios were studied with and without CSI at transmitters in [47] and [48], respectively. Compared with the TS policy proposed in [47], the PS policy proposed in [48] not only gains higher information gain but also harvests more energy. SWIPT technique was also applied in the orthogonal frequency division multiplexing (OFDM) system to coordinate EH and ID operation [49, 50]. The authors in [49] design the resource allocation, the sub-carrier allocation and the PS ratio in a multiuser single-antenna OFDM system in which each receiver employed a power splitter to split the received RF signal. Since the work in [49] was based on the assumption that the PS ratio is different for each subcarrier, a practical OFDM-based SWIPT system with the same PS ratio for all subcarriers was proposed in [50].

2.2.1.2 SWIPT in Multi-Antenna Systems

The practical circuit limitation at the receiver has been overcome in the single antenna system. There still exists another challenge caused by the energy transfer efficiency that needs to be considered when designing WPT systems. In wireless communication systems, the energy transfer efficiency decreases along with the increase of the transmission distance since energy carried by RF signals is more sensitive to the propagation path loss. This drawback is especially severe in single-antenna systems, because the RF signal generated by a single-antenna transmitter has omni-directional radiation characteristic. Multi-antenna techniques have been deemed as an appealing solution to improve efficiency of RF energy transfer. The reason is multi-antenna techniques not only achieve spatial multiplexing but also employ beamforming technique, which is capable to achieve directional transmission, without requiring additional bandwidth and transmit power. Therefore, multi-antenna techniques have been employed to transmit the RF signals toward the target receivers [23, 51–59].

Multi-antenna techniques were first employed to transfer the information and the energy to target receivers in a broadcast MIMO system [23]. Based on the assumption of perfect CSI

at the transmitter, the authors investigated the optimal precoding matrix and transmission strategies to achieve the rate-energy trade-off in either the separated or the co-located ID and EH receiver. It is worth pointing out that the authors proposed two receiving strategies, which allocates the received signal at the co-located receiver to ID circuit and EH circuit from a time and power perspective. Inspired by [23], the authors in [51] extended [23] to a three-node multiple-input single-output (MISO) system under the imperfect CSI assumption. In this work, the transmit beamforming was optimized under the worst-case model to enhance the harvested energy at the ER while satisfying the rate requirement at the IR. The authors also provided the theoretical proof to guarantee the relaxation is always tight. The studies for SWIPT that consider the multiple information receivers and energy receivers were investigated in a MISO downlink broadcast system based on the perfect CSI assumption [54] and the imperfect CSI assumption [55]. In [54], the two types of information receivers that are with and without the capability of canceling the interference were considered. For each type of the information receiver, the authors aimed to jointly design beamforming and power allocation to obtain the maximum weighted sum harvest energy while guaranteeing the signal-to-interference-plus-noise ratio (SINR) requirement of each information receiver. Two approaches (based on the SDR and the uplink-downlink duality) were proposed to solve the non-convex problems for both types of information receivers. In [55], the worst harvested energy maximization problem was proposed to design robust beamforming based on the SINR constraint and the total transmit power constraint. An iterative algorithm based on the bisection method was proposed to solve the problem and obtain the robust solution.

RF Energy transfer was studied under conditions where co-channel interference in a multiple transmitter-receiver pairs MIMO system was considered [52, 53]. In the two studies [52, 53], all receivers were considered to adopt the TS scheme for achieving simultaneously ID and EH. The authors considered a special case which had two pairs of transmitter-receiver [52]. In this case, two receivers were categorized into three modes: both for ID operation, both for EH operation, and one for ID operation and the other one for EH operation. For the

single operation modes, the achievable rate and the harvested energy could be maximized by the information rate maximization problem and the harvested energy maximization problem, respectively. For the different operation mode, the achievable rate-energy region was investigated based on the two rank-one beamforming strategies. Then, the problem investigated in [52] was generalized to k transmitter-receiver pairs [53].

Joint beamforming and power splitting (JBPS) was studied based on the power minimization problem in broadcasting systems [56–58] and multicasting systems [59]. In the broadcasting system, two scenarios were considered: one transmitter with multi-user scenario in [57] and multi-transmitter with multi-user in [56, 58]. In [57], the global design was proposed by applying the SDR method, and two suboptimal designs were proposed based on zero-forcing (ZF) and SINR-Optimal criteria, respectively. In [56], the authors used the semidefinite program (SDP) together with rank relaxation to approximate the optimal solution. Then, four suboptimal algorithms with fixed beamforming design, i.e., ZF, regularized ZF, maximum ratio transmission (MRT), and a hybrid MRT-ZF, were proposed to reduce the computational complexity. The interesting results showed that MRT consumed less power compared with ZF due to the existed co-channel interference in MRT algorithm. However, MRT had higher infeasible probability than ZF. Different to the work in [56], the authors in [58] proposed the centralized algorithm based on the second-order cone programming (SOCP) relaxation and the distributed algorithm based on a primal-decomposition method to solve the JBPS problem, respectively. For cases where optimal solutions were not necessary, a feasible-solution-recovery method was proposed to obtain the close-form of the problem. In addition, the results in [58] indicated that the SOCP relaxation was more efficient than the SDR in [56]. The JBPS problem was addressed based on the perfect and imperfect CSI assumption in a multicast system [59].

2.2.2 SWIPT in Cooperative Networks

Although cooperative techniques are able to overcome fading and attenuation for long distance communication by using relay nodes, the activity of relay nodes may be restricted by limited battery. Therefore, the EH technique is adopted to extend the lifetime of wireless nodes in cooperative networks [60, 61]. Cooperative networks with the EH technique not only increase the transmission efficiency and reliability but also maintain the activity of networks. Based on the advantage of the EH technique, the applications of this technique have been investigated in single relaying networks [62–69] and multiple relaying networks [70–74].

RF Energy transfer was first applied in an orthogonal space-time block codes (OSTBC) MIMO relay system to design the optimal source and relay precoding with discharged relay [62]. Then, the authors in [63, 64] extended works in [62] by considering the charging relay. In [63], a simple greedy switching policy, which was designed based on the idea of TS scheme, was proposed to intelligently switch the operation mode of the relay node. Specifically, the relay node is capable to decide when to harvest energy and when to forward information based on the proposed policy. By using Markov chain, the closed-form expression of outage probability was obtained to evaluate the system performance. In [64], a dynamic antenna switching policy, which is capable to allocate a certain number of antennas for the ID operation and remaining antennas for the EH operation, was proposed in a MIMO relay system by exploiting the array configuration.

Inspired by the TS and the PS receiver architecture introduced in [23], two relaying protocols, namely TS-based relaying (TSR) protocol and PS-based relaying (PSR) protocol, were proposed to enable energy harvesting and information processing at the AF relay [65]. Based on the proposed protocols, the authors adopted outage probability and ergodic capacity as two metrics to evaluate the performance of the delay-limited and the delay-tolerant transmission,

respectively. It is worth noting that the throughput of the TSR protocol is better than the PSR protocol at the relatively low signal-to-noise ratio (SNR) and high transmission rates based on the results in [65]. Then, the same authors proposed adaptive TS protocols for two different modes of EH: EH with continuous time and EH with discrete time [66]. The authors found out that the proposed protocols in [66] outperformed the TSR protocol in [65] through comparing the simulation results. In [68], the authors investigated the system performance of a three-node DF relay network with and without direct link by exploiting two relaying protocols in [66]. With the analysis for the considered system, the authors pointed that the optimal coefficient for both protocols depended on the channel conditions and the remaining energy of the relay node. By adopting the DF relaying strategy, energy distribution strategies on the relay were proposed to investigate the impact of different strategies on the system performance [67]. With the same relaying strategy, the transmission rate for the cases with and without direct link were investigated in [68]. The authors in [69] studied the impact of SWIPT on the end-to-end achievable data rate in a two-hop non-regenerative MIMO-OFDM relay system.

Relay selection is very important in multiple relays networks for SWIPT since the preferable relay for information transmission does not necessarily coincide with the relay which has the strongest channel for EH. The impact of cooperative scheme and relay selection on the system performance was investigated in a large-scale network with SWIPT [70]. The authors in [71] proposed three relay selection strategies for the single source case and two distributed game theoretic algorithms for the multiple sources case to investigate the impact of SWIPT on the multiple relays network. Another three relay selection schemes, namely, time-sharing selection, threshold-checking selection and weighted difference selection, were studied in a two relays cooperative network with the separated IR and ER [72]. The Markov chain model was employed to investigate the states of the batteries in [73, 74].

2.2.3 SWIPT in Cognitive Radio Networks

Powering a CR network with RF energy not only solves the spectrum scarcity problems but also prolongs the lifetime of devices [75–80]. The authors in [75] first utilized RF signals as the energy source to power secondary receivers. In the context of complete CSI at the secondary user, an optimal channel selection policy was proposed to implement the information transmission and the EH at the secondary user based on a Markov decision process [76]. However, the computational complexity of the proposed channel selection policy depends on the size of data queue and energy queue. If the size is large, the computational complexity is very high. Therefore, a suboptimal algorithm, namely online learning algorithm, was proposed based on the incomplete CSI assumption at the secondary user [77]. The authors also demonstrated that the performance of the proposed learning algorithm in [77] was close to that of the optimal selection algorithm in [76]. Furthermore, the application of SWIPT was investigated in the underlay MIMO-CR network under the imperfect CSI assumption [78]. In [79], two spectrum access policies, namely, random and prioritized spectrum access, were designed for a device-to-device (D2D) communication in an underlay cognitive cellular network in which energy was harvested from the ambient interference. In this work, the authors employed stochastic geometry to evaluate the performance of the proposed system. The authors in [80] proposed a novel information and energy cooperation model in CR networks, where secondary transmitter assists the primary transmission based on the harvested energy from the primary transmitter. Specifically, the PS scheme and the TS scheme were used at the secondary transmitter to simultaneously decode information and harvest energy. The results demonstrated that the proposed information and energy cooperation model was better than without energy cooperation model [80].

2.3 A Brief Literature Review of Security Issues in SWIPT Systems

In SWIPT systems, the transmitter may need to amplify the power of the transmitted signal in order to satisfy the EH requirement which may cause more information leakage. In addition, ERs are normally deployed closer to the transmitter compared with IRs, because the IR and the ER work on different power sensitivities, e.g., -60 dBm for IRs versus -10 dBm for ERs [23]. These two factors raise a new security issue for SWIPT systems since the information sent to the designed receiver is vulnerable to be attacked by unexpected eavesdroppers or ERs. Therefore, it is desirable to implement some methods to avoid unexpected eavesdroppers and ERs from recovering the confidential message from their observations. Based on the PHY security technology, a very limited number of research papers have considered the secure communication in single-hop networks [81–88], cooperative networks [89–96] and cognitive networks [97–100].

2.3.1 Security Issues in Single-hop Networks with SWIPT

The PHY security technology was first employed to guarantee the secure communication in a MISO downlink network with a desired receiver and multiple ERs in [81]. Specifically, Liu et al. proposed the secrecy rate maximization problem and sum-harvested-energy maximization problem to jointly design the transmit beamforming vectors and the power allocation strategies [81]. By utilizing the separated receiver structure, Shi et al. [82] studied the beamforming design in a simple MIMO information-energy broadcast system, where the energy receiver was considered as a eavesdropper. The works in [81, 82] were based on the perfect CSI assumption.

However, perfect CSI for all receivers is not easy to be obtained by the transmitter due to the existence of channel estimation errors and quantization errors in the practical scenarios. Thus, it is important to design a secure communication strategy under the imperfect CSI condition. A very limited number of research papers had designed robust secure communication strategies in SWIPT systems based on the bounded CSI error model [83–86] and the probabilistic CSI error model [87, 88]. In [83], the authors utilized the AN and energy signals to provide the secure communication and efficient WPT in the presence of passive eavesdroppers and potential eavesdroppers (idle legitimate receivers). A robust secure beamforming algorithm was investigated in the MISO-SWIPT system and the MIMO-SWIPT system through the secrecy rate maximization design [84] and the worst-case secrecy rate design [85], respectively. In [86], a two-step algorithm was proposed to circumvent the rank-one solution in the MISO secure SWIPT system. In addition, a novel SDP relaxation was investigated to guarantee that the relaxed problem yielded rank-one solution. Compared with the bounded CSI error model in [83–86], the probabilistic CSI error model was more suitable to the delay-sensitive communication scenario. In [87], the authors proposed an outage-constrained robust method to design transmit beamforming while satisfying the probability constraints of the secrecy rate and the harvested energy. Then, the work in [87] was extended to the MIMO scenario [88].

2.3.2 Security Issues in Cooperative Networks with SWIPT

Different from the above literature, there exists an alternative way to enhance the information security and the energy efficiency in SWIPT systems by introducing extra helpers. In general, the multiple-antenna relay might be considered as the extra helper since it can enhance the usage of spatial degree of freedom [89, 90]. A very limited number of research works investigated the impact of cooperative relaying on the information security and the energy efficiency [91–96]. In [91], a secrecy rate maximization problem under the constraints of the minimum

relay transmit power and the maximum harvested energy was investigated to design a secure relay beamforming in a nonregenerative multi-antenna relay network in the presence of an eavesdropper. In [92], multiple wireless EH-enabled friendly jammers were used to improve the information security in a multi-antenna AF relay network. Specifically, the authors in [92] jointly designed the AN covariance and relay beamforming by investigating the secrecy rate maximization problem based on the assumption of perfect CSI and imperfect CSI at the relay. In [93], a novel multi-antenna AF relay network was proposed to simultaneously prolong the operation time of the relay and disturb the information at the eavesdropper by using energy signals provided by the destination node. While in [93], the authors investigated the impacts of the massive MIMO relay on the information security and the power transfer efficiency in very adverse environments. The analysis results indicated that the power transfer efficiency could be significantly enhanced by the characteristic of the large array gain, and the information security could be improved by utilizing the high-resolution spatial beamformer. Furthermore, cooperative beamforming and energy signal were jointly designed by solving the proposed optimization problem in an AF relay network [95]. Recently, the authors in [96] proposed a secrecy rate maximization problem under the source and the relay transmit power constraints as well as the EH constraint at each ER to jointly design the source and relay beamforming matrices.

2.3.3 Secure Issues in Cognitive Radio Networks with SWIPT

Security issues in CR networks with SWIPT system have been attracting continuously growing attention due to the inherent characteristics of CR, where ERs and malicious eavesdroppers are allowed to opportunistically access the licensed spectrum. Thus, research works have considered to protect CR-SWIPT networks against eavesdropping [97–100]. In [97], Fang et al. investigated the secure communication in a cognitive MIMO broadcast scenario, where the AN signal was employed to disturb the secondary energy receiver

(SER). The authors in [98] proposed a multi-objective optimization framework to investigate the information security of the secondary system in a multiuser CR network with SWIPT. A Pareto-optimal resource allocation algorithm was designed to enhance the information security of the secondary system by jointly minimizing the total transmit power and the interference-power-leakage-to-transmit-power ratio as well as maximizing the EH efficiency. While in [99], the secrecy outage probability was investigated in a CR network based SWIPT. Recently, Zhou et al. studied the secure communication in a MISO downlink CR network where a secondary transmitter simultaneously transferred the information and power to cognitive receivers [100]. The optimal and suboptimal secure beamforming was designed to enhance the security of the secondary system in the bounded CSI error model and the probabilistic CSI error mode, respectively [100].

2.4 Convex Optimization Theory

The fundamental concepts and some relevant involved works have been introduced in the the aforementioned sections, this section presents a powerful mathematical tool to design and analyze wireless networks. Optimization techniques play a significant role for the design of future wireless communication systems. Convex optimization, which is an important class of optimization techniques, has been considered as a powerful tool for solving various problems in signal processing and wireless communication scenarios [101, 102]. In practical applications, any design with objective function and constraints can be modelled as constrained optimization problems. However, most of problems cannot be directly solved by the existing convex toolboxes (i.e., SeDuMi [103], Yamip [104], and CVX [105]) due to non-convex characteristics. Therefore, how to exploit convex optimization techniques to convert non-convex problems into convex problems has received remarkable attention both in the world of academia and industry. The ensuing subsections will introduce fundamental elements of the convex optimization theory.

2.4.1 Convex Set

A set S is considered to be a convex set if there exists any $x, y \in S$ and any θ with $0 \leq \theta \leq 1$ satisfy the following condition

$$\theta x + (1-\theta)y \in S. \tag{2.4}$$

The condition (2.4) means that a set can be defined as a convex set if this set is continuous and every points in the set can be seen by each other without any obstacles. In other words, the line segment between any two points in a convex set is lying in this set [101]. Based on the definition of convex set, we know that every affine set is convex set since the entire line between any two distinct points is included in the affine set. Figure 2.5 shows the examples about the convex and non-convex sets [101]. It obviously indicates that (a) is convex set

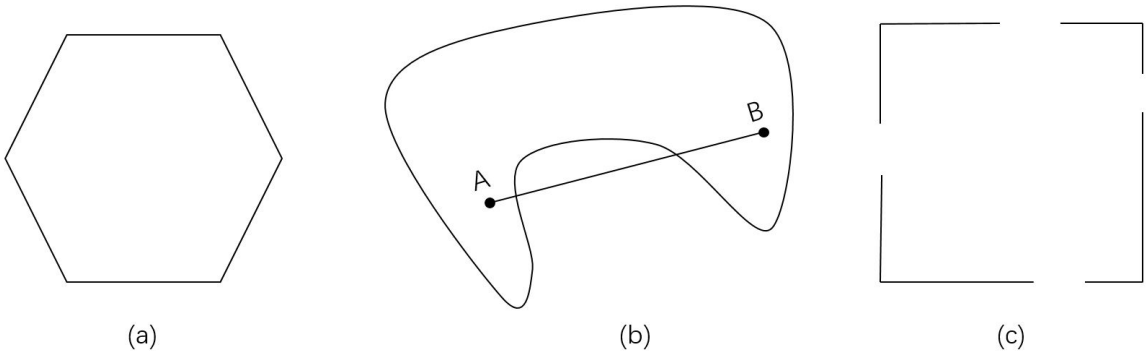

Fig. 2.5 Convex set (a) and non-convex sets (b), (c).

since (a) is hexagon with continuous boundary. Figure 2.5 (b) is the non-convex set since the line segment between point A and point B is not lying the graphic. Also, Figure 2.5 (c) is non-convex set due to the discontinuous boundary.

Next, we introduce a special convex set, namely convex cone. According to the definition of cone in [101], we know that a set S is defined as a *cone* if for every $x \in S$ and nonnegative α we also hold $x\alpha \in S$. Then, the convex cone can be defined based on the convex set

definition (2.4). In other words, a set can be called convex cone if this set is convex and cone. The concept of convex set has been introduced in this subsection. This is the first step to understand the concepts of convex optimization. In the next subsection, we will introduce convex function, which is an important part for understanding convex optimization.

2.4.2 Convex Function

Similar to the convex set introduced in the above subsection, convex function is also an important step to define convex optimization problem. The concepts of convex function and how to define a function whether is convex or not is presented in the ensuing part.

2.4.2.1 Fundamental Definition of Convex Function

If the domain of a function f is convex set and for all $x,\ y \in \mathbf{dom}\ f$ as well as $0 \leq \theta \leq 1$ satisfy the following inequality

$$f(\theta x + (1-\theta)y) \leq \theta f(x) + (1-\theta) f(y), \tag{2.5}$$

this function f can be defined as a convex function [101]. Geometrically, the definition of the convex function f means that the graph of $f(\theta x + (1-\theta)y)$ lies below the line segment between $(x, f(x))$ to $(y, f(y))$ [101]. In other words, the graph of a convex function looks like a faceup bowl as illustrated in Figure 2.6 [101]. If strict inequality holds in (2.5) when $x \neq y$ and $0 < \theta < 1$, the function f is defined as *strictly convex*. Then, if function f is said to be concave if $-f$ is convex.

The basic definition of a convex function is very useful approach for proving or checking whether a function is convex or not. The more important is that the convexity verification of a high-dimensional function can be instead to verify the convexity of a one-dimensional

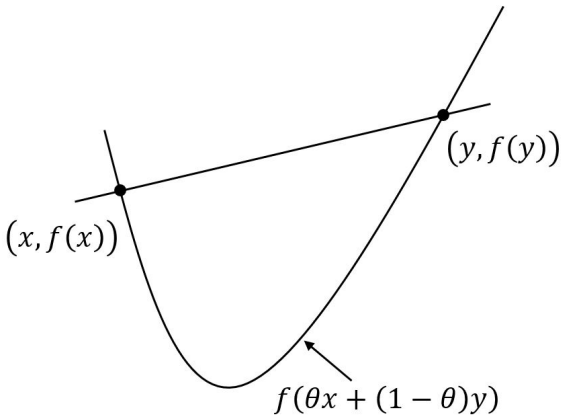

Fig. 2.6 Graph of a convex function.

function. To verify the convexity of a function based on the definition is a general way, we introduce two powerful conditions to verify the convexity for differentiable functions in the ensuing parts.

2.4.2.2 First-order Condition

We assume that f is a first order differentiable function which means that the gradient of f exists at each point in its domain. Then, f is convex function if and only if its domain is convex set and it satisfies the following inequality condition

$$f(y) \geq f(x) + \nabla f(x)^T (y - x), \;\; x, y \in \mathbf{dom} f. \tag{2.6}$$

The inequality (2.6) is called the first-order condition. The right hand side of inequality in (2.6) is the first-order Taylor series approximation of $f(y)$ near x. In addition, this condition provides a tight lower bound for convex function f. Figure 2.7 illustrates the graph for this condition [101].

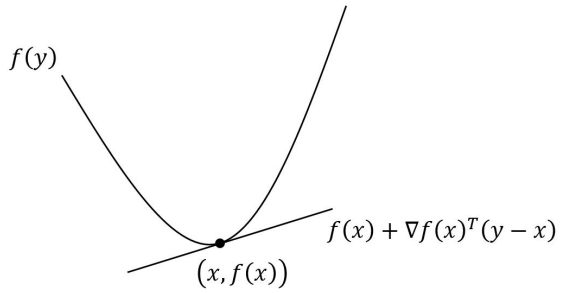

Fig. 2.7 First-order condition for a convex function f.

2.4.2.3 Second-order Condition

Suppose that f is a twice differentiable function. Then, we can define that function f is convex if and only if its domain is convex and its Hessian matrix is positive semidefinite (PSD), which can be written as follows:

$$\nabla^2 f(x) = \left\{ \frac{\partial^2 f(x)}{\partial x_i \partial x_j} \right\}_{m \times m} \succeq \mathbf{0}, \quad \forall x \in \mathbb{R}^m. \tag{2.7}$$

According to the second-order condition, a quadratic function $f(\mathbf{x}) = \mathbf{x}^H \mathbf{A}\mathbf{x} + \mathbf{b}^T \mathbf{x} + c$ is convex if and only if $\mathbf{A} \succeq \mathbf{0}$.

2.4.3 Convex Optimization Problems

The notions of convex sets and convex functions have been introduced in the previous two subsections. In this subsection, we move forward to introduce the concepts of convex optimization, which is the most important part of the convex optimization problem. In

general, a standard optimization problem can be expressed as

$$\begin{aligned} \min \;\; & f_0(x) \\ s.t. \;\; & f_i(x) \leq 0, \;\; i = 1, \ldots, m, \\ & h_i(x) = 0, \;\; i = 1, \ldots, p, \end{aligned} \tag{2.8}$$

where $x \in \mathbb{R}^n$ is the optimization variable; $f_0(x)$ denotes the objective function; $f_i(x)$ and $h_i(x)$ are inequality constraints and equality constraints, respectively. The problem domain of (2.8) can be defined as

$$\mathscr{D} = \left\{ \bigcap_{i=0}^{m} \mathbf{dom}\, f_i \right\} \bigcap \left\{ \bigcap_{i=1}^{p} \mathbf{dom}\, h_i \right\}. \tag{2.9}$$

If a point $x \in \mathscr{D}$ satisfies all constraints in problem (2.8), then this point is called feasible point of this problem. The set of all feasible points is called the feasible set. The problem (2.8) can be defined as convex optimization problem if its objective function $f_0(x)$ is convex and constraints are convex as well as domain is convex set. An optimization problem is either convex or non-convex once it is formulated. For the naturally convex problem, it can be solved directly.

2.4.3.1 Linear Program

A optimization problem is said to be a linear program (LP) when the objective and all constraint functions are affine. Then, a general linear program can be formulated as

$$\begin{aligned} \min_{\mathbf{x}} \;\; & \mathbf{c}^T \mathbf{x} + d \\ s.t. \;\; & \mathbf{G}\mathbf{x} \preceq \mathbf{h}, \\ & \mathbf{A}\mathbf{x} = \mathbf{b}, \end{aligned} \tag{2.10}$$

where $\mathbf{G} \in \mathbb{R}^{m \times n}$, $\mathbf{A} \in \mathbb{R}^{p \times n}$, $\mathbf{x}$, $\mathbf{h}$ and $\mathbf{b}$ are vector. Note that if inequality constraints in (2.10) are only componentwise nonnegativity constraints, this problem is called *standard form LP*. If the problem in (2.10) only contains inequality constraints, the problem is said to be *inequality form LP*. Based on the the definition of convex function in (2.5) and the first-order condition in (2.6), linear programs are said to be convex optimization problems [101]. Note that the maximization of an LP is equivalent to the minimization of this LP since the polarity of the objective function can be reversed.

2.4.3.2 Quadratic program

A optimization problem is called as a quadratic program (QP) if the objective function is quadratic and the constraint functions are affine. The structure of a QP can be given by

$$\begin{aligned} \min_{\mathbf{x}} \quad & \mathbf{x}^T \mathbf{P}\mathbf{x} + \mathbf{q}^T \mathbf{x} + d \\ s.t. \quad & \mathbf{G}\mathbf{x} \preceq \mathbf{h}, \\ & \mathbf{A}\mathbf{x} = \mathbf{b}, \end{aligned} \tag{2.11}$$

where $\mathbf{P} \in \mathbb{S}^n$, $\mathbf{G} \in \mathbb{R}^{m \times n}$, $\mathbf{A} \in \mathbb{R}^{p \times n}$ and $\mathbf{x}$ is a vector. If and only if symmetric matric $\mathbf{P}$ is PSD, QP in (2.11) is convex problem. The key idea of QP is to find the minimum value of a quadratic function over a polyhedral set. LP is a special case of QP by taking $\mathbf{P} = 0$.

On the other hand, if the inequality constraint in (2.11) is a quadratic inequality constraint, the new problem is said to be a quadratically constrained quadratic program (QCQP) as

follows:

$$\begin{aligned} \min_{\mathbf{x}} \;\; & \mathbf{x}^T\mathbf{P}_0\mathbf{x}+\mathbf{q}^T\mathbf{x}+d \\ s.t. \;\; & \mathbf{x}^T\mathbf{P}_i\mathbf{x}+\mathbf{q}_i^T\mathbf{x}+d_i \leq 0, \;\; i=1,\ldots,m, \\ & \mathbf{A}\mathbf{x}=\mathbf{b}, \end{aligned} \tag{2.12}$$

where $\mathbf{P}_i \in \mathbb{S}^n,\ i=0,1,\ldots,m$ and $\mathbf{x}$ is a vector.

2.4.3.3 Second-Order Cone Program

In this part, we introduce another convex optimization problem which is related to QP. This problem is called second-order cone program (SOCP), which has the following structure

$$\begin{aligned} \min_{\mathbf{x}} \;\; & \mathbf{b}^T\mathbf{x} \\ s.t. \;\; & \|\mathbf{A}_i\mathbf{x}+\mathbf{b}_i\|_2 \leq \mathbf{a}_i^T\mathbf{x}+d_i, \;\; i=1,\ldots,m, \\ & \mathbf{G}\mathbf{x}=\mathbf{g}, \end{aligned} \tag{2.13}$$

where $\mathbf{A}_i \in \mathbb{R}^{n_i \times n}$ and $\mathbf{x}$ is a vector. The inequality constraint in (2.13) is called the second-order cone constraint. This second-order cone constraint means that an affine function $\mathbf{a}_i^T\mathbf{x}+d_i$ is lying in the second-order cone. Some QCQPs can be converted to the SOCPs. Similarly, if $\mathbf{A}_i=0,\ \forall_i$ in (2.13), problem (2.13) is transferred to the LP.

2.4.3.4 Semidefinite Program

In this part, anther powerful optimization problem is introduced. The conic form problem can be called as Semidefinite program (SDP), which has the following structure

$$\begin{aligned} \min_{\mathbf{x}} \ & \mathbf{b}^T\mathbf{x} \\ s.t. \ & x_1\mathbf{F}_1 + x_2\mathbf{F}_2 + \ldots + x_n\mathbf{F}_n + \mathbf{G} \preceq \mathbf{0}, \\ & \mathbf{A}\mathbf{x} = \mathbf{b}, \end{aligned} \tag{2.14}$$

where $\mathbf{G},\ \mathbf{F}_1,\ldots,\ \mathbf{F}_n \in \mathbb{S}^k$, $\mathbf{x} = [x1,x2,\ldots,x_n] \in \mathbb{R}^n$ and $\mathbf{b} \in \mathbb{R}^n$. It notes that the inequality in (2.14) is the linear matrix inequality (LMI). If replacing $\mathbf{G},\ \mathbf{F}_1,\ldots,\ \mathbf{F}_n$ by their diagonal matrixes, then the LMI in (2.14) is equivalent to a set of n linear inequalities, and the SDP (2.14) reduces to a LP.

A briefly description about how to convert QCQP into SDP for the real-variable case is introduced. The complex-variable case can be similarly performed by the real-variable case. First, a relationship between a linear inequality and a LMI is defined. Based on the principle of the inequality transformation, the following convex quadratic inequality

$$(\mathbf{A}\mathbf{x}+\mathbf{b})^T(\mathbf{A}\mathbf{x}+\mathbf{b}) - \mathbf{a}^T\mathbf{x} - c \leq 0, \ \ \forall \mathbf{x} \in \mathbb{R}^n \tag{2.15}$$

holds true if and only if the following LMI

$$\begin{bmatrix} \mathbf{I} & \mathbf{A}\mathbf{x}+\mathbf{b} \\ (\mathbf{A}\mathbf{x}+\mathbf{b})^T & \mathbf{a}^T\mathbf{x}+c \end{bmatrix} \succeq \mathbf{0}, \ \ \forall \mathbf{x} \in \mathbb{R}^n \tag{2.16}$$

is true.

Next, an example is provided to prove how to convert QCQP into SDP. Consider the following optimization problem

$$\begin{aligned} \min_{\mathbf{x}} \ & \|\mathbf{A}_0\mathbf{x}+\mathbf{b}_0\|_2^2 - \mathbf{c}_0^T\mathbf{x} - d_0 \\ s.t. \ & \|\mathbf{A}_m\mathbf{x}+\mathbf{b}_m\|_2^2 - \mathbf{c}_m^T\mathbf{x} - d_m \leq 0, \ \ m = 1,\ldots,n. \end{aligned} \tag{2.17}$$

where $\mathbf{A}_m \in \mathbb{R}^{n\times n}$ and $\mathbf{x},\ \mathbf{c}_m,\ \mathbf{b}_m \in \mathbb{R}^n$. According to the definition of the QCQP problem in (2.12), which consists of quadratic objective function and quadratic constraints, problem (2.17) can be defined as a QCQP problem. The reason is that problem (2.17) includes the quadratic objective function and quadratic constraints. Then, by exploiting epigraph representation, problem (2.17) can be converted to the following problem

$$\begin{aligned} \min_{\mathbf{x},t} \ & t \\ s.t. \ & (\mathbf{A}_0\mathbf{x}+\mathbf{b}_0)^T(\mathbf{A}_0\mathbf{x}+\mathbf{b}_0) - \mathbf{c}_0^T\mathbf{x} - d_0 \leq t \\ & (\mathbf{A}_m\mathbf{x}+\mathbf{b}_m)^T(\mathbf{A}_m\mathbf{x}+\mathbf{b}_m) - \mathbf{c}_m^T\mathbf{x} - d_m \leq 0, \ \ m = 1,\ldots,n. \end{aligned} \tag{2.18}$$

Based on the relationship between the quadratic inequality (2.15) and the LMI (2.16), it is easily to convert the quadratic inequality constraints in (2.18) into the following LMI constraints

$$\begin{aligned} &\begin{bmatrix} \mathbf{I} & \mathbf{A}_0\mathbf{x}+\mathbf{b}_0 \\ (\mathbf{A}_0\mathbf{x}+\mathbf{b}_0)^T & \mathbf{c}_0^T\mathbf{x}+d_0+t \end{bmatrix} \succeq \mathbf{0} \\ &\begin{bmatrix} \mathbf{I} & \mathbf{A}_m\mathbf{x}+\mathbf{b}_m \\ (\mathbf{A}_m\mathbf{x}+\mathbf{b}_m)^T & \mathbf{c}_m^T\mathbf{x}+d_m+t \end{bmatrix} \succeq \mathbf{0}, \ \ m = 1,\ldots,n. \end{aligned} \tag{2.19}$$

Finally, problem (2.17) can be expressed by the following problem

$$\begin{aligned} &\min_{\mathbf{x},t} \quad t \\ &s.t. \quad (2.19). \end{aligned} \tag{2.20}$$

Note that problem (2.20) is a SDP problem since the objective function of (2.20) is a linear function and the inequality constraints of (2.20) are LMI constraints. The objective and constraint functions satisfy the definition of SDP problem in (2.14).

2.4.3.5 Duality and KKT Conditions

We consider the standard optimization problem (2.8) and its nonempty domain $\mathscr{D}$ in (2.9). We assume that the optimal value of problem (2.8) is p^*. In the following, we consider to use problem (2.8) as an example to introduce the Lagrange duality. The key idea to obtain the Langrange dual function of problem (2.8) is to combine the objective and weighted sum constraint functions into one expression. Then, the Lagrangian function associated with problem (2.8) can be defined as

$$\mathscr{L}(x,\lambda,\nu) = f_0(x) + \sum_{i=1}^{m} \lambda_i f_i(x) + \sum_{i=1}^{p} \nu_i h_i(x), \tag{2.21}$$

where λ and ν are the vector of λ_i and ν_i; λ_i and ν_i are called dual variable or Lagrange multiplier associated with the ith inequality constraint $f_i(x) \leq 0$ and equality constraint $h_i(x) = 0$, respectively. It notes that $\mathscr{L}(x,\lambda,\nu)$ is affine function of (λ,ν) with fixed x. Based on the Lagrangian function $\mathscr{L}$ in (2.21), the associated dual function can be defined by minimizing the Lagrangian function over x as follows:

$$g(\lambda,\nu) = \inf_{x\in\mathscr{D}} \mathscr{L}(x,\lambda,\nu), \tag{2.22}$$

with

$$\textbf{dom}\ g = \{(\lambda, \nu) | g(\lambda, \nu) > -\infty\}, \tag{2.23}$$

where $\inf(A)$ denotes the infimum of A. The dual function g is always concave in terms of λ and ν regardless of whether the primal problem is convex or not as the dual function is the pointwise infimum of a family of affine functions of (λ, ν) [101].

The dual function $g(\lambda, \nu)$ is the lower bound of the optimal value p^* of the primal problem (2.8). This fact can be expressed as

$$g(\lambda, \nu) \leq f_0(x^*) = p^* \tag{2.24}$$

for any nonnegative λ_i and any ν. This important property can be easily proved. We assume x^* is a feasible point of problem (2.8), then we have

$$\mathscr{L}(x^*, \lambda, \nu) = f_0(x^*) + \sum_{i=1}^{m} \lambda_i f_i(x^*) + \sum_{i=1}^{p} \nu_i h_i(x^*) \leq f_0(x^*) \tag{2.25}$$

since

$$\sum_{i=1}^{m} \lambda_i f_i(x^*) + \sum_{i=1}^{p} \nu_i h_i(x^*) \leq 0. \tag{2.26}$$

On the other hand, since $g(\lambda, \nu)$ is the minimum value of $\mathscr{L}(x^*, \lambda, \nu)$ over x^*, we can obtain

$$g(\lambda, \nu) \leq \mathscr{L}(x^*, \lambda, \nu) \leq f_0(x^*). \tag{2.27}$$

It indicates that the inequality holds true since every feasible point of problem (2.8) satisfies inequality in (2.25). Duality gap denotes the difference between the optimal value of the primal problem and the dual problem. If inequality in (2.24) holds, it calls weak duality

which means the gap is non-zero. If only equality holds in (2.24), it calls strong duality which means the gap is zero. Note that strong duality requires the primal problem is convex.

Suppose that the inequality and equality constraints in (2.8) are differentiable. Then, we provide Karush-Kuhn-Tucker (KKT) conditions with considering the primal optimal point x^* and dual optimal Lagrange multipliers λ^* and ν^* as follows:

$$\nabla f_0(x^*) + \sum_{i=1}^{m} \lambda_i^* f_i(x^*) + \sum_{i=1}^{p} \nu_i^* h_i(x^*) = 0, \tag{2.28a}$$

$$f_i(x^*) \leq 0,\ i = 1, \ldots, m, \tag{2.28b}$$

$$h_i(x^*) = 0,\ i = 1, \ldots, p, \tag{2.28c}$$

$$\lambda_i^* \geq 0,\ i = 1, \ldots, m, \tag{2.28d}$$

$$\lambda_i^* f_i(x^*) = 0,\ i = 1, \ldots, m. \tag{2.28e}$$

Based on the provided KKT conditions, we discuss their impacts on optimization problems. For the optimization problem with weak duality, the KKT conditions are the necessary conditions to obtain the local optimality. For the optimization problem with strong duality, any pair of primal and dual optimal points must satisfy KKT conditions. For convex problems with strong duality, then the KKT conditions provide necessary and sufficient conditions for optimality [101].

Chapter 3

Transmit Power Minimization in a Multi-Antenna Relay Network

The remainder of this chapter is organized as follows. The main contributions are first introduced in Section 3.1. The system model is presented in Section 3.2. The proposed robust relay transmit power minimization problem based on imperfect CSI are solved in Section 3.3. Section 3.4 provides the numerical results for the proposed the problem. Conclusions are drawn in Section 3.5.

3.1 Introduction

The application of SWIPT is considered in cooperative networks. In the considered network, multiple antenna relay adopts AF protocol to send information to destinations and the power splitter is fitted at each destination node. On the standpoint of joint optimizing beamforming and PS ratio, a robust relay transmit power minimization problem is proposed. The original non-convex problem is formulated into SDP problem by using SDR method. Then, a proof is given to guarantee the relaxation for the original problem is tight. Finally, the performances of the robust schemes are evaluated by simulations.

3.2 Network Model

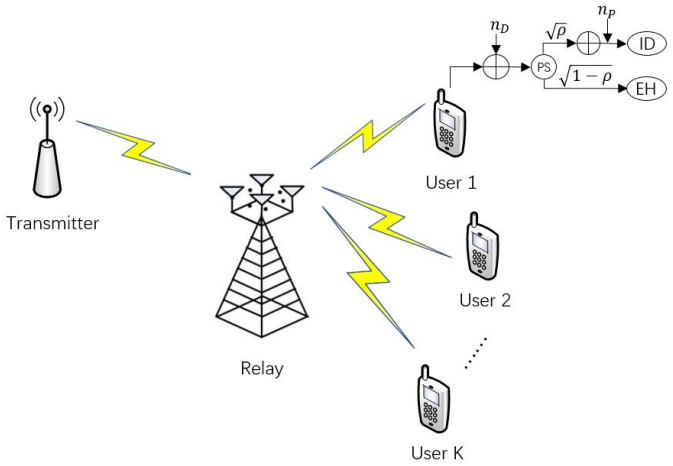

Fig. 3.1 System model.

An AF relay cooperative network consisting of a source, a multi-antenna relay and $K > 1$ destination nodes is considered. The source node and destination nodes are equipped with single antenna, whereas the relay is equipped with $M > 1$ antennas. It is assumed that the source communicates with each destination via the multi-antenna relay node, and the direct links between the source and destinations nodes are sufficiently weak to be ignored. The received signal at the relay can be written as

$$\mathbf{y} = \mathbf{h}x + \mathbf{n}_{s,r}, \tag{3.1}$$

where $\mathbf{h} = [h_1, h_2, ..., h_M]^T \in \mathbb{C}^{M\times 1}$ and x denote channel response vector from the source to the relay and transmitted signal, respectively; $\mathbf{n}_{s,r} \sim \mathrm{CN}(\mathbf{0}, \sigma_{s,r}^2\mathbf{I})$ is the additive white Gaussian noise at the multi-antenna relay. The transmit power of the source is $P_s = E\left[|x^2|\right]$.

The received signal at the relay is amplified by a beamforming matrix $\mathbf{W} \in \mathbb{C}^{M\times M}, \mathbf{W} = \mathrm{diag}(\mathbf{w}_j)$ and then forwarded to the destination. Hence, the transmitted signal by the relay is

given by

$$\mathbf{t} = \mathbf{W}\mathbf{y}. \tag{3.2}$$

The power splitter is fitted at each receiver to dynamically split the received signals. The received signal at the kth receiver is splitted into two portions by a parameter $\rho_k \in [0,1]$, one part is fed to ID and the remaining part is used for EH. Hence, the received signal split for ID at the kth receiver is given by

$$y_k = \sqrt{\rho_k}\left(\mathbf{g}_k^H \mathbf{W}\mathbf{h}x + \mathbf{g}_k^H \mathbf{W}\mathbf{n}_{s,r} + n_k\right) + z_k, \tag{3.3}$$

where $\mathbf{g}_k = [g_{1k}, g_{2k}, ..., g_{Mk}]^T \in \mathbb{C}^{M\times 1}$ presents the channel coefficients from the relay to the kth destination. $n_k \sim CN(0,\sigma_k^2)$ and $z_k \sim CN(0,\delta_k^2)$ denote the antenna noise at the kth destination node and the additional noise introduced by the ID at the kth destination node, respectively. The transmitted power by the relay can be expressed as

$$P_T = \|\mathbf{t}\|^2 = P_s\|\mathbf{h}^H\mathbf{W}\|^2 + \sigma_{s,r}^2\|\mathbf{W}\|^2. \tag{3.4}$$

Then, the received SNR at the kth receiver can be written as

$$\Gamma_k = \frac{\rho_k P_s |\mathbf{g}_k^H \mathbf{W}\mathbf{h}|^2}{\rho_k \sigma_{s,r}^2 \|\mathbf{g}_k^H \mathbf{W}\|^2 + \rho_k \sigma_k^2 + \delta_k^2}, \quad \forall_k \tag{3.5}$$

The harvested energy at the kth receiver can be expressed as

$$P_E = \xi_k(1-\rho_k)\left(|\mathbf{g}_k^H \mathbf{W}\mathbf{h}|^2 + \sigma_{s,r}^2\|\mathbf{g}_k^H \mathbf{W}\|^2 + \sigma_k^2\right), \tag{3.6}$$

in which $\xi_k \in (0,1]$ denotes the energy conversion efficiency of the EH at the kth receiver.

By jointly optimizing the transmit beamforming, $\{\mathbf{W}\}$, and PS ratio, $\{\rho_k\}$, the relay transmit power minimization problem can be expressed as

$$\begin{aligned} \min_{\mathbf{W},\rho_k} \quad & P_s\|\mathbf{h}^H\mathbf{W}\|^2 + \sigma_{s,r}^2\|\mathbf{W}\|^2 \\ s.t. \quad & \Gamma_k \geq \gamma_k, P_E \geq e_k, 0 < \rho_k < 1, \forall_k. \end{aligned} \tag{3.7}$$

The achieved SNR for each destination should be higher than a threshold γ_k. Similarly, EH constraint requires that the harvested energy at the kth receiver should be higher than a threshold e_k. It is assumed that this problem is feasible throughout this chapter.

3.3 Problem Formulation and Solution

In this section, a robust optimization problem is proposed to jointly design beamforming and PS ratio based on the bounded CSI error model. Since the relay is used to help the communication between the source and the destinations, it is assumed that the channel between the source and the relay is perfectly known by the source. Meanwhile, it is also assumed that the relay only knows the imperfect CSI of the destinations. The channel uncertainty model is considered based on the assumption of the actual channel lying in an ellipsoid, which is centred at the channel mean. The actual channels can be modelled as

$$G_k = \{\mathbf{g}_k | \mathbf{g}_k = \tilde{\mathbf{g}}_k + \Delta\mathbf{g}_k, \Delta\mathbf{g}_k^H \mathbf{C}_k \Delta\mathbf{g}_k \leq 1\}, \forall_k, \tag{3.8}$$

where $\tilde{\mathbf{g}}_k$ denotes the estimation of the corresponding channel; $\Delta\mathbf{g}_k$ represent the channel error, which are bounded by ellipsoid; $\mathbf{C}_k \succ \mathbf{0}$ determine the quality of CSI and are assumed known by the relay. Without loss of generality, it sets $\mathbf{C}_k = (1/\varepsilon_k)\mathbf{I}$, where ε_k represent the size of the bounded error region. By taking into the account the actual channel for the

optimization problem in (3.7), the robust power minimization problem can be formulated as

$$\begin{aligned}
\min_{\mathbf{W},\rho_k} \quad & P_s\|\mathbf{h}^H\mathbf{W}\|^2+\sigma_{s,r}^2\|\mathbf{W}\|^2 \\
s.t. \quad & \frac{P_s|(\tilde{\mathbf{g}}_k+\Delta\mathbf{g}_k)^H\mathbf{W}\mathbf{h}|^2}{\sigma_{s,r}^2\|(\tilde{\mathbf{g}}_k+\Delta\mathbf{g}_k)^H\mathbf{W}\|^2+\sigma_k^2+\frac{\delta_k^2}{\rho_k}}\geq\gamma_k,\ \forall_k, \\
& |(\tilde{\mathbf{g}}_k+\Delta\mathbf{g}_k)^H\mathbf{W}\mathbf{h}|^2+\sigma_{s,r}^2\|(\tilde{\mathbf{g}}_k+\Delta\mathbf{g}_k)^H\mathbf{W}\|^2+\sigma_k^2\geq\frac{e_k}{\xi_k(1-\rho_k)}\ \forall_k, \\
& 0<\rho_k<1,\ \forall_k. \qquad (3.9)
\end{aligned}$$

The formulated robust problem is non-convex due to the quadratic function and error function [101]. In the following parts, this non-convex problem is solved by two approximation approaches.

3.3.1 Coefficient Uncertainty Model

In order to solve the non-convex problem (3.9), the quadratic terms need to be transformed to the easy-handled functions. The aim of the SNR constraint is to guarantee the minimum SNR greater than a threshold. It means that the numerator can be expressed by its underestimation value and the denominator can be expressed by its overestimation value. Based on the definition of vec$(\cdot)$ [106] and *Cauchy-Schwarz inequality* [107], the numerator and the denominator in the SNR constraint can be approximated as

$$\begin{aligned}
&|(\tilde{\mathbf{g}}_k+\Delta\mathbf{g}_k)^H\mathbf{W}\mathbf{h}|^2\geq|\mathbf{b}_k^H\mathbf{f}|^2+(\varepsilon_k-2\sqrt{\varepsilon_k}\|\tilde{\mathbf{g}}_k\|)\|\mathbf{h}\|^2\|\mathbf{f}\|^2, \\
&\|(\tilde{\mathbf{g}}_k+\Delta\mathbf{g}_k)^H\mathbf{W}\|^2\leq\|\mathbf{G}_k\mathbf{f}\|^2+M(\varepsilon_k+2\sqrt{\varepsilon_k}\|\tilde{\mathbf{g}}_k\|)\|\mathbf{f}\|^2, \qquad (3.10)
\end{aligned}$$

where $\mathbf{b}_k=\text{vec}(\tilde{\mathbf{g}}_k\mathbf{h}^H)$, $\mathbf{G}_k=(\tilde{\mathbf{g}}_k\otimes\mathbf{I})$, $\mathbf{f}=\text{vec}(\mathbf{W})$, and vec$(\cdot)$ denots vectorization of matrix. Similarly, the quadratic term in EH constraint can also be approximated to the same expression with the first inequality in (3.10). After solving the channel errors, the

optimization problem is still non-convex. The semidefinite relaxation (SDR) method is adopted to convert problem (3.9) into SDP problem by setting $\mathbf{Q} = \mathbf{f}\mathbf{f}^H$. Then, the relaxed problem is given by

$$\begin{aligned} \min_{\mathbf{Q},\rho_k} \quad & P_s \mathrm{Tr}(\mathbf{H}\mathbf{Q}) + \sigma_{s,r}^2 \mathrm{Tr}(\mathbf{Q}) \\ s.t. \quad & \frac{P_s}{\gamma_k}\mathrm{Tr}(\mathbf{B}_k\mathbf{Q}) - \sigma_{s,r}^2 \mathrm{Tr}(\mathbf{G}_{k1}\mathbf{Q}) - \sigma_k^2 \geq \frac{\delta_k^2}{\rho_k}, \ \forall_k, \\ & P_s \mathrm{Tr}(\mathbf{B}_k\mathbf{Q}) + \sigma_{s,r}^2 \mathrm{Tr}(\mathbf{G}_{k1}\mathbf{Q}) + \sigma_k^2 \geq \frac{e_k}{1-\rho_k}, \forall_k \\ & 0 < \rho_k < 1, \ \mathbf{Q} \succeq \mathbf{0}, \ \mathrm{rank}(\mathbf{Q}) = 1, \end{aligned} \tag{3.11}$$

where $\mathbf{H} = (\mathbf{h} \otimes \mathbf{I})(\mathbf{h} \otimes \mathbf{I})^H$, $\mathbf{B}_k = \mathbf{b}_k\mathbf{b}_k^H + (\varepsilon_k - 2\sqrt{\varepsilon_k}\|\tilde{\mathbf{g}}_k\|)\mathbf{h}\mathbf{h}^H$, $\mathbf{G}_{k1} = \mathbf{G}_k\mathbf{G}_k^H + M(\varepsilon_k + 2\sqrt{\varepsilon_k}\|\tilde{\mathbf{g}}_k\|)$. Note that the problem (3.11) is still non-convex due to the rank-one constraint. By dropping the rank-one constraint, the problem (3.11) becomes a convex problem and can be solved easily by using the existing tool box [105]. Note that If the problem in (3.11) yields a rank-one (i.e. $rank(Q) \leq 1$) solution, then the optimal solution of the problem in (3.9) can be obtained by eigenvalue decomposition (EVD); otherwise, the solutions obtained by problem (3.11) is only the lower-bound solution. Based on the following lemma, $rank(\mathbf{Q}) = 1$ condition can be proved.

Lemma 1. *If the problem* (3.9) *is feasible, thus the optimal solution* $\mathbf{Q}^*$ *for problem* (3.11) *is rank-one.*

Proof. Please refer to Section 3.6. □

3.3.2 Covariance Uncertainty Model

In this subsection, a channel covariance uncertainty model is considered. Based on the assumption, the actual channel covariance matrix can be expressed as

$$\mathbf{D}_k = \hat{\mathbf{D}}_k + \Delta D_k, \mathbf{R}_k = \hat{\mathbf{R}}_k + \Delta R_k, \tag{3.12}$$

where $\hat{\mathbf{D}}_k = \text{vec}(\tilde{\mathbf{g}}_k\mathbf{h}^H)\text{vec}(\tilde{\mathbf{g}}_k\mathbf{h}^H)^H$, $\Delta D_k = 2\text{vec}(\tilde{\mathbf{g}}_k\mathbf{h}^H)\text{vec}(\Delta\mathbf{g}_k\mathbf{h}^H)^H + \text{vec}(\Delta\mathbf{g}_k\mathbf{h}^H)\text{vec}(\Delta\mathbf{g}_k\mathbf{h}^H)^H$, $\hat{\mathbf{R}}_k = (\tilde{\mathbf{g}}_k \otimes \mathbf{I})(\tilde{\mathbf{g}}_k \otimes \mathbf{I})^H$ and $\Delta R_k = 2(\tilde{\mathbf{g}}_k \otimes \mathbf{I})(\Delta\mathbf{g}_k \otimes \mathbf{I})^H + (\Delta\mathbf{g}_k \otimes \mathbf{I})(\Delta\mathbf{g}_k \otimes \mathbf{I})^H$. The covariance error can be bounded as follows:

$$\begin{aligned} \|\Delta D_k\|_F &\leq (\varepsilon_k + 2\sqrt{\varepsilon_k}\|\tilde{\mathbf{g}}_k\|)\|\mathbf{h}\|^2 = \varepsilon_{D_k}, \\ \|\Delta R_k\|_F &\leq (\varepsilon_k + 2\sqrt{\varepsilon_k}\|\tilde{\mathbf{g}}_k\|)\|M = \varepsilon_{R_k}. \end{aligned} \tag{3.13}$$

By substituting (3.13) into problem (3.9), the robust power minimization problem is formulated as follows:

$$\min_{\mathbf{Q},\rho_k} \quad P_s\text{Tr}(\mathbf{HQ}) + \sigma_{s,r}^2\text{Tr}(\mathbf{Q}) \tag{3.14a}$$

$$s.t. \quad \min_{\|\Delta D_k\|,\|\Delta R_k\|} \frac{P_s\text{Tr}(\hat{\mathbf{D}}_k + \Delta D_k)\mathbf{Q})}{\sigma_{s,r}^2\text{Tr}((\hat{\mathbf{R}}_k + \Delta R_k)\mathbf{Q}) + \sigma_k^2 + \frac{\delta_k^2}{\rho_k}} \geq \gamma_k, \quad \forall k, \tag{3.14b}$$

$$\min_{\|\Delta D_k\|,\|\Delta R_k\|} P_s\text{Tr}((\hat{\mathbf{D}}_k + \Delta D_k)\mathbf{Q}) + \sigma_{s,r}^2\text{Tr}((\hat{\mathbf{R}}_k + \Delta R_k)\mathbf{Q}) + \sigma_k^2 \geq \frac{e_k}{1-\rho_k}, \quad \forall k, \tag{3.14c}$$

$$\mathbf{Q} \succeq \mathbf{0}, \ \|\Delta D_k\| \leq \varepsilon_{D_k}, \ \|\Delta R_k\| \leq \varepsilon_{R_k}, \ 0 < \rho_k < 1, \ \forall k, \tag{3.14d}$$

It obviously shows that the objective function of problem (3.14) is a linear function and the constraints of problem (3.14) are infinite functions. Therefore, the above problem (3.14) is non-convex due to the non-convex constraints. In the following parts, the non-convex

constraints are solved by dealing with the error parts. Lagrangian dual method is considered to convert these non-convex constraints into the convex functions. Also, the duality gap between the relaxed and original problems is investigated. By applying the Lagrangian duality, the constraint in (3.14b) can be expressed as

$$\max_{\mathbf{Y}_k^D,\mathbf{Y}_k^R} -\varepsilon_{D_k}\|\mathbf{Y}_k^D - \frac{P_s}{\gamma_k}\mathbf{Q}\| - \varepsilon_{R_k}\|\mathbf{Y}_k^R + \sigma_{s,r}^2\mathbf{Q}\| - \mathrm{Tr}\Big(\hat{\mathbf{D}}_k(\mathbf{Y}_k^D - \frac{P_s}{\gamma_k}\mathbf{Q})\Big) - \sigma_k^2 - \frac{\delta_d^2}{\rho_k}$$
$$- \mathrm{Tr}\Big(\hat{\mathbf{R}}_k(\mathbf{Y}_k^R + \sigma_{s,r}^2\mathbf{Q})\Big) \geq 0, \ \ \forall_k \tag{3.15}$$

and the EH constraint in (3.14c) can be written as

$$\max_{\mathbf{Z}_k^D,\mathbf{Z}_k^R} \ -\varepsilon_{D_k}\|\mathbf{Z}_k^D - P_s\mathbf{Q}\| - \varepsilon_{R_k}\|\mathbf{Z}_k^R - \sigma_{s,r}^2\mathbf{Q}\| + \sigma_k^2 - \mathrm{Tr}\Big(\hat{\mathbf{D}}_k(\mathbf{Z}_k^D - P_s\mathbf{Q})\Big) - \frac{e_k}{1-\rho_k}$$
$$- \mathrm{Tr}\Big(\hat{\mathbf{R}}_k(\mathbf{Z}_k^R - \sigma_{s,r}^2\mathbf{Q})\Big) \geq 0, \ \ \forall_k. \tag{3.16}$$

It is assumed that there exist the Lagrangian multipliers $\mathbf{Y}_k^D$, $\mathbf{Y}_k^R$, $\mathbf{Z}_k^D$ and $\mathbf{Z}_k^R$, which satisfy the first and the second constraints (3.14b) and (3.14c). With the help of (3.15) and (3.16), the robust power minimization problem can be reformulated as

$$\begin{aligned}\min_{\mathbf{Q}_j,\mathbf{Y}_k^D,\mathbf{Y}_k^R,\mathbf{Z}_k^D,\mathbf{Z}_k^R,\rho_k} \quad & P_s\mathrm{Tr}(\mathbf{HQ}) + \sigma_{s,r}^2\mathrm{Tr}(\mathbf{Q}) \\ s.t. \quad & (3.15),(3.16), \quad 0<\rho_k<1, \quad \forall_k, \\ & \mathbf{Q}\succeq\mathbf{0},\ \mathbf{Y}_k^D\succeq\mathbf{0},\ \mathbf{Y}_k^R\succeq\mathbf{0},\ \mathbf{Z}_k^D\succeq\mathbf{0},\ \mathbf{Z}_k^R\succeq\mathbf{0},\forall_k. \end{aligned} \tag{3.17}$$

The above problem is convex, and can be directly solved by using convex optimization software [105]. If the problem in (3.17) yield a rank-one (i.e. $\mathrm{rank}(\mathbf{Q}) = 1$) solution, then the optimal solution of the problem in (3.14) can be obtained by eigenvalue decomposition (EVD). However, if $\mathrm{rank}(\mathbf{Q}) \geq 1$, the randomization technique can be considered to obtain a best rank-one solution [108, 109].

3.4 Numerical Results

In this section, the performances of the proposed robust scheme are validated through simulation. It is assumed that there are three users (K = 3), and the relay is equipped with four antennas (M = 4), where the other nodes consist of single antenna. All channels are generated by using the zero-mean and unit variance Gaussian random variables. For simplicity, some parameters is set as $\sigma_{s,r}^2 = \sigma_k^2 = -70$ dBm, $\delta_k^2 = -50$ dBm, $e_k = e$, $\gamma_k = \gamma$, $\rho_k = \rho$, and $\varepsilon_k = \varepsilon$, $k = 1, \ldots, K$. The performance of proposed robust power minimization scheme is evaluated by averaging over 100 randomly generated channel realizations.

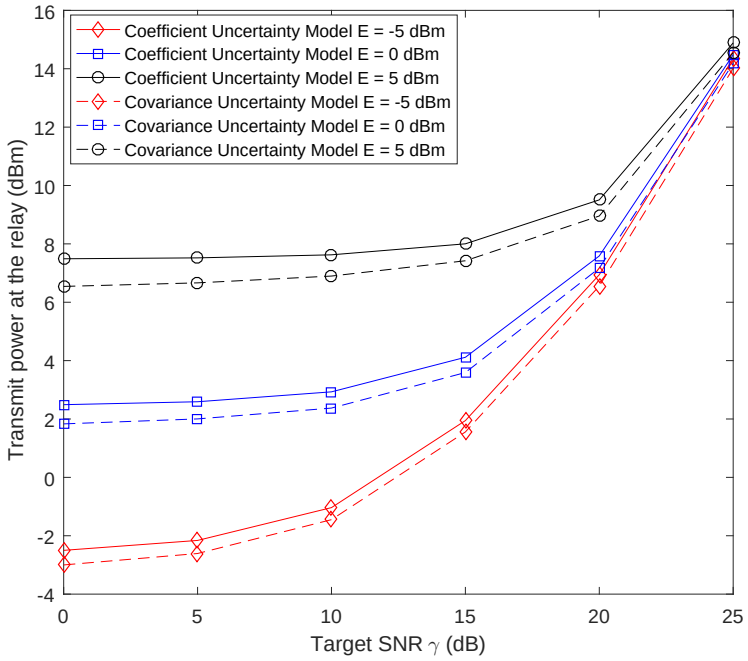

Fig. 3.2 Transmit power at the relay versus the required SNR γ with $P_s = 5$ dBm, $\varepsilon^2 = 0.1$.

In Figure 3.2, the performance of the proposed robust algorithms based on the channel coefficient and channel covariance uncertainty models versus the required SNR γ with different value of harvested energy constraint e is compared. From this result, it can be observed that the required transmit power at the relay increases with the increase of in the

required SNR targets for both channel uncertainties. In addition, the relay transmits less power for covariance model compared with coefficient model. However, the required transmit power for both uncertainty models becomes the same at high target SNR. Also, the relay need consume more power as the EH requirement increases for all cases.

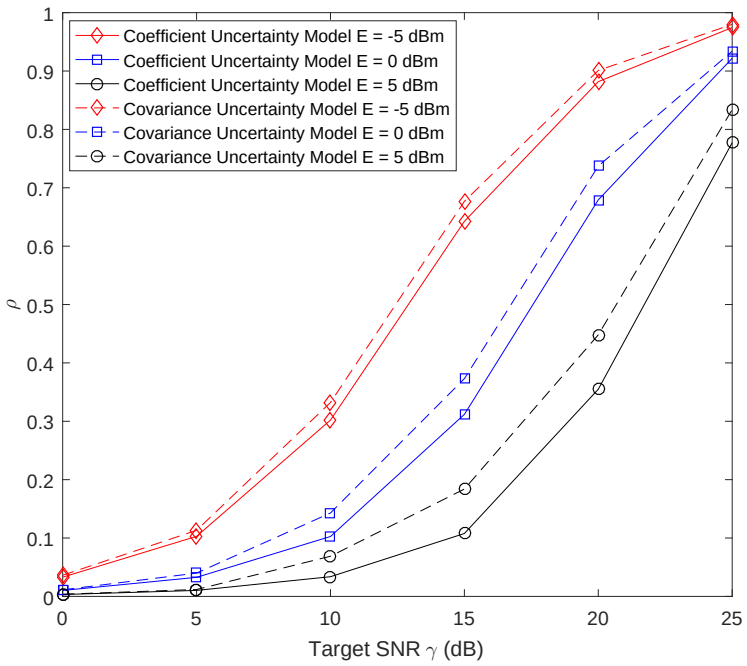

Fig. 3.3 Optimal PS ratio versus the SNR threshold with $\gamma = 5$ dB, $P_s = 5$ dBm, and $\varepsilon^2 = 0.1$.

Next, the PS ratio performance for the proposed robust schemes is evaluated. Figure 3.3 shows the optimal PS ratio versus the SNR constraint γ with different energy requirements e for both uncertainty models. Notice that the average value of ρ is adopted to evaluate the performance. This result confirms that more received power is allocated to the ID receivers by the power splitter for both channel uncertainty models as the SNR increasing. The covariance uncertainty model distributes more power to the ID receivers compared with the coefficient uncertainty model under the same target SNR. One possible reason is that the ID receiver is more sensitive under covariance uncertainty model and it needs more energy to overcome the channel effect.

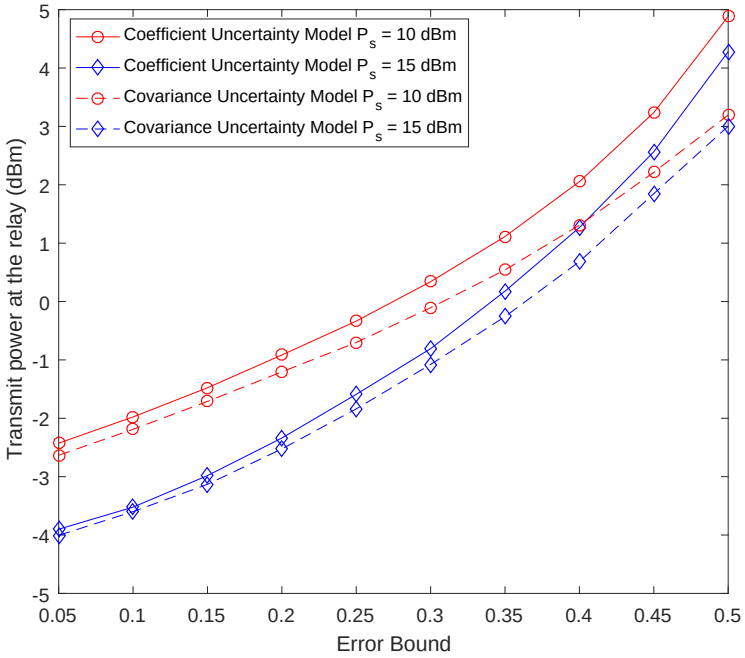

Fig. 3.4 Relay power versus the error bound ε with $\gamma = 5$ dB and $e = 0$ dBm

Finally, the required transmit power is evaluated for the two proposed robust schemes. Figure 3.4 shows the transmit power with different error bound based on two uncertainty models. This result confirms that the covariance uncertainty model consumes less power than that of the coefficient uncertainty model. In addition, the difference between these two channel uncertainty models becomes small as the error bound increases.

3.5 Summary

In this chapter, a SWIPT scheme is investigated in a MISO downlink system. For this network, a robust power minimization problem is proposed. The relay beamforming and PS ratio are jointly optimized based on two robust algorithms. Due to non-convexity of the original problem, the original problem is converted into SDP by using SDR. Simulation results have been provided to validate the performance of the proposed robust schemes.

3.6 Appendix

3.6.1 Proof of Lemma 1

By dropping the rank-one constraint, (3.11) is a convex SDP problem. It is easy to verify that this problem satisfies the Slater's condition [101] and the corresponding duality gap is zero. Therefore, the Lagrangian of (3.11) can be expressed as

$$\mathrm{L}(\mathbf{Q},\mathbf{C}_j,\lambda_j,\mu_j)=\sum_{j=1}^{K}\left(\lambda_j(\frac{\delta_d^2}{\rho_k}+\sigma_k^2)+\mu_j(\frac{e_k}{1-\rho_k}-\sigma_k^2)\right)+\sum_{j=1}^{K}\mathrm{Tr}(\mathbf{C}_j\mathbf{Q}), \tag{3.18}$$

where $\mathbf{C}_j=P_s\mathbf{H}+\sigma_{s,r}^2\mathbf{I}-\sum_{j=1}^{K}(\frac{\lambda_j}{\gamma_k}+\mu_j)P_s\mathbf{B}_k+\sum_{j=1}^{K}((\lambda_j-\mu_j)\sigma_{s,r}^2\mathbf{G}_{k1})$ and $\lambda_j\geq 0$, $\mu_j\geq 0$ are the dual variables associated with kth SNR and EH constraints, respectively. The dual problem of (3.11) is then defined as

$$\begin{aligned}\max_{\lambda_j,\mu_j,\rho_k}\quad & \sum_{j=1}^{K}\left(\lambda_j(\frac{\delta_d^2}{\rho_k}+\sigma_k^2)+\mu_j(\frac{e_k}{1-\rho_k}-\sigma_k^2)\right)\\ s.t.\quad & \mathbf{C}_j\succeq\mathbf{0},\forall_j.\end{aligned} \tag{3.19}$$

It is assumed that $\left\{\lambda_j^*\right\}$ and $\left\{\mu_j^*\right\}$ are the optimal dual variables for problem (3.19). The resulting $\mathbf{C}_j$ becomes $\mathbf{C}_j^*$. Then by complementary slackness condition, it obtains

$$\mathrm{Tr}(\mathbf{C}_j^*\mathbf{Q}^*)=0,\forall_j, \tag{3.20}$$

where $\mathbf{Q}^*$ is the optimal solution of (3.11) and the equation (3.20) is equivalent $\mathbf{C}_j^*\mathbf{Q}^*=\mathbf{0},\forall_j$. Due to $0<\rho_k<1$, condition, two cases of the dual variables: $\lambda_j^*>0,\mu_j^*=0$ and $\lambda_j^*=0,\mu_j^*>0$ is not possible. If $\lambda_j^*=0$ and $\mu_j^*=0$, then $\mathbf{C}_j^*=\sigma_{s,r}^2\mathbf{I}+P_s\mathbf{H}\succ\mathbf{0}$ and $\mathrm{Rank}(\mathbf{C}_j^*)=M$ is full rank. Combining $\mathrm{Rank}(\mathbf{c}_j^*)=M$ and $\mathbf{C}_j^*\mathbf{Q}^*=\mathbf{0}$ conditions, I can obtain $\mathbf{Q}^*=\mathbf{0}$, which

cannot be the optimal solution for problem (3.11). Therefore, both $\lambda_j^*, \mu_j^* = 0$ must be great than zero.

Due to $P_s\mathbf{H} + \sigma_{s,r}^2\mathbf{I} \succ \mathbf{0}$, it has $\text{Rank}(\mathbf{C}_j^*) = \text{Rank}(M - (\sum_{j=1}^{K}(\frac{\lambda_j}{\gamma_k} + \mu_j)P_s\mathbf{B}_k))$, then it gets $\text{Rank}(\mathbf{C}_j^*) \geq M - 1$. Note that if $\text{Rank}(\mathbf{C}_j^*)$ is full rank matrix, it has $\mathbf{Q}^* = \mathbf{0}$, which cannot be the optimal solution. Hence, it follows that $\text{Rank}(\mathbf{C}_j^*) = M - 1, \forall_j$. According to $\mathbf{C}_j^*\mathbf{Q}^* = \mathbf{0}$, then $\text{Rank}(\mathbf{Q}^*) = 1, \forall_j$. Therefore, the proof of Lemma 1 is completed.

Chapter 4

Secure Beamforming and Power Splitting Designs in a Multi-antenna Relay Network

This chapter is organized as follows. The main contributions of this work is first introduced in 4.1. The system model is described in Section 4.2. The PM optimization problems based on perfect CSI is solved in Section 4.3, whereas the robust PM optimization problem is considered in Section 4.4. Section 4.5 presents simulation results to validate the performance of the proposed algorithms for both perfect and imperfect CSI cases. Finally, conclusions are presented in Section 4.6.

4.1 Introduction

In this chapter, a secure transmission in a multi-antenna AF relay network based on perfect CSI and imperfect CSI assumption is investigated. In the considered scenario, multiple idle receivers attempt to overheard the transmission message. PS receiver architecture is employed at each receiver. The main objective is to jointly design secure beamforming and the PS ratio by a proposed PM problem subject to the constraints on secrecy rate and EH under the assumption of perfect and imperfect CSI at the transmitter and the relay. The

proposed PM problem for both channel model is non-convex and challenge to solve due to the coupled variables [101]. Two methods are proposed to tackle the difficulties. One is based on 1-D search and the other one is based on SPCA [110]. The primary contributions of this chapter are summarized as follows.

- For the model with perfect CSI at the transmitter and the relay, the PM problem is transformed into a two-level optimization problem. In the inner level, the PM problem can be relaxed as a SDP problem by using SDR method [108]. In the outer level, the problem can be solved by using 1-D line search respect to a single variable. In addition, a rank reduction algorithm is proposed to guarantee the tightness of the relaxation based on the concept in [111]. On the other hand, a low-complexity algorithm based on the SPCA method is proposed to iteratively solve the PM problem.

- For the imperfect CSI model with bounded CSI error, SDR method, 1-D linear search, and the rank reduction method can be still adopted to solve the difficulties caused by the quadratic terms, the coupled variables, and rank constraint. Furthermore, S-procedure method is used to convert the semi-infinite constraints into LMI. In order to reduce the computational complexity, an SPCA-based iterative algorithm is also proposed.

4.2 Network Model

In this chapter, a cooperative relay network is considered as shown in Figure 4.1 which consists of a transmitter, $(K+1)$th receiver, and a half duplex (HD) AF relay. All nodes are deployed in a same cluster. It is assumed that there is no direct link from the transmitter to all the receivers since the transmitter is relative far away from the receivers. The transmitter and all receivers are equipped with single antenna as well as the relay is equipped with M antennas $(M > 1)$. All receivers are able to decode information and harvest energy from radio signals.

Two types of receiver are considered in the system; one desired receiver and K idle receivers. In addition, it is assumed that only the desired receiver is active to decode information and harvest energy simultaneously. The other idle receivers are supposed to harvest energy from the RF signal when they are inactive. However, these idle receivers may attempt to eavesdrop the information for the desired receiver rather than to harvest energy since all receivers are deployed in the range of service coverage. Hence, the secure communication should be provided by taking into account for the idle receivers as the potential eavesdroppers.

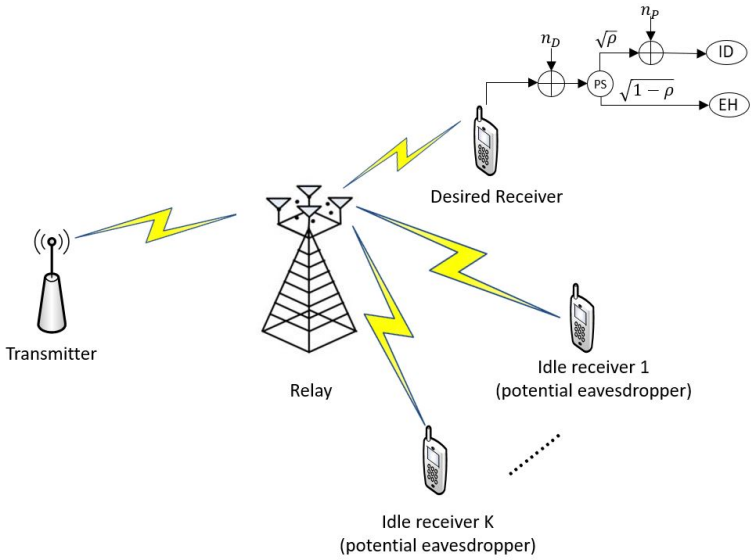

Fig. 4.1 System model.

In the first transmission phase, the transmitter sends coded confidential information s to the AF relay. Thus, the received signal at the relay is given by

$$\mathbf{y}_r = \sqrt{P_s}\mathbf{h}_r s + \mathbf{n}_r, \tag{4.1}$$

where P_s denotes the average transmit power at the transmitter; $s \sim \mathrm{CN}(0,1)$ is a transmit signal and $\mathbf{n}_r \sim \mathrm{CN}(\mathbf{0}, \sigma_r^2\mathbf{I})$ is an additive complex noise at the relay; $\mathbf{h}_r \in \mathbb{C}^{M\times 1}$ represents the channel vector from the transmitter to the relay.

In the second transmission phase, the relay employs the AF transformation matrix $\mathbf{W} \in \mathbb{C}^{N_t \times N_t}$ to amplify the received signal and then forwards to the DR. Thus, the transmitted signal at the relay can be expressed as

$$\mathbf{x}_r = \mathbf{W}\mathbf{y}_r. \tag{4.2}$$

Note that the transmit power at the relay is given by

$$P_r = \mathbb{E}\{\mathbf{x}_r \mathbf{x}_r^H\} = P_s \|\mathbf{W}\mathbf{h}_r\|^2 + \sigma_r^2 \|\mathbf{W}\|_F^2. \tag{4.3}$$

Then, the received signal at the DR and the k-th idle receiver is given by

$$y_d = \sqrt{P_s}\mathbf{h}_d^H \mathbf{W}\mathbf{h}_r s + \mathbf{h}_d^H \mathbf{W}\mathbf{n}_r + n_D, \tag{4.4a}$$

$$y_{e,k} = \sqrt{P_s}\mathbf{g}_k^H \mathbf{W}\mathbf{h}_r s + \mathbf{g}_k^H \mathbf{W}\mathbf{n}_r + n_k, \tag{4.4b}$$

where $\mathbf{h}_d \in \mathbb{C}^{M\times 1}$ and $\mathbf{g}_k \in \mathbb{C}^{M\times 1}$ denote the channel vector from the relay to the DR and the k-th idle receiver, respectively; $n_D \sim \mathrm{CN}(0, \sigma_D^2)$ and $n_k \sim \mathrm{CN}(0, \sigma_k^2)$ represent the additive complex noise at the DR and the k-th idle receiver, respectively.

It assumes that power splitter is employed at the DR to perform ID and EH simultaneously. Hence, the received signal for ID can be expressed as

$$y_d^{ID} = \sqrt{\rho}\left(\sqrt{P_s}\mathbf{h}_d^H \mathbf{W}\mathbf{h}_r s + \mathbf{h}_d^H \mathbf{W}\mathbf{n}_r + n_D\right) + n_P, \tag{4.5}$$

where ρ $(0 \le \rho \le 1)$ is PS ratio and $n_P \sim \mathrm{CN}(0, \sigma_P^2)$ is the signal processing noise power at the receiver. On the other hand, the total harvested energy at the DR can be expressed as

$$E = \xi(1-\rho)(P_s|\mathbf{h}_d^H \mathbf{W}\mathbf{h}_r|^2 + \sigma_r^2 \|\mathbf{h}_d^H \mathbf{W}\|^2 + \sigma_D^2), \tag{4.6}$$

where $\xi \in (0,1]$ denotes the energy conversion efficiency.

According to Equations (4.5) and (4.4b), the SNR at the DR and the k-th idle receiver is given, respectively

$$\gamma_d = \frac{\rho P_s |\mathbf{h}_d^H \mathbf{W} \mathbf{h}_r|^2}{\rho(\sigma_r^2 \|\mathbf{h}_d^H \mathbf{W}\|^2 + \sigma_D^2) + \sigma_P^2}, \tag{4.7a}$$

$$\begin{aligned} \gamma_{e,k} &= \frac{\rho_k P_s |\mathbf{g}_k^H \mathbf{W} \mathbf{h}_r|^2}{\rho_k(\sigma_r^2 \|\mathbf{g}_k^H \mathbf{W}\|^2 + \sigma_k^2) + \sigma_P^2} \\ &\overset{(a)}{\leq} \frac{P_s |\mathbf{g}_k^H \mathbf{W} \mathbf{h}_r|^2}{\sigma_r^2 \|\mathbf{g}_k^H \mathbf{W}\|^2 + \sigma_k^2 + \sigma_P^2}, \end{aligned} \tag{4.7b}$$

where ρ_k is the PS ratio at the k-th idle receiver. (a) is due to the fact that the SNR of the k-th idle receiver is a monotonically increasing function of ρ_k. The physical meaning of (4.7b) is that the idle receivers give up the opportunity to harvest energy and use all the received power to eavesdropping.

Based on the aforementioned settings, the achievable secrecy rate at the DR can be expressed as [30]

$$\begin{aligned} R_s &= \frac{1}{2}\left[\min_k \{\log(1+\gamma_d) - \log(1+\gamma_{e,k})\}\right]^+, \\ &= \frac{1}{2}\left[\log(1+\gamma_d) - \max_k \log(1+\gamma_{e,k})\right]^+, \forall_k, \end{aligned} \tag{4.8}$$

where $[x]^+$ denotes $\max(0,x)$.

4.3 Problem Design Based on Perfect CSI

In this section, a PM problem is proposed to jointly optimize the AF beamforming matrix $\mathbf{W}$ and the PS ratio ρ. The channel between the transmitter and the AF relay is perfectly known by the transmitter since the direct link is very week and the relay needs to obtain more

corrected signal to improve the secure communication. As the idle receivers are deployed in the same range of service coverage with the desired receiver, it assumes that the CSI of all the receivers is perfectly known by the relay.

4.3.1 Problem Formulation

The aim of this problem is to minimize the total power consumption at the relay subject to the secrecy rate constraint and the EH constraint. Specifically, the PM problem can be formulated as

$$\min_{\mathbf{W},\rho} P_s\|\mathbf{W}\mathbf{h}_r\|^2+\sigma_r^2\|\mathbf{W}\|_F^2 \tag{4.9a}$$

$$s.t.\ \ \frac{1}{2}\log\left(1+\frac{P_s|\mathbf{h}_d^H\mathbf{W}\mathbf{h}_r|^2}{\sigma_r^2\|\mathbf{h}_d^H\mathbf{W}\|^2+\sigma_D^2+\frac{\sigma_P^2}{\rho}}\right)-\max_k\frac{1}{2}\log\left(1+\frac{P_s|\mathbf{g}_k^H\mathbf{W}\mathbf{h}_r|^2}{\sigma_r^2\|\mathbf{g}_k^H\mathbf{W}\|^2+\sigma_k^2+\sigma_P^2}\right)\geq R,\forall_k, \tag{4.9b}$$

$$\xi(1-\rho)(P_s|\mathbf{h}_d^H\mathbf{W}\mathbf{h}_r|^2+\sigma_r^2\|\mathbf{h}_d^H\mathbf{W}\|^2+\sigma_D^2)\geq\eta, \tag{4.9c}$$

$$0\leq\rho\leq 1, \tag{4.9d}$$

where $R\geq 0$ represents the target secrecy rate and η is the predefined harvested power. Notably, problem (4.9) is non-convex and includes the high complexity forms, which are hard to be solved. In order to facilitate the analysis in the sequel, the quadratic terms in (4.9) can be equivalently transformed into the following easy-handled functions based on the

definition of vec$(\cdot)$ [106]:

$$\begin{aligned}
|\mathbf{h}_d^H\mathbf{W}\mathbf{h}_r|^2 &= |\mathrm{vec}(\mathbf{h}_d\mathbf{h}_r^H)^H\mathrm{vec}(\mathbf{W})|^2 = |\mathbf{f}^H\mathbf{w}|^2,\\
\|\mathbf{h}_d^H\mathbf{W}\|^2 &= \|(\mathbf{h}_d\otimes\mathbf{I})^H\mathrm{vec}(\mathbf{W})\|^2 = \|\mathbf{H}_d^H\mathbf{w}\|^2,\\
\|\mathbf{g}_k^H\mathbf{W}\mathbf{h}_r\|^2 &= |\mathrm{vec}(\mathbf{g}_k\mathbf{h}_r^H)^H\mathrm{vec}(\mathbf{W})|^2 = |\mathbf{t}_k^H\mathbf{w}|^2,\\
\|\mathbf{g}_k^H\mathbf{W}\|^2 &= \|(\mathbf{g}_k\otimes\mathbf{I})^H\mathrm{vec}(\mathbf{W})\|^2 = \|\mathbf{G}_k^H\mathbf{w}\|^2.
\end{aligned} \tag{4.10}$$

According to the transformation in (4.10), problem (4.9) can be equivalently expressed as

$$\min_{\mathbf{w},\rho_1,\rho_2} \ \mathbf{w}^H\bar{\Phi}\mathbf{w} \tag{4.11a}$$

$$s.t. \quad \log\left(1+\frac{P_s\mathbf{w}^H\mathbf{F}\mathbf{w}}{\sigma_r^2\mathbf{w}^H\bar{\mathbf{H}}_d\mathbf{w}+\sigma_D^2+\rho_1\sigma_P^2}\right)-\max_k \log\left(1+\frac{P_s\mathbf{w}^H\mathbf{T}_k\mathbf{w}}{\sigma_r^2\mathbf{w}^H\bar{\mathbf{G}}_k\mathbf{w}+\sigma_k^2+\sigma_P^2}\right)\geq 2R, \forall_k, \tag{4.11b}$$

$$P_s\mathbf{w}^H\mathbf{F}\mathbf{w}+\sigma_r^2\mathbf{w}^H\bar{\mathbf{H}}_d\mathbf{w}+\sigma_D^2 \geq \frac{\rho_2\eta}{\xi}, \tag{4.11c}$$

$$\rho_1\geq 1, \rho_2\geq 1, \frac{1}{\rho_1}+\frac{1}{\rho_2}\leq 1, \tag{4.11d}$$

in which $\mathbf{F}=\mathbf{f}\mathbf{f}^H$, $\bar{\mathbf{H}}_d=\mathbf{H}_d\mathbf{H}_d^H$, $\mathbf{T}_k=\mathbf{t}_k\mathbf{t}_k^H$, $\bar{\mathbf{G}}_k=\mathbf{G}_k\mathbf{G}_k^H$, $\bar{\Phi}=\Phi\Phi^H$, and $\Phi=(\mathbf{I}_{N_t}\otimes\Theta)^{1/2}$ with $\Theta=P_s\mathbf{h}_r\mathbf{h}_r^H+\sigma_r^2\mathbf{I}_{N_t}$; the PS ratio is replaced with two variables $\rho_1\geq\frac{1}{\rho}$ and $\rho_2\geq\frac{1}{1-\rho}$. In the following parts, the non-convex problem (4.11) is solved by two methods, i.e. 1) 1-D line search method, 2) low-complexity SPCA method.

4.3.2 One-Dimensional Line Search Method

By introducing a slack variable β, the PM problem (4.11) can be rewritten as

$$\min_{\mathbf{w},\rho_1,\rho_2} \mathbf{w}^H \bar{\Phi} \mathbf{w} \tag{4.12a}$$

$$s.t. \quad \log\left(1+\frac{P_s \mathbf{w}^H \mathbf{F} \mathbf{w}}{\sigma_r^2 \mathbf{w}^H \bar{\mathbf{H}}_d \mathbf{w} + \sigma_D^2 + \rho_1 \sigma_P^2}\right) + \log(\beta) \geq 2R, \tag{4.12b}$$

$$\log\left(1+\frac{P_s \mathbf{w}^H \mathbf{T}_k \mathbf{w}}{\sigma_r^2 \mathbf{w}^H \bar{\mathbf{G}}_k \mathbf{w} + \sigma_k^2 + \sigma_P^2}\right) \leq \log\left(\frac{1}{\beta}\right), \forall_k, \tag{4.12c}$$

$$P_s \mathbf{w}^H \mathbf{F} \mathbf{w} + \sigma_r^2 \mathbf{w}^H \bar{\mathbf{H}}_d \mathbf{w} + \sigma_D^2 \geq \frac{\rho_2 \eta}{\xi}, \tag{4.12d}$$

$$\rho_1 \geq 1, \rho_2 \geq 1, \frac{1}{\rho_1} + \frac{1}{\rho_2} \leq 1. \tag{4.12e}$$

Note that $\log(\beta)$ can be considered as the maximal allowable data rate of eavesdroppers' link. The secret transmission can be achieved by adjusting β. It obviously shows that problem (4.12) is non-convex due to the quadratic term and coupled variables. The original problem (4.12) can be reformulated as a two-level optimization problem. More specifically, in the inner level, problem (4.12) can be converted into a standard quadratic problem w.r.t. $\mathbf{Q}$ and ρ for a given β [101]. In the outer level, problem (4.12) can be considered as a single-variable optimization problem respect to β. Clearly, the inner quadratic problem can be relaxed to the

following standard SDP problem by defining $\mathbf{Q} = \mathbf{w}\mathbf{w}^H$:

$$
\begin{aligned}
f(\beta) = \min_{\mathbf{Q},\rho_1,\rho_2} \quad & \mathrm{Tr}(\bar{\Phi}\mathbf{Q}) && \text{(4.13a)}\\
s.t. \quad & \log\left(1+\frac{P_s\mathrm{Tr}(\mathbf{F}\mathbf{Q})}{\sigma_r^2\mathrm{Tr}(\bar{\mathbf{H}}_d\mathbf{Q})+\sigma_D^2+\rho_1\sigma_P^2}\right)+\log(\beta)\geq 2R, && \text{(4.13b)}\\
& \log\left(1+\frac{P_s\mathrm{Tr}(\mathbf{T}_k\mathbf{Q})}{\sigma_r^2\mathrm{Tr}(\bar{\mathbf{G}}_k\mathbf{Q})+\sigma_k^2+\sigma_P^2}\right)\leq\log\left(\frac{1}{\beta}\right),\forall_k, && \text{(4.13c)}\\
& P_s\mathrm{Tr}(\mathbf{F}\mathbf{Q})+\sigma_r^2\mathrm{Tr}(\bar{\mathbf{H}}_d\mathbf{Q})+\sigma_D^2\geq\frac{\rho_2\eta}{\xi}, && \text{(4.13d)}\\
& \mathbf{Q}\succeq\mathbf{0},\mathrm{rank}(\mathbf{Q})=1,\text{(4.11d)}, && \text{(4.13e)}\\
& \mathrm{rank}(\mathbf{Q})=1, && \text{(4.13f)}
\end{aligned}
$$

where $f(\beta)$ represents the optimal value of problem (4.13). SDP problem (4.13) is still not easily to solve due to the rank constraint of matrix $\mathbf{Q}$ (4.13f). By deleting the rank constraint, problem (4.13) can be expressed as:

$$
\begin{aligned}
f(\beta) = \min_{\mathbf{Q},\rho_1,\rho_2} \quad & \mathrm{Tr}(\bar{\Phi}\mathbf{Q})\\
s.t. \quad & \text{(4.13b)}-\text{(4.13e)}. && \text{(4.14)}
\end{aligned}
$$

It verifies that problem (4.14) is convex and can be efficiently solved by available solvers such as CVX [105]. Then, the single variable β can be optimized by solving the following outer level problem

$$
\begin{aligned}
\min_{\beta} \quad & f(\beta)\\
s.t. \quad & \beta_{min}\leq\beta\leq\beta_{max}, && \text{(4.15)}
\end{aligned}
$$

where β_{max} and β_{min} are the upper and lower bound of β, respectively. According to the characteristic of Shannon capacity, the upper bound β_{max} is set to equal to one. In addition, the lower bound of β can be expressed by the following inequality based on the character of

the non-negative secrecy rate

$$\beta \geq \left(1+\frac{P_s \mathbf{w}^H \mathbf{F} \mathbf{w}}{\sigma_r^2 \mathbf{w}^H \bar{\mathbf{H}}_d^H \mathbf{w}+\sigma_D^2+\sigma_P^2}\right)^{-1} \geq e^{2R}\lambda_{min}\left((\mathbf{A}+\mathbf{B})^{-1}\mathbf{B}\right), \tag{4.16}$$

where $\mathbf{A}=\frac{P_s}{\sigma_D^2+\sigma_P^2}\mathbf{F}$ and $\mathbf{B}=\frac{\sigma_r^2}{\sigma_D^2+\sigma_P^2}\bar{\mathbf{H}}_d$. The optimal solution of (4.15) can be found by using 1-D line search.

Notice that the optimal solutions to (4.14) is obtained by dropping the rank-one constraint. Assume that $\mathbf{Q}^*$ is the optimal solution to SDP problem (4.14). If $\mathbf{Q}^*$ is rank-one, then the optimal vector $\mathbf{w}^*$ to problem (4.11) can be obtained from EVD of $\mathbf{Q}^*$; otherwise, randomization method, which generates a near-optimal solution to the problem, can be used to find a suitable solution [108]. However, randomization method results in high computational complexity. In this work, an alternative reduction method is employed to obtain the optimal solution if the rank-one constraint cannot be satisfied [111]. It defines that $\Lambda=\frac{\beta P_s}{2R-\beta}\mathbf{F}-\sigma_r^2\bar{\mathbf{H}}_d$, $\varpi_k=\frac{\beta P_s}{1-\beta}\mathbf{T}_k-\sigma_r^2\bar{\mathbf{G}}_k$ and $\Theta=P_s\mathbf{F}-\sigma_r^2\bar{\mathbf{H}}_d$.

Theorem 2. *If the matrix* $\mathbf{Q}^*$ *obtained from* (4.14) *has a rank higher than one, the rank of* $\mathbf{Q}^*$ *can be reduced to one via the following procedure.*

1. ***Repeat***

   (a) *Decompose* $\mathbf{Q}^*$ *as* $\mathbf{Q}^*=\mathbf{U}\mathbf{U}^H$ *with* $\mathbf{U}\in\mathbb{C}^{M^2\times x}$*, in which x is the rank of* $\mathbf{Q}^*$.

   (b) *Find a non-zero* $x\times x$ *Hermitian matrix* $\mathbf{A}$ *to satisfy the following linear equations:* $\mathrm{Tr}(\mathbf{U}^H\Lambda\mathbf{U}\mathbf{A})=0$, $\mathrm{Tr}(\mathbf{U}^H\varpi_k\mathbf{U}\mathbf{A})=0$ *and* $\mathrm{Tr}(\mathbf{U}^H\Theta\mathbf{U}\mathbf{A})=0$.

   (c) *Evaluate all eigenvalues of matrix* $\mathbf{A}$ *and find the maximum eigenvalue* λ_{max}.

   (d) *Update* $\mathbf{Q}^*=\mathbf{Q}^{'}$ *with* $\mathbf{Q}^{'}=\mathbf{U}(\mathbf{I}_x-\frac{\mathbf{A}}{\lambda_{max}})\mathbf{U}^H$.

2. ***Until*** $\mathrm{rank}(\mathbf{Q}^*)=1$.

Proof. The specific proof of this theorem is provided in [111], a brief explanation is provided here. A nonzero matrix $\mathbf{A}$ is always found to satisfy the linear equations in step b) if the real elements of $\mathbf{A}$ greater than 3, $x^2 > 3$. This means that the rank of the new matrix $\mathbf{Q}^{'}$ not only reduce at least one compared to the original matrix $\mathbf{Q}^{*}$ but also is the feasible point of (4.14). In other words, $\mathbf{Q}^{'}$ is also the optimal solution to (4.14) but with lower rank. Hence, the rank one matrix $\mathbf{Q}^{*}$ can be found by repeating the above procedures. □

4.3.3 Low-Complexity SPCA Algorithm

The methods, 1-D linear search and rank reduction approach, used in the above section to solve problem (4.11) cause high computational complexity. Hence, in this subsection, a low complexity method, which is embedded in the concept of SPCA method, is proposed to solve the PM problem . Problem (4.11) can be transformed into the following equivalent problem by introducing two positive slack variables α and ν:

$$\min_{\mathbf{w},\rho_1,\rho_2,\alpha,\nu} \quad \mathbf{w}^H\bar{\Phi}\mathbf{w} \tag{4.17a}$$

$$s.t \qquad \alpha\nu \geq e^{2R} \tag{4.17b}$$

$$1+\frac{P_s\mathbf{w}^H\mathbf{F}\mathbf{w}}{\sigma_r^2\mathbf{w}^H\bar{\mathbf{H}}_d\mathbf{w}+\sigma_D^2+\rho_1\sigma_P^2} \geq \alpha, \tag{4.17c}$$

$$1+\frac{P_s\mathbf{w}^H\mathbf{T}_k\mathbf{w}}{\sigma_r^2\mathbf{w}^H\bar{\mathbf{G}}_k\mathbf{w}+\sigma_k^2+\sigma_P^2} \leq \frac{1}{\nu}, \forall_k, \tag{4.17d}$$

$$(4.11c), (4.11d). \tag{4.17e}$$

Problem (4.17) is non-convex and cannot be solved directly due to non-convex constraints. Hence, the non-convex constraints in (4.17) can be converted into tractable forms one by one in the sequel. Based on the feature of the bilinear product, the inequality in (4.17b) is

equivalent to

$$4e^{2R} + (\alpha - \nu)^2 \leq (\alpha + \nu)^2. \tag{4.18}$$

Furthermore, the inequality (4.18) can be represented by the following conic quadratic function

$$\left\| \left[2\sqrt{e^2 R} \quad (\alpha - \nu) \right]^T \right\|_2 \leq \alpha + \nu. \tag{4.19}$$

Next, the constraint (4.17c) can be transformed into the following form

$$\sigma_r^2 \mathbf{w}^H \bar{\mathbf{H}}_d \mathbf{w} + \sigma_D^2 + \rho_1 \sigma_P^2 \leq \frac{P_s \mathbf{w}^H \mathbf{F} \mathbf{w}}{\alpha - 1}. \tag{4.20}$$

The above inequality is a non-convex function because of the quadratic term on the left side and quadratic-over-linear term on the right side of the inequality [101]. Hence, the quadratic-over-linear function can be transferred to the linear function by its first order Taylor series around $\mathbf{w}^q$, α^q based on SPCA method [110]. Specifically, it defines

$$\begin{aligned} \frac{P_s \mathbf{w}^H \mathbf{F} \mathbf{w}}{\alpha - 1} &\geq \frac{2P_s \Re\{\mathbf{w}^{qH} \mathbf{F} \mathbf{w}\}}{\alpha^q - 1} - \frac{P_s \mathbf{w}^{qH} \mathbf{F} \mathbf{w}^q}{(\alpha^q - 1)^2}(\alpha - 1) \\ &= f(\mathbf{w}^q, \mathbf{w}, \alpha, \alpha^q). \end{aligned} \tag{4.21}$$

Replacing quadratic-over-linear term by $f(\mathbf{w}^q, \mathbf{w}, \alpha, \alpha^q)$, the overall approximation of the constraint in (4.20) reads as

$$\sigma_r^2 \mathbf{w}^H \bar{\mathbf{H}}_d \mathbf{w} + \sigma_D^2 + \rho_1 \sigma_P^2 \leq f(\mathbf{w}^q, \mathbf{w}, \alpha, \alpha^q). \tag{4.22}$$

Similarly, the constraint (4.17d) can be converted into the following convex form by replacing the quadratic-over-line function with its Taylor expansion

$$\mathbf{w}^H(P_s\mathbf{T}_k+\sigma_r^2\bar{\mathbf{G}}_k)\mathbf{w}+\sigma_k^2+\sigma_P^2\leq g(\mathbf{w}^q,\mathbf{w},\nu,\nu^q), \tag{4.23}$$

where $g(\mathbf{w}^q,\mathbf{w},\nu,\nu^q)=\frac{2\sigma_r^2\Re\{\mathbf{w}^{qH}\bar{\mathbf{G}}_k\mathbf{w}\}}{\nu^q}-\frac{\nu\sigma_r^2\mathbf{w}^{qH}\bar{\mathbf{G}}_k\mathbf{w}^q}{\nu^{q2}}$. Denoting $\varsigma=f(\mathbf{w}^q,\mathbf{w},\alpha,\alpha^q)-\sigma_D^2-\rho_1\sigma_P^2$ and $\vartheta_k=g(\mathbf{w}^q,\mathbf{w},\nu,\nu^q)-\sigma_k^2$, (4.22) and (4.23) can be transferred to the following second-order cone (SOC) constraints [112]

$$\|[2\sigma_r\mathrm{vec}(\mathbf{w}^H\mathbf{H}_d),\varsigma-1]^T\|\leq\varsigma+1, \tag{4.24}$$

$$\|[2\sqrt{P_s}\mathbf{w}^H\mathbf{t}_k,2\sigma_r\mathrm{vec}(\mathbf{w}^H\mathbf{G}_k),\vartheta_k-1]^T\|\leq\vartheta_k+1,\forall_k. \tag{4.25}$$

The constraint (4.11c) is non-convex due to the quadratic terms on the left side of the inequality. Based on the above approximation, this constraint can be converted into the linear function by using SPCA method. By defining $\mathbf{w}=\mathbf{w}^q+\Delta\mathbf{w}$ and substituting it into the quadratic terms, it obtains

$$\begin{aligned}
&P_s\mathbf{w}^H\mathbf{F}\mathbf{w}+\sigma_r^2\mathbf{w}^H\bar{\mathbf{H}}_d\mathbf{w}\\
&=(\mathbf{w}^q+\Delta\mathbf{w})^H(P_s\mathbf{F}+\sigma_r^2\bar{\mathbf{H}}_d)(\mathbf{w}^q+\Delta\mathbf{w})\\
&\geq\mathbf{w}^{qH}(P_s\mathbf{F}+\sigma_r^2\bar{\mathbf{H}}_d)\mathbf{w}^q+2\Re\{\mathbf{w}^{qH}(P_s\mathbf{F}+\sigma_r^2\bar{\mathbf{H}}_d)\Delta\mathbf{w}\},
\end{aligned} \tag{4.26}$$

where $\Delta\mathbf{w}$ denotes the difference between $\mathbf{w}$ and $\mathbf{w}^q$. Note that the inequality is given by ignoring the quadratic terms $\Delta\mathbf{w}^H(P_s\mathbf{F}+\sigma_r^2\bar{\mathbf{H}}_d)\Delta\mathbf{w}$. Then, the non-convex constraint (4.11c) can be reformulated by its convex form

$$\mathbf{w}^{qH}(P_s\mathbf{F}+\sigma_r^2\bar{\mathbf{H}}_d)\mathbf{w}^q+2\Re\{\mathbf{w}^{qH}(P_s\mathbf{F}+\sigma_r^2\bar{\mathbf{H}}_d)\Delta\mathbf{w}\}\geq\frac{\rho_2\eta}{\xi}-\sigma_D^2. \tag{4.27}$$

Algorithm 4.1: Proposed iterative algorithm to solve (4.28)

1. **Initialize**: randomly generated $\mathbf{w}^q$, α^q and v^q feasible to (4.28), set $q = 0$.
2. **Repeat**
   (a) Solve the problem (4.28) with $\mathbf{w}^q$, α^q and v^q to obtain the optimal solutions $\mathbf{w}^*$, α^* and v^*.
   (b) Update $\mathbf{w}^{q+1} = \mathbf{w}^*$, $\alpha^{q+1} = \alpha^*$ and $v^{q+1} = v^*$.
   (c) Set q = q+1.
3. **Until** Convergence or required number of iterations.

Using the above equivalent transformations and approximations, problem (4.11) can be rewritten as the following SOCP problem

$$\begin{aligned} \min_{\mathbf{w},\rho_1,\rho_2,\alpha,v,z} \quad & z \\ s.t. \quad & \left\| \left[2\mathbf{w}^H \bar{\Phi}^{\frac{1}{2}} \quad z-1 \right]^T \right\| \leq z+1 \\ & (4.19),(4.24),(4.25),(4.27),\Delta\mathbf{w} = \mathbf{w} - \mathbf{w}^q \\ & \alpha \geq 1, 0 \leq v \leq 1, z \geq 0, (4.11\text{d}). \end{aligned} \tag{4.28}$$

For a given $\mathbf{w}^q$, α^q and v^q, problem (4.28) is convex and can be directly addressed by the software tools such as CVX [105]. The iterative algorithm to solve the problem (4.28) is summarized in Algorithm 4.1. The optimal solutions can be iteratively updated through Algorithm 4.1. The convergence analysis of the proposed iterative algorithm is provided in the following. It assumes that $\mathbf{w}^q$, α^q, v^q and f^q are the optimal solutions and optimal value to problem (4.28) in the qth iteration of Algorithm 4.1, respectively. Thus, $\mathbf{w}^q$, α^q and v^q satisfy all constraints in (4.28). This means that $\mathbf{w}^q$, α^q and v^q are the feasible solutions to (4.28) in the $q+1$st iteration due to the iteratively updated optimal solutions. The optimal value f^{q+1} can be obtained in the $q+1$st iteration based on the optimal solutions $\mathbf{w}^q$, α^q and v^q. Thus, it holds that $f^{q+1} \leq f^q$. That is to say, Algorithm 4.1 generates a non-increasing sequence of objective values. Hence, Algorithm 4.1 converges to some local optimum solution of (4.11).

4.4 Problem Design Based on Imperfect CSI

In the previous section, the PM problem is proposed based on the assumption that CSI of the relay and the desired receiver as well as the idle receivers is perfectly known by the transmitter and the relay, respectively. In order to improve the secure communication, it is still assumed that CSI between the transmitter and the relay is perfectly known by the transmitter. Perfect CSI of all receivers is not always practical to be available at the relay due to the channel feedback, which may cause quantization errors and delay error. Therefore, a robust PM problem under the imperfect CSI scenario is proposed. Two efficient algorithms are proposed to solve this robust PM problem.

4.4.1 Channel model and Problem Formulation

The deterministic model for the imperfect CSI case is considered where the true channel lies in an ellipsoid that is centred at the channel mean [113, 114]. The actual channels between the relay and the DR as well as the k-th Eva can be modelled as

$$H_d = \{\mathbf{h}_d | \mathbf{h}_d = \tilde{\mathbf{h}}_d + \Delta\mathbf{h}_d, \Delta\mathbf{h}_d^H \mathbf{C}_d \Delta\mathbf{h}_d \leq 1\}, \tag{4.29a}$$

$$G_k = \{\mathbf{g}_k | \mathbf{g}_k = \tilde{\mathbf{g}}_k + \Delta\mathbf{g}_k, \Delta\mathbf{g}_k^H \mathbf{C}_k \Delta\mathbf{g}_k \leq 1\}, \forall_k, \tag{4.29b}$$

where $\tilde{\mathbf{h}}_d$ and $\tilde{\mathbf{g}}_k$ denote the estimates of the corresponding channels; $\Delta\mathbf{h}_d$ and $\Delta\mathbf{g}_k$ represent the channel errors, which are bounded by ellipsoids; $\mathbf{C}_d \succ \mathbf{0}$ and $\mathbf{C}_k \succ \mathbf{0}$ determine the quality of CSI and are assumed known by transmitter. Without loss of generality, it sets $\mathbf{C}_d = (1/\varepsilon_d)\mathbf{I}$ and $\mathbf{C}_k = (1/\varepsilon_k)\mathbf{I}$, where ε_d and ε_k represent the size of the bounded error region.

Based on the designs of channel uncertainties in (4.29a) and (4.29b), the robust PM problem can be formulated as:

$$\min_{\mathbf{w},\rho} \ \mathbf{w}^H \bar{\Phi} \mathbf{w} \tag{4.30a}$$

$$s.t. \min_{\Delta\mathbf{h}_d,\Delta\mathbf{g}_k,k} \frac{1}{2}\left\{\log\left(1+\frac{\rho P_s \mathbf{w}^H \mathbf{F}\mathbf{w}}{\rho(\sigma_r^2 \mathbf{w}^H \bar{\mathbf{H}}_d \mathbf{w}+\sigma_D^2)+\sigma_P^2}\right)-\log\left(1+\frac{P_s \mathbf{w}^H \mathbf{T}_k \mathbf{w}}{\sigma_r^2 \mathbf{w}^H \bar{\mathbf{G}}_k \mathbf{w}+\sigma_k^2+\sigma_P^2}\right)\right\} \geq R, \forall_k, \tag{4.30b}$$

$$\min_{\Delta\mathbf{h}_d} \quad P_s \mathbf{w}^H \mathbf{F}\mathbf{w}+\sigma_r^2 \mathbf{w}^H \bar{\mathbf{H}}_d \mathbf{w}+\sigma_D^2 \geq \frac{\eta}{\xi(1-\rho)}, \tag{4.30c}$$

$$0 \leq \rho \leq 1, \|\Delta\mathbf{h}_d\|^2 \leq \varepsilon, \|\Delta\mathbf{g}_k\|^2 \leq \varepsilon. \tag{4.30d}$$

Problem (4.30) is harder to solve than the problem proposed in perfect CSI case due to the infinity constraints. However, the two methods proposed in section III still can be employed to deal with the quadratic term and coupled variables. Additional method is considered to solve the infinity constraints.

4.4.2 One-Dimensional Line Search Method

With following similar steps in handling (4.11), I recast problem (4.30) as a two-level optimization problem by introducing a slack variable τ. The outer-level problem is then formulated as

$$\begin{aligned} &\min_{\tau} \ f(\tau) \\ &s.t. \ \tau_{min} \leq \tau \leq 1. \end{aligned} \tag{4.31}$$

The lower bound of τ has defined in (4.16). $f(\tau)$ denotes the optimal value of the following problem after dropping the rank-one constraint

$$f(\tau) = \min_{\mathbf{Q},\rho,\omega,\varsigma} \mathrm{Tr}(\bar{\Phi}\mathbf{Q}) \tag{4.32a}$$

$$s.t. \quad \min_{\Delta\mathbf{h}_d} \ \frac{P_s \mathrm{Tr}(\mathbf{F}\mathbf{Q})}{\sigma_r^2 \mathrm{Tr}(\bar{\mathbf{H}}_d\mathbf{Q}) + \sigma_D^2 + \omega\sigma_P^2} \geq \frac{e^{2R}}{\tau} - 1, \tag{4.32b}$$

$$\max_{\Delta\mathbf{g}_k} \ \frac{P_s \mathrm{Tr}(\mathbf{T}_k\mathbf{Q})}{\sigma_r^2 \mathrm{Tr}(\bar{\mathbf{G}}_k\mathbf{Q}) + \sigma_k^2 + \sigma_P^2} \leq \frac{1}{\tau} - 1, \forall_k, \tag{4.32c}$$

$$\min_{\Delta\mathbf{h}_d} \ P_s \mathrm{Tr}(\mathbf{F}\mathbf{Q}) + \sigma_r^2 \mathrm{Tr}(\bar{\mathbf{H}}_d\mathbf{Q}) + \sigma_D^2 \geq \frac{\varsigma\eta}{\xi}, \tag{4.32d}$$

$$\mathbf{Q} \succeq \mathbf{0}, \mathbf{V} \succeq \mathbf{0}, \frac{1}{\omega} + \frac{1}{\varsigma} \leq 1, \omega \geq 1, \varsigma \geq 1, \tag{4.32e}$$

where $\omega \geq \frac{1}{\rho}$ and $\upsilon \geq \frac{1}{1-\rho}$. Problem (4.32) is still non-convex due to the potentially infinite number of constraints in (4.32b)-(4.32d). Applying the matrix equalities, $\mathrm{vec}(\mathbf{AXB}) = (\mathbf{B}^T \otimes \mathbf{A})\mathrm{vec}(\mathbf{X})$, $\mathrm{Tr}(\mathbf{A}^T\mathbf{B}) = \mathrm{vec}(\mathbf{A})^T\mathrm{vec}(\mathbf{B})$ and $(\mathbf{A}\otimes\mathbf{B})^T = \mathbf{A}^T \otimes \mathbf{B}^T$, it obtains

$$\mathrm{Tr}(\mathbf{F}\mathbf{Q}) = \mathbf{h}_{r,d}^H (\mathbf{I}_{N_t^2} \otimes \mathbf{h}_r)\mathbf{Q}(\mathbf{I}_{N_t^2} \otimes \mathbf{h}_r)^H \mathbf{h}_{r,d}, \tag{4.33a}$$

$$\mathrm{Tr}(\bar{\mathbf{H}}_d\mathbf{Q}) = \mathbf{h}_{r,d}^H (\mathbf{I}_{N_t} \otimes \mathbf{Q})\mathbf{h}_{r,d}, \tag{4.33b}$$

$$\mathrm{Tr}(\mathbf{T}_k\mathbf{Q}) = \mathbf{g}_{r,k}^H (\mathbf{I}_{N_t^2} \otimes \mathbf{h}_r)\mathbf{Q}(\mathbf{I}_{N_t^2} \otimes \mathbf{h}_r)^H \mathbf{g}_{r,k}, \tag{4.33c}$$

$$\mathrm{Tr}(\bar{\mathbf{G}}_k\mathbf{Q}) = \mathbf{g}_{r,k}^H (\mathbf{I}_{N_t} \otimes \mathbf{Q})\mathbf{g}_{r,k}, \tag{4.33d}$$

where $\mathbf{h}_{r,d} = \mathrm{vec}(\mathbf{h}_d \otimes \mathbf{I}_{N_t})$ and $\mathbf{g}_{r,k} = \mathrm{vec}(\mathbf{g}_k \otimes \mathbf{I}_{N_t})$. The actual transformed channel $\mathbf{h}_{r,d}$ and $\mathbf{g}_{r,k}$ can be expressed as $\mathbf{h}_{r,d} = \tilde{\mathbf{h}}_{r,d} + \Delta\mathbf{h}_{r,d}$ and $\mathbf{g}_{r,k} = \tilde{\mathbf{g}}_{r,k} + \Delta\mathbf{g}_{r,k}$, respectively. According to the channel definitions in (4.29), the transformed channel error $\Delta\mathbf{h}_{r,d}$ and $\Delta\mathbf{g}_{r,k}$ can be defined as $\|\Delta\mathbf{h}_{r,d}\|^2 \leq N_t\varepsilon_d$ and $\|\Delta\mathbf{g}_{r,k}\|^2 \leq N_t\varepsilon_k$, respectively. Based on the aforementioned transformations, the constraint (4.32b) can be rewritten as

$$\Delta\mathbf{h}_{r,d}^H \Xi \Delta\mathbf{h}_{r,d} + 2\Re\{\Delta\mathbf{h}_{r,d}^H \Xi \tilde{\mathbf{h}}_{r,d}\} + c_d \geq 0, \tag{4.34}$$

where $\Xi = \frac{\tau P_s}{e^{2R}-\tau}(\mathbf{I}_{N_t^2} \otimes \mathbf{h}_r)\mathbf{Q}(\mathbf{I}_{N_t^2} \otimes \mathbf{h}_r)^H - \sigma_r^2(\mathbf{I}_{N_t} \otimes \mathbf{Q})$ and $c_d = \tilde{\mathbf{h}}_{r,d}^H \Xi \tilde{\mathbf{h}}_{r,d} - \sigma_D^2 - \omega\sigma_P^2$. Considering (4.34) is still an infinite constraint, *S-Procedure* lemma is employed to transform it to a tractable form.

Lemma 3 (*S-Procedure* [101])**.** *Define the function* $f_k(x) = \mathbf{x}^H \mathbf{A}_k \mathbf{x} + 2\Re\{\mathbf{b}_k^H \mathbf{x}\} + c_k$ *for* $k \in \{1,2\}$*, where* $\mathbf{A}_k \in \mathbb{C}^{N\times N}$*,* $\mathbf{b}_k \in \mathbb{C}^{N\times 1}$ *and* $c_k \in \mathbb{R}$*. The implication* $f_1(\mathbf{x}) \geq 0 \Rightarrow f_2(\mathbf{x}) \geq 0$ *holds if and only if there exists* $\mu \geq 0$ *such that*

$$\begin{bmatrix} \mathbf{A}_2 & \mathbf{b}_2 \\ \mathbf{b}_2^H & c_2 \end{bmatrix} - \mu \begin{bmatrix} \mathbf{A}_1 & \mathbf{b}_1 \\ \mathbf{b}_1^H & c_1 \end{bmatrix} \succeq \mathbf{0}, \tag{4.35}$$

provided that there exists a value $\mathbf{x}$ *satisfies* $f_k(\mathbf{x}) \geq 0$*.*

Applying *S-Procedure* lemma to (4.34), if there exists a positive variable λ_d, it obtains

$$\begin{bmatrix} \Xi + \lambda_d \mathbf{I}_{N_t^3} & \Xi\tilde{\mathbf{h}}_{r,d} \\ \tilde{\mathbf{h}}_{r,d}^H \Xi & c_d - \lambda_d N_t \varepsilon_d \end{bmatrix} \succeq \mathbf{0}. \tag{4.36}$$

With (4.33c) and (4.33d), (4.32c) can be rewritten as

$$\Delta\mathbf{g}_{r,k}^H \Pi \Delta\mathbf{g}_{r,k} + 2\Re\{\Delta\mathbf{g}_{r,k}^H \Pi \tilde{\mathbf{g}}_{r,k}\} + c_k \geq 0, \tag{4.37}$$

where $\Pi = \sigma_r^2(\mathbf{I}_{N_t} \otimes \mathbf{Q}) - \frac{\tau P_s}{1-\tau}(\mathbf{I}_{N_t^2} \otimes \mathbf{h}_r)\mathbf{Q}(\mathbf{I}_{N_t^2} \otimes \mathbf{h}_r)^H$ and $c_k = \tilde{\mathbf{g}}_{r,k}^H \Pi \tilde{\mathbf{g}}_{r,k} + \sigma_k^2 + \sigma_P^2$. Based on Lemma 1, there always exist positive variables λ_k such that (4.37) can be converted into the following tractable LMI constraint

$$\begin{bmatrix} \Pi + \lambda_k \mathbf{I}_{N_t^3} & \Pi\tilde{\mathbf{g}}_{r,k} \\ \tilde{\mathbf{g}}_{r,k}^H \Pi & c_k - \lambda_k N_t \varepsilon_k \end{bmatrix} \succeq \mathbf{0}. \tag{4.38}$$

At last, following the similar steps, the harvested energy constraint (4.32d) can be transformed into the following LMI by applying Lemma 3

$$\begin{bmatrix} \Psi+\varphi\mathbf{I}_{N_t^3} & \Psi\tilde{\mathbf{h}}_{r,d} \\ \tilde{\mathbf{h}}_{r,d}^H\Psi & \vartheta-\varphi N_t\varepsilon_d \end{bmatrix} \succeq \mathbf{0}, \tag{4.39}$$

where $\Psi = P_s(\mathbf{I}_{N_t^2}\otimes\mathbf{h}_r)\mathbf{Q}(\mathbf{I}_{N_t^2}\otimes\mathbf{h}_r)^H+\sigma_r^2(\mathbf{I}_{N_t}\otimes\mathbf{Q})$ and $\vartheta = \tilde{\mathbf{h}}_{r,d}^H\Psi\tilde{\mathbf{h}}_{r,d}+\sigma_D^2-\varsigma x$.

According to (4.36)-(4.39), the robust PM problem (4.32) is now simplified as

$$\begin{aligned} f(\tau) = \min_{\mathbf{Q},\lambda_d,\lambda_k,\varphi,\omega,\varsigma} \ & \mathrm{Tr}(\bar{\Phi}\mathbf{Q}) \\ s.t. \quad & (4.36),(4.38),(4.39),(4.32e). \end{aligned} \tag{4.40}$$

The above problem (4.40) is convex and can be solved by CVX [105] with given τ. Then, the optimal value $f(\tau)$ can be found by using one-dimensional line search w.r.t. τ. The rank of matrix $\mathbf{Q}$ can be reduced to one by using the rank reduction theorem proposed in the above section.

4.4.3 Low-Complexity SPCA Algorithm

In this subsection, a low-complexity iterative algorithm is proposed based on the SPCA method to deal with the robust PM problem (3.14). First, the robust secrecy rate (3.14b) can be rewritten as

$$\frac{1}{2}\log(r_1 r_2) \geq R, \tag{4.41a}$$

$$1+\frac{\rho P_s\mathbf{w}^H\mathbf{F}\mathbf{w}}{\rho(\sigma_r^2\mathbf{w}^H\bar{\mathbf{H}}_d\mathbf{w}+\sigma_D^2)+\sigma_P^2} \geq r_1, \tag{4.41b}$$

$$1+\frac{P_s\mathbf{w}^H\mathbf{T}_k\mathbf{w}}{\sigma_r^2\mathbf{w}^H\bar{\mathbf{G}}_k\mathbf{w}+\sigma_k^2+\sigma_P^2} \leq \frac{1}{r_2}, \tag{4.41c}$$

where $r_1 \geq 1$ and $r_2 \leq 1$ denote the slack variables. The constraint (4.41a) is equivalent to

$$4e^{2R} + (r_1 - r_2)^2 \leq (r_1 + r_2)^2. \tag{4.42}$$

Based on the concept of the SOC representation [112], inequality (4.42) can be converted into its conic representable function

$$\left\| \begin{bmatrix} 2e^R & (r_1 - r_2) \end{bmatrix}^T \right\|_2 \leq r_1 + r_2. \tag{4.43}$$

In order to implement SPCA algorithm, I derive the actual combinative channels $\mathbf{F}$, $\bar{\mathbf{H}}_d$, $\tilde{\mathbf{H}}_d$, $\mathbf{T}_k$, $\bar{\mathbf{G}}_k$, $\tilde{\mathbf{G}}_k$ and their corresponding errors $\Delta\mathbf{F}$, $\Delta\bar{\mathbf{H}}_d$, $\Delta\mathbf{T}_k$, $\Delta\bar{\mathbf{G}}_k$as follows:

$$\begin{aligned}\mathbf{F} = &\operatorname{vec}(\tilde{\mathbf{h}}_d\mathbf{h}_r^H)\operatorname{vec}(\tilde{\mathbf{h}}_d\mathbf{h}_r^H)^H + \operatorname{vec}(\tilde{\mathbf{h}}_d\mathbf{h}_r^H)\operatorname{vec}(\Delta\mathbf{h}_d\mathbf{h}_r^H)^H \\ &+ \operatorname{vec}(\Delta\mathbf{h}_d\mathbf{h}_r^H)\operatorname{vec}(\tilde{\mathbf{h}}_d\mathbf{h}_r^H)^H + \operatorname{vec}(\Delta\mathbf{h}_d\mathbf{h}_r^H)\operatorname{vec}(\Delta\mathbf{h}_d\mathbf{h}_r^H)^H,\end{aligned} \tag{4.44a}$$

$$\bar{\mathbf{H}}_d = (\mathbf{I}\otimes\tilde{\mathbf{h}}_d)(\mathbf{I}\otimes\tilde{\mathbf{h}}_d)^H + (\mathbf{I}\otimes\tilde{\mathbf{h}}_d)(\mathbf{I}\otimes\Delta\mathbf{h}_d)^H + (\mathbf{I}\otimes\Delta\mathbf{h}_d)(\mathbf{I}\otimes\tilde{\mathbf{h}}_d)^H + (\mathbf{I}\otimes\Delta\mathbf{h}_d)(\mathbf{I}\otimes\Delta\mathbf{h}_d)^H, \tag{4.44b}$$

$$\begin{aligned}\mathbf{T}_k = &\operatorname{vec}(\tilde{\mathbf{g}}_k\mathbf{h}_r^H)\operatorname{vec}(\tilde{\mathbf{g}}_k\mathbf{h}_r^H)^H + \operatorname{vec}(\tilde{\mathbf{g}}_k\mathbf{h}_r^H)\operatorname{vec}(\Delta\mathbf{g}_k\mathbf{h}_r^H)^H \\ &+ \operatorname{vec}(\Delta\mathbf{g}_k\mathbf{h}_r^H)\operatorname{vec}(\tilde{\mathbf{g}}_k\mathbf{h}_r^H)^H + \operatorname{vec}(\Delta\mathbf{g}_k\mathbf{h}_r^H)\operatorname{vec}(\Delta\mathbf{g}_k\mathbf{h}_r^H)^H,\end{aligned} \tag{4.44c}$$

$$\bar{\mathbf{G}}_k = (\mathbf{I}\otimes\tilde{\mathbf{g}}_k)(\mathbf{I}\otimes\tilde{\mathbf{g}}_k)^H + (\mathbf{I}\otimes\tilde{\mathbf{g}}_k)(\mathbf{I}\otimes\Delta\mathbf{g}_k)^H + (\mathbf{I}\otimes\Delta\mathbf{g}_k)(\mathbf{I}\otimes\tilde{\mathbf{g}}_k)^H + (\mathbf{I}\otimes\Delta\mathbf{g}_k)(\mathbf{I}\otimes\Delta\mathbf{g}_k)^H, \tag{4.44d}$$

where $\tilde{\mathbf{F}} = \operatorname{vec}(\tilde{\mathbf{h}}_d\mathbf{h}_r^H)\operatorname{vec}(\tilde{\mathbf{h}}_d\mathbf{h}_r^H)^H$; $\tilde{\bar{\mathbf{H}}}_d = (\mathbf{I}\otimes\tilde{\mathbf{h}}_d)(\mathbf{I}\otimes\tilde{\mathbf{h}}_d)^H$; $\tilde{\mathbf{T}}_k = \operatorname{vec}(\tilde{\mathbf{g}}_k\mathbf{h}_r^H)\operatorname{vec}(\tilde{\mathbf{g}}_k\mathbf{h}_r^H)^H$; $\tilde{\bar{\mathbf{G}}}_k = (\mathbf{I}\otimes\tilde{\mathbf{g}}_k)(\mathbf{I}\otimes\tilde{\mathbf{g}}_k)^H$. Note that the remaining components, except $\tilde{\mathbf{F}}$, $\tilde{\bar{\mathbf{H}}}_d$, $\tilde{\mathbf{T}}_k$ and $\tilde{\bar{\mathbf{G}}}_k$ denote their corresponding error parts in (4.44a)-(4.44d). The error regions can be expressed

as

$$\|\Delta\mathbf{F}\|_F \leq (\varepsilon_d + 2\sqrt{\varepsilon_d}\|\tilde{\mathbf{h}}_d\|)\|\mathbf{h}_r\|^2 = \varepsilon_F, \tag{4.45a}$$

$$\|\Delta\bar{\mathbf{H}}_d\|_F \leq (\varepsilon_d + 2\sqrt{\varepsilon_d}\|\tilde{\mathbf{h}}_d\|)N_t = \varepsilon_{\bar{H}_d}, \tag{4.45b}$$

$$\|\Delta\mathbf{T}_k\|_F \leq (\varepsilon_k + 2\sqrt{\varepsilon_k}\|\tilde{\mathbf{g}}_k\|)\|\mathbf{h}_r\|^2 = \varepsilon_{T_k} \tag{4.45c}$$

$$\|\Delta\bar{\mathbf{G}}_k\|_F \leq (\varepsilon_k + 2\sqrt{\varepsilon_k}\|\tilde{\mathbf{g}}_k\|)N_t = \varepsilon_{\bar{G}_k}. \tag{4.45d}$$

According to the channel uncertainties, the constraint (4.41b) can be represented as

$$\max_{\|\Delta\bar{\mathbf{H}}_d\|_F, \|\Delta\bar{\mathbf{H}}_d\|_F} \sigma_r^2\mathbf{w}^H\mathbf{A}_{\bar{H}_d}\mathbf{w} + \sigma_D^2 + \frac{\sigma_P^2}{\rho} \leq \min_{\|\Delta\mathbf{F}\|_F} \frac{P_s\mathbf{w}^H\mathbf{A}_F\mathbf{w}}{r_1 - 1}. \tag{4.46}$$

where $\mathbf{A}_{\bar{H}_d} = \tilde{\bar{\mathbf{H}}}_d + \Delta\bar{\mathbf{H}}_d$ and $\mathbf{A}_F = \tilde{\mathbf{F}} + \Delta\mathbf{F}$. The RHS and the LHS of (4.46) can be approximated by a loose approximation method proposed in [115]

$$\begin{aligned} &\text{LHS} : \sigma_r^2\mathbf{w}^H\mathbf{A}_{\bar{H}_d}\mathbf{w} + \sigma_D^2 + \frac{\sigma_P^2}{\rho} \leq \sigma_r^2\mathbf{w}^H\mathbf{B}_{\bar{H}_d}\mathbf{w} + \sigma_D^2 + \frac{\sigma_P^2}{\rho}, \\ &\text{RHS} : \frac{P_s\mathbf{w}^H\mathbf{A}_F\mathbf{w}}{r_1 - 1} \geq \frac{P_s\mathbf{w}^H\mathbf{B}_F\mathbf{w}}{r_1 - 1}, \end{aligned} \tag{4.47}$$

where $\mathbf{B}_{\bar{H}_d} = \tilde{\bar{\mathbf{H}}}_d + \varepsilon_{\bar{H}_d}\mathbf{I}_{N_t^2}$ and $\mathbf{B}_F = \tilde{\mathbf{F}} - \varepsilon_F\mathbf{I}_{N_t^2}$. Based on the above approximation, (4.46) can be transformed to

$$\sigma_r^2\mathbf{w}^H\mathbf{B}_{\bar{H}_d}\mathbf{w} + \sigma_D^2 + \frac{\sigma_P^2}{\rho} \leq \frac{P_s\mathbf{w}^H\mathbf{B}_F\mathbf{w}}{r_1 - 1}. \tag{4.48}$$

Although all functions are convex on both sides of (4.48), it is still not a convex constraint. Hence, the method in (4.21) is adopted to convert (4.48) to a convex form

$$\sigma_r^2\mathbf{w}^H\mathbf{B}_{\bar{H}_d}\mathbf{w} + \sigma_D^2 + \frac{\sigma_P^2}{\rho} \leq f(\mathbf{w}, \mathbf{w}^q, r_1, r_1^q), \tag{4.49}$$

where $f(\mathbf{w},\mathbf{w}^q,r_1,r_1^q)=\frac{2P_s\Re\{\mathbf{w}^{qH}\mathbf{B}_F\mathbf{w}\}}{r_1^q-1}-\frac{P_s\mathbf{w}^{qH}\mathbf{B}_F\mathbf{w}^q}{(r_1^q-1)^2}(r_1-1)$. According to (4.45c)-(4.45d) and the first Taylor approximation, (4.41c) can be rewritten as

$$\mathbf{w}^H(P_s\mathbf{B}_{T_k}+\sigma_r^2\mathbf{B}_{\bar{G}_k})\mathbf{w}+\sigma_k^2+\sigma_P^2\leq g(\mathbf{w}^q,\mathbf{w},r_2,r_2^q), \tag{4.50}$$

where $\mathbf{B}_{T_k}=\tilde{\mathbf{T}}_k+\varepsilon_{T_k}\mathbf{I}_{N_t^2}$, $\mathbf{B}_{\bar{G}_k}=\tilde{\bar{\mathbf{G}}}_k+\varepsilon_{\bar{G}_k}\mathbf{I}_{N_t^2}$, $g(\mathbf{w}^q,\mathbf{w},r_2,r_2^q)=\frac{2\sigma_r^2\Re\{\mathbf{w}^{qH}\mathbf{D}_{\bar{G}_k}\mathbf{w}\}}{r_2^q}-\frac{r_2\sigma_r^2\mathbf{w}^{qH}\mathbf{D}_{\bar{G}_k}\mathbf{w}^q}{r_2^{q2}}$ with $\mathbf{D}_{\bar{G}_k}=\tilde{\bar{\mathbf{G}}}_k-\varepsilon_{\bar{G}_k}\mathbf{I}_{N_t^2}$. Next, the transmit power constraint (3.14c) can be rewritten as follows based on the channel model in (4.44a) and (4.44b)

$$\min_{\|\Delta\mathbf{h}_d\|} P_s\mathbf{w}^H(\tilde{\mathbf{F}}+\Delta\mathbf{F})\mathbf{w}+\sigma_r^2\mathbf{w}^H(\tilde{\bar{\mathbf{H}}}_d+\Delta\bar{\mathbf{H}}_d)\mathbf{w}+\sigma_D^2\geq\frac{\eta}{\xi(1-\rho)}. \tag{4.51}$$

By exploiting a loose approximation approach for the above constraint, it obtains

$$P_s\mathbf{w}^H\mathbf{B}_F\mathbf{w}+\sigma_r^2\mathbf{w}^H\mathbf{C}_{\bar{H}_d}\mathbf{w}+\sigma_D^2\geq\frac{\eta}{\xi(1-\rho)}, \tag{4.52}$$

where $\mathbf{C}_{\bar{H}_d}=\tilde{\bar{\mathbf{H}}}_d-\varepsilon_{\bar{H}_d}\mathbf{I}_{N_t^2}$. Then, (4.52) can be approximated to the following convex form by using SPCA technique with substituting $\mathbf{w}=\mathbf{w}^q+\Delta\mathbf{w}$

$$\mathbf{w}^{qH}(P_s\mathbf{B}_F+\sigma_r^2\mathbf{C}_{\bar{H}_d})\mathbf{w}^q+2\Re\{\mathbf{w}^{qH}(P_s\mathbf{B}_F+\sigma_r^2\mathbf{C}_{\bar{H}_d})\Delta\mathbf{w}\}+\sigma_D^2\geq\frac{\eta}{\xi(1-\rho)}. \tag{4.53}$$

Finally, the robust power minimization problem can be reformulated as follows by applying SPCA approach

$$\begin{aligned}
&\min_{\mathbf{w},\mathbf{v},\rho,s,r_1,r_2} \quad s \\
&s.t. \quad \left\| \begin{bmatrix} \mathrm{vec}(\mathbf{w}^H \bar{\Phi}^{\frac{1}{2}}) \\ \mathbf{v} \end{bmatrix} \right\|_2 \leq s, \\
&\quad (4.43), (4.49), (4.50), (4.53), \Delta\mathbf{w} = \mathbf{w} - \mathbf{w}^q \\
&\quad r_1 \geq 1, 0 \leq r_2 \leq 1, s \geq 0, 0 \leq \rho \leq 1. \qquad (4.54)
\end{aligned}$$

For a given $\mathbf{w}^q$, r_1^q and r_2^q, problem (4.54) can be efficiently solved by available solver, i.e. CVX [105]. The initial values of each iteration can be updated by the previous iterative optimal values. Problem (4.54) can be iteratively solved based on the algorithm in Algorithm 4.1.

4.5 Numerical Results

In this section, numerical results are provided to validate the performance of the proposed algorithms. It is assuming that all channels in the cooperative network are randomly generated following an independent and identically distributed (i.i.d) complex Gaussian distribution $\mathrm{CN}(0, 10^{-2})$. Specifically, the number of antenna at the relay is set to $M = 5$ and the number of eavesdroppers with $K = 3$. The noise variances is set to the same value $\sigma_r^2 = \sigma_d^2 = \sigma_D^2 = \sigma_P^2 = \sigma^2 = -50$ dBm, the transmit power at the transmitter is $P_s = 30$ dBm, energy conversion efficiency is $\xi = 0.8$ and the error bound is $\varepsilon_d = \varepsilon_k = \varepsilon$. The performance of the proposed algorithms are evaluated by averaging over 300 randomly generated channel realizations.

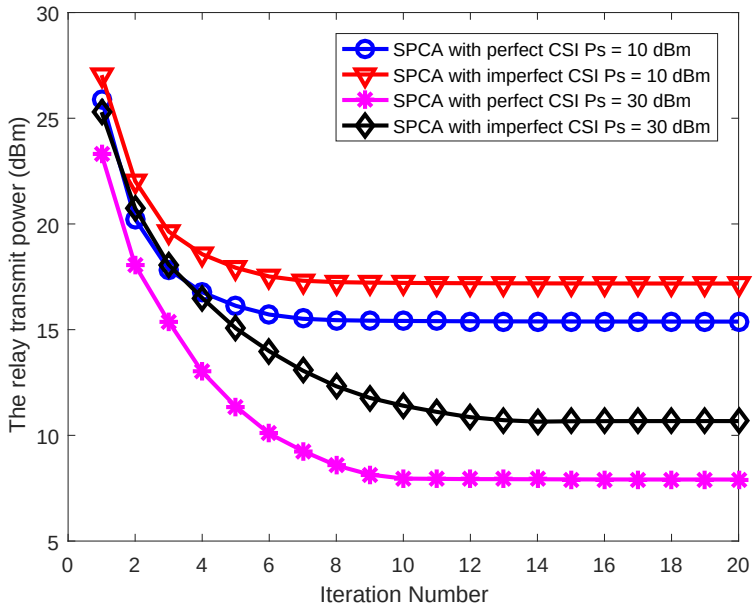

Fig. 4.2 The relay transmit power w.r.t. iteration numbers for the SPCA algorithm with various Ps. Set $R = 1.5$ bps/Hz, $\varepsilon = 0.01$ and $\eta = -5$ dBm.

Figure 4.2 illustrates the convergence performance of the proposed SPCA for perfect CSI and imperfect CSI cases with respect to iteration numbers. It obviously shows that all curves have converged after several iterations, and the proposed SPCA algorithm converges faster when the transmitter provides smaller power. In addition, the relay needs consume more power to support information transmission when the transmit power Ps becomes small. This is due to the fact that the relay needs additional power to overcome the negative effects, such as path loss and shadowing, if the transmitter cannot provide sufficient energy for information transmission.

Figure 4.3 depicts the relay transmit power required by various algorithms versus the target secrecy rate R. From the results, it can be seen that the transmit power consumption at the relay for all considered schemes increases with the growth of the secrecy rate R. In addition, the performance of the iterative algorithm based on the SPCA method closes to that of the 1-D search algorithm in both channel cases. The more interesting is that the performance gap between two algorithms in the perfect CSI case is smaller than that of in the imperfect

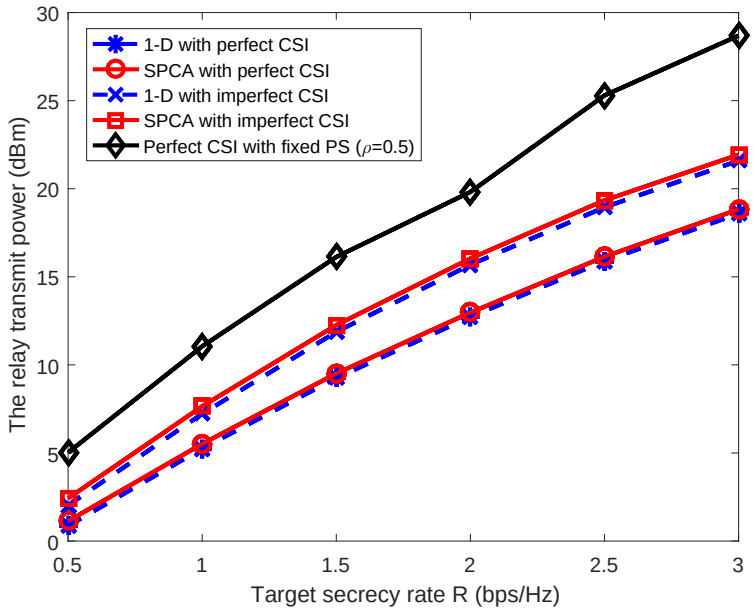

Fig. 4.3 Transmit power at the relay versus the target rate R. Set $\varepsilon = 0.01$ and $\eta = -5$ dBm.

CSI case. Compared with the perfect CSI case, the relay needs more power to achieve the secrecy rate requirement. This is because of the system needs more power to overcome the channel uncertainties. Moreover, it is finding that the proposed scheme with adaptive PS ratio outperforms the scheme with the fixed PS ratio $(\rho = 0.5)$, and the performance gap between them becomes large when the secrecy rate requirement increases.

Figure 4.4 illustrates the relay transmit power required by various algorithms against the EH threshold η. It observes that the relay requires more energy to transmit message to the DR when the EH threshold becomes large for all schemes. As expected, the iterative algorithm generated by SPCA method achieves the similar performance to the 1-D method. Interestingly, the power consumption at the relay has a huge increase when the EH threshold greater than 0 dBm. This phenomenon indicates that the EH at the DR is the major factor for the relay power consumption when EH threshold is sufficiently large and the secrecy rate is prominent to the relay power consumption when the EH threshold is small. In addition, the performance gap between the fixed PS ratio scheme and the adaptive PS ratio scheme

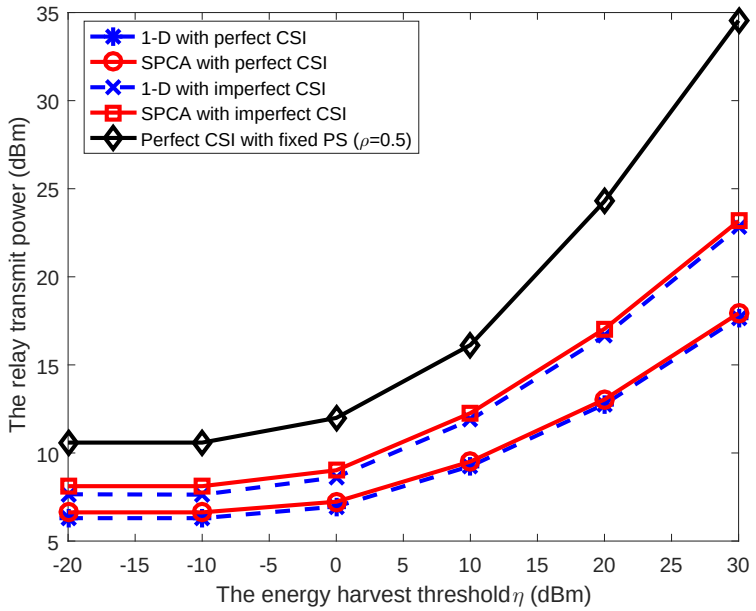

Fig. 4.4 Transmit power at the relay versus the EH threshold η. Set $\varepsilon = 0.01$ and $R = 1.5$ bps/Hz.

becomes large in the high EH threshold region. Moreover, the power consumption under the imperfect CSI case is still lager than the perfect CSI case in the whole EH threshold region.

The impact of the channel uncertainty bound ε on the relay transmit power is investigated in Figure 4.5. It is observed that the demanded transmit power at the relay increases monotonically with an increasing value of the error bound for imperfect CSI schemes. This is due to the fact that the relay needs more power to overcome the effects of the uncertainty channels in order to guarantee successful information transmission. The performance provided by the 1-D search method is better than that of SPCA method, but the gap between them is very small. Moreover, there is no performance impact on perfect CSI schemes with the different channel uncertainty bound. On the other hand, it can be observed that a significant power saving can be achieved by the proposed optimal scheme when the number of antennas increase from $M = 5$ to $M = 8$. This is due to the fact that the degrees of freedom for resource allocation increase if the number of transmit antennas increases, which enables a more power efficient resource allocation.

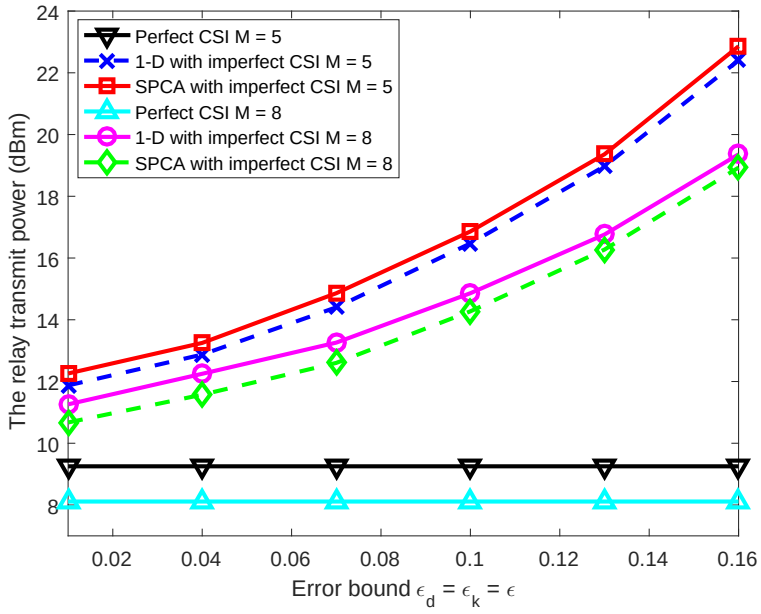

Fig. 4.5 Transmit power at the relay versus the channel uncertainty level ε. Set $R = 1.5$ bps/Hz and $\eta = -5$ dBm.

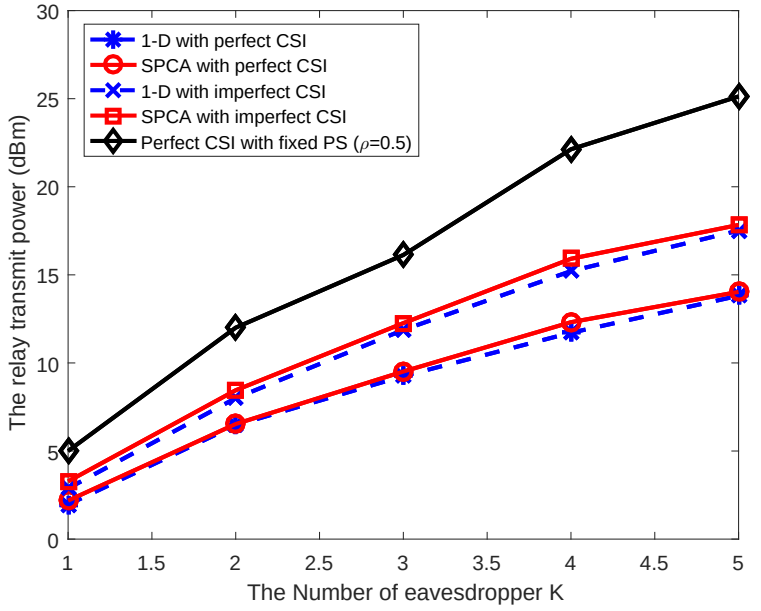

Fig. 4.6 Transmit power at the relay versus the number of eavesdropper K. Set $R = 1.5$ bps/Hz, $\varepsilon = 0.01$ and $\eta = -5$ dBm.

Finally, Figure 4.6 illustrates the effect of the different number of eavesdroppers on the power consumption at the relay. From the figure, the following observations can be made. First, the relay power consumption of all schemes tend to increase with the growth of the number of eavesdropper. Second, the performance gaps between the perfect CSI scheme and the imperfect CSI scheme as well as fixed PS ratio scheme obviously increase when the number of eavesdropper increases. This is because the imperfect CSI scheme consume more power to overcome the channel uncertainties and the fixed PS scheme consume more power to achieve the security requirement. Third, the performance provided by the SPCA method closes to the 1-D method, but the difference between them has a slightly increase when the number of eavesdropper greater than three.

4.6 Summary

In this chapter, the secure communication for SWIPT is studied in a multi-antenna AF relay network based on the assumption of perfect CSI and imperfect CSI. The PM problem is designed to jointly optimize the relay beamforming matrix and PS ratio based on the secrecy rate constraint and the EH constraint. Since the PM problem is non-convex, two algorithms are proposed to solve it. First, a two-level optimization algorithm which including one-dimensional search and SDR is proposed to solve the PM problem for both channel models. Furthermore, a rank reduction theorem is introduced to guarantee the rank constraint of the matrix. Second, a low complexity iterative algorithm, which is designed based on the SPCA method, is proposed to locally solve the PM problem for the two channel models. Simulation results have been provided to demonstrate the performance of the proposed the algorithms.

Chapter 5

Outage Constrained Design with SWIPT in MIMO-CR Systems

This chapter is organized as follows. The main contributions of this chapter are first introduced in Section 5.1. The system model is presented in Section 5.2. The proposed the problems and solutions are formulated in Section 5.3 based on the assumed channel models. The performance of the proposed approaches is validated in Section 5.5. Conclusions are drawn in Section 5.6.

5.1 Introduction

In this chapter, a secrecy rate maximization problem under the probability constraints design is investigated in an underlay CR network, where all receivers and the secondary transmitter are equipped with multiple antennas. The proposed design can achieve the better secrecy performance compared with the worst-case design. The transmit signal and AN signal are jointly designed based on the statistical channel uncertainty model. Due to the nonconvex and nonsmooth secrecy rate function and the complicated probabilistic constraints, the proposed OC-SRM problem is more challenging to obtain the safe and

tractable design. The original OC-SRM problem is decomposed into two subproblems by introducing auxiliary variables based on the theory in [116–118]. To tackle the difficulty arising from probabilistic constraints in each subproblem, a conservative approximation approach, namely BTI introduced in [119, 120], is adopted to transform the probabilistic constraints into the safe and tractable forms. The tractable solution of the proposed OC-SRM problem can be obtained by alternately solving two convex conic subproblems. Finally, the effectiveness of the proposed algorithm is validated by simulation.

5.2 Network Model

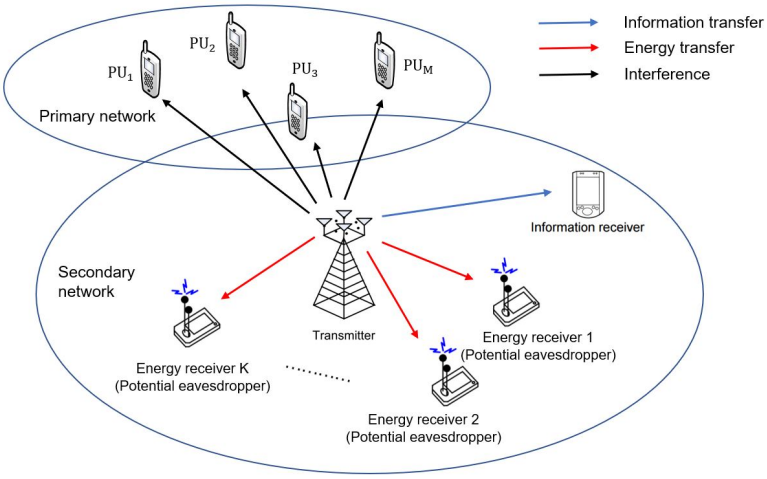

Fig. 5.1 System model.

As shown in Figure 5.1, an underlay cognitive MIMO wiretap scenario is considered where a secondary transmitter (ST) with N_t antennas, a desired secondary information receiver (SIR) with N_d antennas, $(M \geq 1)$ secondary energy receivers (SER) with N_e antennas and $(K \geq 1)$ PUs with N_p antennas. The slow frequency-flat fading channel from the ST to the SIR, the kth PU and the mth SER are denoted by $\mathbf{G}_k \in \mathbb{C}^{N_t \times N_p}$ (PU), $\mathbf{H}_d \in \mathbb{C}^{N_t \times N_d}$ (SIR) and $\mathbf{H}_m \in \mathbb{C}^{N_t \times N_e}$ (SER), respectively. In each scheduling slot, it is assumed that only one secondary receiver is active as the IR to decode its own information and other secondary

receivers are active as the ERs to harvest and store energy for future use. However, If the SERs are malicious, they may attempt to eavesdrop the information rather than to harvest energy since all receivers are deployed in the range of service coverage. In order to protect the received information by the SIR, the secure communication should be considered by regarding the SERs as the potential eavesdroppers. The received signals at the SIR, the kth PU and the mth SER may be written as

$$\mathbf{y}_d = \mathbf{H}_d^H \mathbf{x} + \mathbf{n}_d, \tag{5.1}$$

$$\mathbf{y}_k = \mathbf{G}_k^H \mathbf{x} + \mathbf{n}_k, k \in K, \tag{5.2}$$

$$\mathbf{y}_m = \mathbf{H}_m^H \mathbf{x} + \mathbf{n}_m, m \in M, \tag{5.3}$$

respectively, where $\mathbf{n}_d \sim \mathrm{CN}(\mathbf{0}, \mathbf{I}), \mathbf{n}_k \sim \mathrm{CN}(\mathbf{0}, \mathbf{I})$ and $\mathbf{n}_m \sim \mathrm{CN}(\mathbf{0}, \mathbf{I})$ denote i.i.d. standard complex Gaussian noise; $\mathbf{x} \in \mathbb{C}^{N_t}$ is the transmit signal of ST, which can be formed as $\mathbf{x} = \mathbf{s} + \mathbf{v}$, where $\mathbf{s} \in \mathbb{C}^{N_t}$ denotes the coded confidential signal, the distribution of which follows $\mathrm{CN}(\mathbf{0}, \mathbf{Q})$ with the transmit covariance $\mathbf{Q} \succeq \mathbf{0}$ and $\mathbf{v} \sim \mathrm{CN}(\mathbf{0}, \mathbf{V})$ is AN-aided signal with the covariance $\mathbf{V} \succeq \mathbf{0}$ to enhance physical layer security [32]. It is assumed that all SERs are linear models. Thus, the harvested energy at the mth SU-ER is given by $E_m = \xi_m \mathrm{Tr}(\mathbf{H}_m^H(\mathbf{Q} + \mathbf{V})\mathbf{H}_m, m \in M$, where $\xi \in (0, 1]$ is the energy conversion efficiency. Since all SERs are potential eavesdroppers, the achievable secrecy rate of SIR can be expressed by [30]

$$R_s = \min_{m \in M} \{C_d(\mathbf{Q}, \mathbf{V}) - C_m(\mathbf{Q}, \mathbf{V})\}, \tag{5.4}$$

where $C_d(\mathbf{Q}, \mathbf{V}) = \log|\mathbf{I} + (\mathbf{H}_d^H \mathbf{V} \mathbf{H}_d + \mathbf{I})^{-1} \mathbf{H}_d^H \mathbf{Q} \mathbf{H}_d|$ and $C_m(\mathbf{Q}, \mathbf{V}) = \log|\mathbf{I} + (\mathbf{H}_m^H \mathbf{V} \mathbf{H}_m + \sigma_e^2 \mathbf{I})^{-1} \mathbf{H}_m^H \mathbf{Q} \mathbf{H}_m|$ are the mutual information of the SIR and the mth SER, respectively. Note that the perfect secrecy rate is achieved when SU-IR can correctly decode the confidential information at R_s bits per channel use, while all SU-ER can retrieve almost nothing about the secret message. Since the secondary system and the primary system share the same

spectrum resource in the underlay CR network, the interference power at the kth PU from ST is considered as $I_k = \mathrm{Tr}(\mathbf{G}_k^H(\mathbf{Q}+\mathbf{V})\mathbf{G}_k), k \in K$.

5.3 Robust Secure Communication Design

In this section, the OC-SRM problem based on the imperfect CSI assumption is proposed since there exist the channel estimation and quantization errors in practical scenarios.

5.3.1 Channel Models

In this subsection, two models of statistical channel uncertainty are introduced in the following.

- Partial Channel Uncertainty (PCU): A particular channel uncertainty scenario is considered where ST has the perfect CSI of SIR and the imperfect CSI of all SERs and PUs. Accordingly, the actual channels of the mth SER and the kth PU can be respectively modeled as

$$\mathbf{H}_m = \widehat{\mathbf{H}}_m + \triangle\mathbf{H}_m, m \in M, \quad \mathbf{G}_k = \widehat{\mathbf{G}}_k + \triangle\mathbf{G}_k, k \in K, \tag{5.5}$$

  where $\widehat{\mathbf{H}}_m$ and $\widehat{\mathbf{G}}_k$ are the estimated channel matrixes; $\mathrm{vec}(\triangle\mathbf{H}_m) \sim \mathrm{CN}(0, \mathbf{C}_m)$ and $\mathrm{vec}(\triangle\mathbf{G}_k) \sim \mathrm{CN}(0, \mathbf{D}_k)$ denote the corresponding statistical errors, where $\mathbf{C}_m$ and $\mathbf{D}_k$ are the positive semidefinite matrixes.

- Full Channel Uncertainty (FCU): Next, A general uncertainty case is considered in which ST has the imperfect CSI of all receivers. Thus, the actual channel of SIR is

determined as

$$\mathbf{H}_d = \widehat{\mathbf{H}}_d + \triangle\mathbf{E}_d, \tag{5.6}$$

where $\widehat{\mathbf{H}}_d$ is the estimated CSI and corresponding error satisfies the complex Gaussian distribution, $\text{vec}(\triangle\mathbf{E}_d) \sim \text{CN}(0, \mathbf{Z}_d)$, where $\mathbf{Z}_d$ is a positive semidefinite matrix.

Based on the above uncertainty models, the OC-SRM problem can be expressed as

$$\max_{\mathbf{Q},\mathbf{V},R} \quad R \tag{5.7a}$$

$$s.t.\ \Pr\{\min_{m\in M}\{C_d(\mathbf{Q},\mathbf{V}) - C_m(\mathbf{Q},\mathbf{V})\} \geq R\} \geq 1-\rho, \forall_m, \tag{5.7b}$$

$$\Pr\{\xi \text{Tr}(\mathbf{H}_m^H(\mathbf{Q}+\mathbf{V})\mathbf{H}_m) \geq \eta_m\} \geq 1-\rho_m, \forall_m, \tag{5.7c}$$

$$\Pr\{\text{Tr}(\mathbf{G}_k^H(\mathbf{Q}+\mathbf{V})\mathbf{G}_k) \leq \Gamma_k\} \geq 1-\rho_k, \forall_k, \tag{5.7d}$$

$$\text{Tr}(\mathbf{Q}+\mathbf{V}) \leq P, \mathbf{Q} \succeq \mathbf{0}, \mathbf{V} \succeq \mathbf{0}, \tag{5.7e}$$

where η_m is the harvested energy target at the mth SER; Γ_k denotes tolerable interference power at the kth PU; P is the power budget at the ST; $\rho \in (0,1]$, $\rho_m \in (0,1]$ and $\rho_k \in (0,1]$ indicate the maximum allowable outage probabilities associated with the secrecy rate of SIR, harvested energy of the mth SER and received interference power of the kth PU.

5.3.2 Robust SRM Problem in PCU Model

Problem (5.7) is non-convex and computationally intractable due to the Shannon capacity expression in secrecy rate function and the outage probability constraints (5.7b)-(5.7d) [101]. It considers to replace $\{C_d - C_m\}$ in outage secrecy function (5.7b) by an easy-to-handle function, which also satisfies the probabilistic requirement. First, the expressions of C_d and

$C_{e,m}$ can be rewritten as follows based on the concept of log function

$$C_d = \log|\mathbf{H}_d^H(\mathbf{Q}+\mathbf{V})\mathbf{H}_d+\mathbf{I}| - \log|\mathbf{H}_d^H\mathbf{V}\mathbf{H}_d+\mathbf{I}|, \tag{5.8}$$

$$C_m = \log|\mathbf{H}_m^H(\mathbf{Q}+\mathbf{V})\mathbf{H}_m+\mathbf{I}| - \log|\mathbf{H}_m^H\mathbf{V}\mathbf{H}_m+\mathbf{I}|. \tag{5.9}$$

Then, the following lemma is adopted to solve log det function in (5.8) and (5.9) efficiently

Lemma 4. *[116]: Let's define a positive matrix* $\mathbf{E} \succ \mathbf{0}$, $\mathbf{E} \in \mathbb{C}^{N\times N}$ *with integer N, there exist a function,* $v(\mathbf{S},\mathbf{E}) = -\mathrm{Tr}(\mathbf{S}\mathbf{E}) + \ln|\mathbf{S}| + N$, *satisfies the following equation*

$$\ln|\mathbf{E}^{-1}| = \max_{\mathbf{S}\in\mathbb{C}^{N\times N}, \mathbf{S}\succeq\mathbf{0}} v(\mathbf{S},\mathbf{E}) \tag{5.10}$$

By invoking Lemma 4, the second term of (5.8) and the first term of (5.9) can be rewritten as follows, respectively

$$-\log|(\mathbf{H}_d^H\mathbf{V}\mathbf{H}_d+\mathbf{I})^{-1}| = \min_{\mathbf{S}_d\succeq\mathbf{0}} \mathrm{Tr}(\mathbf{S}_d(\mathbf{H}_d^H\mathbf{V}\mathbf{H}_d+\mathbf{I})) - \ln|\mathbf{S}_d| - N_d \tag{5.11}$$

$$-\log|(\mathbf{H}_m^H(\mathbf{Q}+\mathbf{V})\mathbf{H}_m+\mathbf{I})^{-1}| = \min_{\mathbf{S}_m\succeq\mathbf{0}} \mathrm{Tr}(\mathbf{S}_m(\mathbf{H}_m^H(\mathbf{Q}+\mathbf{V})\mathbf{H}_m+\mathbf{I})) - \ln|\mathbf{S}_m| - N_e. \tag{5.12}$$

The authors in [117] give the following expression to approximate the mutual information at low SNR for MIMO channel

$$\log|\mathbf{I}+\frac{1}{\sigma^2}\mathbf{H}\mathbf{Q}\mathbf{H}^H| = \frac{1}{\sigma^2}\mathrm{Tr}\{\mathbf{H}\mathbf{Q}\mathbf{H}^H\} + \mathscr{O}(\frac{1}{\sigma^2}\|\mathbf{H}\mathbf{Q}\mathbf{H}^H\|). \tag{5.13}$$

Based on Lemma 1 and low SNR approximation, the secrecy rate outage constraint (5.7b) can be reformulated as

$$\Pr\Big\{\mathrm{Tr}(\mathbf{H}_d^H(\mathbf{Q}+\mathbf{V})\mathbf{H}_d) - \mathrm{Tr}(\mathbf{S}_d(\mathbf{H}_d^H\mathbf{V}\mathbf{H}_d+\mathbf{I})) + \ln|\mathbf{S}_d| + N_d - \mathrm{Tr}(\mathbf{S}_m(\mathbf{H}_m^H(\mathbf{Q}+\mathbf{V})\mathbf{H}_m + \mathbf{I})) + \ln|\mathbf{S}_m| + N_e + \mathrm{Tr}(\mathbf{H}_m^H\mathbf{V}\mathbf{H}_m) - R \geq 0\Big\} \geq 1-\rho. \tag{5.14}$$

Next, probabilistic constraints, in (5.7c), (5.7d) and (5.14) have become the new challenges. Since $\mathbf{e}_m = \text{vec}(\triangle\mathbf{H}_m)$ and $\mathbf{e}_k = \text{vec}(\triangle\mathbf{G}_k)$, it can define $\mathbf{e}_m \sim \text{CN}(0, \mathbf{C}_m)$ and $\mathbf{e}_k \sim \text{CN}(0, \mathbf{D}_k)$. Then, the transformation is given in the following

$$\mathbf{e}_m = \mathbf{C}_m^{\frac{1}{2}}\mathbf{v}_m, \;\; \mathbf{e}_k = \mathbf{D}_k^{\frac{1}{2}}\mathbf{x}_k, \tag{5.15}$$

where $\mathbf{v}_m \sim \text{CN}(0, \mathbf{I}_{N_t \times N_e})$ and $\mathbf{x}_k \sim \text{CN}(0, \mathbf{I}_{N_t \times N_p})$. By substituting the uncertainty channel models into the outage constraints in (5.7) and invoking the identity function $\text{Tr}(\mathbf{A}^H\mathbf{BCD}) = \text{vec}(\mathbf{A})^H(\mathbf{D}^T \otimes \mathbf{B})\text{vec}(\mathbf{C})$, the secrecy outage constraint (5.14) can be expressed as

$$\Pr\{\mathbf{v}_m^H\mathbf{C}_m^{\frac{1}{2}}\Theta_m\mathbf{C}_m^{\frac{1}{2}}\mathbf{v}_m + 2\Re(\mathbf{v}_m^H\mathbf{C}_m^{\frac{1}{2}}\Theta_m\mathbf{h}_m) + \widehat{\mathbf{h}}_m^H\Theta_m\widehat{\mathbf{h}}_m \leq c_m\} \geq 1-\rho. \tag{5.16}$$

where $\widehat{\mathbf{h}}_m = \text{vec}(\widehat{\mathbf{H}}_m)$, $\Theta_m = (\mathbf{S}_m^T \otimes (\mathbf{Q}+\mathbf{V}) - \mathbf{I}_{N_t} \otimes \mathbf{V})$ and $c_m = \text{Tr}(\mathbf{H}_d^H(\mathbf{Q}+\mathbf{V})\mathbf{H}_d) - \text{Tr}(\mathbf{S}_d(\mathbf{H}_d^H\mathbf{V}\mathbf{H}_d + \mathbf{I})) + \ln|\mathbf{S}_d| + N_d - \text{Tr}(\mathbf{S}_m) + \ln|\mathbf{S}_m| + N_e - R$. The harvested energy outage constraint (5.7c) can be reformulated as

$$\Pr\{\mathbf{v}_m^H\mathbf{C}_m^{\frac{1}{2}}\Xi\mathbf{C}_m^{\frac{1}{2}}\mathbf{v}_m + 2\Re(\mathbf{v}_m^H\mathbf{C}_m^{\frac{1}{2}}\Xi\widehat{\mathbf{h}}_m) + \widehat{\mathbf{h}}_m^H\Xi\widehat{\mathbf{h}}_m \geq \frac{\eta_m}{\xi}\} \geq 1-\rho_m, \tag{5.17}$$

where $\Xi = \mathbf{I}_{N_t}^T \otimes (\mathbf{Q}+\mathbf{V})$. Similarly, the interference outage constraint (5.7d) can be converted into the following form

$$\Pr\{\mathbf{x}_k^H\mathbf{D}_k^{\frac{1}{2}}\Phi\mathbf{D}_k^{\frac{1}{2}}\mathbf{x}_k + 2\Re(\mathbf{x}_k^H\mathbf{D}_k^{\frac{1}{2}}\Phi\widehat{\mathbf{g}}_k) + \widehat{\mathbf{g}}_k^H\Phi\widehat{\mathbf{g}}_k \leq \Gamma_k\} \geq 1-\rho_k, \tag{5.18}$$

where $\widehat{\mathbf{g}}_k = \text{vec}(\widehat{\mathbf{G}}_k)$ and $\Phi = \mathbf{I}_{N_t \times N_p}^T \otimes (\mathbf{Q}+\mathbf{V})$.

The above transformation still cannot provide a convex approximation of the original problem due to the intractable outage constraints in (5.16)-(5.18). In order to convert the intractable outage constraints into tractable deterministic constraints, the BTI approach is adopted to

provide a conservative approximation of the outage constraint based on large deviation inequalities for complex Gaussian quadratic vector functions.

Lemma 5 (*BTI* [120, 121])**.** *Consider the following outage constraint*

$$f(\mathbf{A},\mathbf{u},c) \Leftrightarrow \Pr\{\mathbf{x}^H\mathbf{A}\mathbf{x}+2\Re\{\mathbf{x}^H\mathbf{u}\}+c\geq 0\}\geq 1-\rho, \tag{5.19}$$

where $\mathbf{A}\in\mathbb{C}^{N\times N}$ *is a complex Hermitian matrix,* $\mathbf{u}\in\mathbb{C}^{N\times 1}$*,* $\mathbf{x}\sim\mathscr{CN}(\mathbf{0},\mathbf{I})$ *and fixed* $\rho\in(0,1]$*. With any slack variables* λ *and* μ*, the outage constraint can be equivalently transformed into the following three inequalities*

$$\begin{cases} \mathrm{Tr}(\mathbf{A})-\sqrt{-2\ln(\rho)}\lambda+\ln(\rho)\mu+c\geq 0, \\ \left\|\begin{bmatrix}\mathrm{vec}(\mathbf{A})\\ \sqrt{2}\mathbf{u}\end{bmatrix}\right\|\leq\lambda, \\ \mu\mathbf{I}_N+\mathbf{A}\succeq 0,\quad \mu\geq 0. \end{cases} \tag{5.20}$$

By involving Lemma 5, the convex approximation of the secrecy outage constraint in (5.16) can be reformulated into the following inequalities:

$$\begin{cases} \mathrm{Tr}(\mathbf{C}_m^{\frac{1}{2}}\Theta_m\mathbf{C}_m^{\frac{1}{2}})+\sqrt{-2\ln(\rho)}\lambda_m-\ln(\rho)\mu_m+\widehat{\mathbf{h}}_m^H\Theta_m\widehat{\mathbf{h}}_m-c_m\leq 0, \\ \left\|\begin{bmatrix}\mathrm{vec}(\mathbf{C}_m^{\frac{1}{2}}\Theta_m\mathbf{C}_m^{\frac{1}{2}})\\ \sqrt{2}\mathbf{C}_m^{\frac{1}{2}}\Theta_m\mathbf{h}_m\end{bmatrix}\right\|\leq\lambda_m, \\ \mu_m\mathbf{I}_{N_t\times N_e}-\mathbf{C}_m^{\frac{1}{2}}\Theta_m\mathbf{C}_m^{\frac{1}{2}}\succeq 0,\quad \mu_m\geq 0,\quad \forall_m, \end{cases} \tag{5.21}$$

and that of the energy outage constraint in (5.17) can be represented by

$$\begin{cases} \mathrm{Tr}(\mathbf{C}_m^{\frac{1}{2}}\Xi\mathbf{C}_m^{\frac{1}{2}}) - \sqrt{-2\ln(\rho_m)}\alpha_m + \ln(\rho_m)\beta_m + \widehat{\mathbf{h}}_m^H\Xi\widehat{\mathbf{h}}_m - \dfrac{\eta_m}{\xi} \geq 0, \\ \left\| \begin{bmatrix} \mathrm{vec}(\mathbf{C}_m^{\frac{1}{2}}\Xi\mathbf{C}_m^{\frac{1}{2}}) \\ \sqrt{2}\mathbf{C}_m^{\frac{1}{2}}\Xi\widehat{\mathbf{h}}_m \end{bmatrix} \right\| \leq \alpha_m, \\ \beta_m\mathbf{I}_{N_t\times N_e} + \mathbf{C}_m^{\frac{1}{2}}\Xi\mathbf{C}_m^{\frac{1}{2}} \succeq \mathbf{0}, \quad \beta_m \geq 0, \quad \forall_m. \end{cases} \tag{5.22}$$

Due to the similarly transformation of the previous function, the outage constraint (5.18) can be recast into

$$\begin{cases} \mathrm{Tr}(\mathbf{D}_k^{\frac{1}{2}}\Phi\mathbf{D}_k^{\frac{1}{2}}) + \sqrt{-2\ln(\rho_k)}\nu_k - \ln(\rho_k)\omega_k + \widehat{\mathbf{g}}_k^H\Phi\widehat{\mathbf{g}}_k - \Gamma_k \leq 0, \\ \left\| \begin{bmatrix} \mathrm{vec}(\mathbf{D}_k^{\frac{1}{2}}\Phi\mathbf{D}_k^{\frac{1}{2}}) \\ \sqrt{2}\mathbf{C}_m^{\frac{1}{2}}\Phi\widehat{\mathbf{g}}_k \end{bmatrix} \right\| \leq \nu_k, \\ \omega_k\mathbf{I}_{N_t\times N_p} - \mathbf{D}_k^{\frac{1}{2}}\Phi\mathbf{D}_k^{\frac{1}{2}} \succeq \mathbf{0}, \quad \omega_k \geq 0, \quad \forall_k. \end{cases} \tag{5.23}$$

It is worth to note that the outage constraints of the original problem (5.7) have been converted into the tractable deterministic forms based on the above three transformations. The new problem (5.7) is still not jointly convex for all variables after replacing (5.7b)-(5.7d) by (5.21)-(5.23). In order to overcome this challenge, an AO algorithm is proposed. Then, the secrecy rate maximization problem (5.7) can be solved by fixing $\mathbf{S}_s$ and $\mathbf{S}_m$

$$\begin{aligned} \max_{\mathbf{Q},\mathbf{V},R,\lambda_m,\mu_m,\alpha_m,\beta_m,\nu_k,\omega_k} \quad & R \\ s.t. \quad & (5.21)-(5.23),(5.7\text{e}). \end{aligned} \tag{5.24}$$

Algorithm 5.1: AO Algorithm for (5.7) in PCU

1. **Initialize:** Set $ln = 1, \varepsilon > 0, \mathbf{S}_d^0 = \mathbf{I}, \mathbf{S}_m^0 = \mathbf{I}, m = 1, \ldots, M$;
2. **Repeat:**
   (a) Solving (5.24) with fixed $\mathbf{S}_d = \mathbf{S}_d^{l-1}$ and $\mathbf{S}_m = \mathbf{S}_m^{l-1}$ to obtain $(\mathbf{Q}^{l-1}, \mathbf{V}^{l-1}, R^{l-1})$;
   (b) Solving (5.25) with fixed $\mathbf{Q} = \mathbf{Q}^{l-1}$ and $\mathbf{V} = \mathbf{V}^{l-1}$ to get $(\mathbf{S}_d^l, \mathbf{S}_m^l, R^l)$;
   (c) $l = l + 1$;
3. **Until** $|R^l - R^{l-1}| \leq \varepsilon$
4. Output $(\mathbf{Q}^l, \mathbf{V}^l, R^l)$.

Assuming $\mathbf{Q}$ and $\mathbf{V}$ are the optimal solutions to problem (5.24), $\mathbf{S}_s$ and $\mathbf{S}_m$ can be optimized by fixing $\mathbf{Q}$ and $\mathbf{V}$ as follows:

$$\begin{aligned} \max_{\mathbf{S}_s, \mathbf{S}_m, R, \lambda_m, \mu_m} \quad & R \\ s.t. \quad & (5.21), \mathbf{S}_s \succeq \mathbf{0}, \mathbf{S}_m \succeq \mathbf{0}. \end{aligned} \tag{5.25}$$

The AO algorithm is summarized in Algorithm 5.1. Subproblems (5.24) and (5.25) can be efficiently solved by using CVX tool box [105]. It is notable that the optimal solutions generated at the $(l-1)$th iteration are also the feasible values at the lth iteration. For this reason, the proposed AO algorithm generates a nondecreasing sequence of the secrecy rate. In addition, the smaller tolerance ε is, the more iterative steps are need. Hence, the time of solving the proposed algorithm can be roughly estimated as the time of solving the two subproblems multiplied with the number of iterations.

5.3.3 Robust SRM Problem in FCU Model

In this subsection, a robust secrecy rate maximization based on the FCU model is investigated. The proposed method used to solve the problems of the PCU model can be employed to the FCU model. Since $\mathbf{e}_d = \text{vec}(\Delta E_d)$, the distribution of $\mathbf{e}_d$ is $\mathbf{e}_d \sim \text{CN}(0, \mathbf{U}_d)$. With a standard

complex Gaussian random vector $\mathbf{z}_d$, it obtains

$$\mathbf{e}_d = \mathbf{U}_d^{\frac{1}{2}} \mathbf{v}_d, \tag{5.26}$$

where $\mathbf{v}_d \sim \mathrm{CN}(0, \mathbf{I}_{N_t \times N_d})$. By substituting the channel errors (5.15) and (5.26) into (5.14), the secrecy outage constraint under FCU model can be expressed as

$$\begin{aligned} \Pr \Bigg\{ & \begin{bmatrix} \mathbf{v}_d^H & \mathbf{v}_m^H \end{bmatrix} \begin{bmatrix} \mathbf{U}_d^{\frac{1}{2}} \boldsymbol{\varpi}_d \mathbf{U}_d^{\frac{1}{2}} & \mathbf{0} \\ \mathbf{0} & \mathbf{C}_m^{\frac{1}{2}} \Psi_m \mathbf{C}_m^{\frac{1}{2}} \end{bmatrix} \begin{bmatrix} \mathbf{v}_d^H & \mathbf{v}_m^H \end{bmatrix}^H \\ & + 2\Re \left(\begin{bmatrix} \mathbf{v}_d^H & \mathbf{v}_m^H \end{bmatrix} \begin{bmatrix} \mathbf{U}_d^{\frac{1}{2}} \boldsymbol{\varpi}_d & \mathbf{0} \\ \mathbf{0} & \mathbf{C}_m^{\frac{1}{2}} \Psi_m \end{bmatrix} \begin{bmatrix} \widehat{\mathbf{h}}_d^H & \widehat{\mathbf{h}}_m^H \end{bmatrix}^H \right) \\ & + \begin{bmatrix} \widehat{\mathbf{h}}_d^H & \widehat{\mathbf{h}}_m^H \end{bmatrix} \begin{bmatrix} \boldsymbol{\varpi}_d & \mathbf{0} \\ \mathbf{0} & \Psi_m \end{bmatrix} \begin{bmatrix} \widehat{\mathbf{h}}_d^H & \widehat{\mathbf{h}}_m^H \end{bmatrix}^H - c_m \leq 0 \Bigg\} \geq 1 - \rho, \end{aligned} \tag{5.27}$$

where $\widehat{\mathbf{h}}_d = \mathrm{vec}(\widehat{\mathbf{H}}_d), \boldsymbol{\varpi}_d = \mathbf{S}_d^T \otimes \mathbf{V} - \mathbf{I}_{N_t} \otimes (\mathbf{Q} + \mathbf{V}), \Psi_m = \mathbf{S}_m^T \otimes (\mathbf{Q} + \mathbf{V}) - \mathbf{I}_{N_t} \otimes \mathbf{V}$ and $c_m = -\mathrm{Tr}(\mathbf{S}_s) + \ln|\mathbf{S}_d| + N_d - \mathrm{Tr}(\mathbf{S}_m) + \ln|\mathbf{S}_m| - N_e - R$. In order to involve Lemma 5 to transform secrecy outage constraint (5.27) into more tractable form, it sets

$$\begin{cases} \mathbf{v}_{d,m} = \begin{bmatrix} \mathbf{v}_d^H & \mathbf{v}_m^H \end{bmatrix}^H \\ \mathbf{A}_{d,m} = \begin{bmatrix} \mathbf{U}_d^{\frac{1}{2}} \boldsymbol{\varpi}_d \mathbf{U}_d^{\frac{1}{2}} & \mathbf{0} \\ \mathbf{0} & \mathbf{C}_m^{\frac{1}{2}} \Psi_m \mathbf{C}_m^{\frac{1}{2}} \end{bmatrix} \\ \mathbf{B}_{d,m} = \begin{bmatrix} \mathbf{U}_d^{\frac{1}{2}} \boldsymbol{\varpi}_d & \mathbf{0} \\ \mathbf{0} & \mathbf{C}_m^{\frac{1}{2}} \Psi_m \end{bmatrix} \begin{bmatrix} \widehat{\mathbf{h}}_d^H & \widehat{\mathbf{h}}_m^H \end{bmatrix}^H \\ \sigma_{d,m} = \begin{bmatrix} \widehat{\mathbf{h}}_d^H & \widehat{\mathbf{h}}_m^H \end{bmatrix} \begin{bmatrix} \boldsymbol{\varpi}_d & \mathbf{0} \\ \mathbf{0} & \Psi_m \end{bmatrix} \begin{bmatrix} \widehat{\mathbf{h}}_d^H & \widehat{\mathbf{h}}_m^H \end{bmatrix}^H - c_m \end{cases}$$

to simplify (5.27) as

$$\Pr\{\mathbf{v}_{d,m}^H \mathbf{A}_{d,m} \mathbf{v}_{d,m} + 2\Re(\mathbf{v}_{d,m}^H \mathbf{B}_{d,m}) + \sigma_{d,m} \leq 0\} \geq 1 - \rho, \tag{5.28}$$

which has the similar form with (5.19). By applying Lemma 5, the secrecy outage constraint (5.27) can be equivalently represented by the following three inequalities

$$\begin{cases} \mathrm{Tr}(\mathbf{A}_{d,m}) + \sqrt{-2\ln(\rho)}\theta_{d,m} - \ln(\rho)\delta_{d,m} + \sigma_{d,m} \leq 0, \\ \left\| \begin{bmatrix} \mathrm{vec}(\mathbf{A}_{d,m}) \\ \sqrt{2}\mathbf{B}_{d,m} \end{bmatrix} \right\| \leq \theta_{d,m}, \\ \delta_{d,m}\mathbf{I}_{N_t \times N_e} - \mathbf{A}_{d,m} \succeq 0, \quad \delta_{d,m} \geq 0. \end{cases} \tag{5.29}$$

The harvested energy and interference outage constraints based on FCU model are same as that of PCU model. Hence, the OC-SRM problem based on FCU is reformulated by

$$\begin{aligned} \max_{\mathbf{Q},\mathbf{V},\mathbf{S}_d,\mathbf{S}_m,R,\delta_{d,m},\theta_{d,m},\alpha_m,\beta_m,\nu_k,\omega_k} \quad & R \\ s.t. \quad & (5.22),(5.23),(5.29),(5.7\mathrm{e}). \end{aligned} \tag{5.30}$$

After replacing the outage constraints (5.7b)-(5.7d) with their tractable deterministic constraints (5.29), (5.22) and (5.23), the approximated optimization problem based on FCU model is still nonconvex w.r.t. all the variables jointly. With the similar AO algorithm proposed in PCU model, problem (5.30) first can be solved by CVX tool box [105] based on the fixed $\mathbf{S}_s$ and $\mathbf{S}_m$ to obtain the optimal $\mathbf{Q}^*$ and $\mathbf{V}^*$. Then, it sets $\mathbf{Q} = \mathbf{Q}^*$ and $\mathbf{V} = \mathbf{V}^*$ to optimize the following problem to obtain the optimal $\mathbf{S}_s^*$ and $\mathbf{S}_m^*$,

$$\begin{aligned} \max_{\mathbf{S}_d,\mathbf{S}_m,R,\delta_{d,m},\theta_{d,m}} \quad & R \\ s.t. \quad & (5.29), \mathbf{S}_d \succeq \mathbf{0}, \mathbf{S}_m \succeq \mathbf{0}. \end{aligned} \tag{5.31}$$

Since the AO algorithm of the FCU model and that of the PCU model are similar, as shown in Algorithm 5.1, the summary of the AO algorithm of the FCU model is omitted.

5.4 Baseline Design

For comparison, the worst case design and non-robust design are considered as two baselines.

5.4.1 Non-Robust Design

The aim of the non-robust design is to reflect the effects of the proposed the outage design on the system performance. For the non-robust design, beamforming and AN matrix should be optimized under the perfect CSI case by the following secrecy rate maximization problem

$$\begin{aligned} \max_{\mathbf{Q},\mathbf{V}} \ \min_{m\in M} \ & \{C_d(\mathbf{Q},\mathbf{V}) - C_m(\mathbf{Q},\mathbf{V})\} \\ s.t. \ \ & \xi \mathrm{Tr}(\mathbf{H}_m^H(\mathbf{Q}+\mathbf{V})\mathbf{H}_m) \geq \eta_m, \ \forall_m, \\ & \mathrm{Tr}(\mathbf{G}_k^H(\mathbf{Q}+\mathbf{V})\mathbf{G}_k) \leq \Gamma_k, \ \forall_k, \\ & \mathrm{Tr}(\mathbf{Q}+\mathbf{V}) \leq P, \mathbf{Q} \succeq \mathbf{0}, \mathbf{V} \succeq \mathbf{0}. \end{aligned} \tag{5.32}$$

The above problem (5.32) is non-convex due to the non-convex objective function. Based on Lemma 4 and several transformations, problem (5.32) can be converted to the following

convex problem

$$\begin{aligned}
&\max_{\mathbf{Q},\mathbf{V},t,v} \; t-v \\
&\quad s.t. \quad \log|\mathbf{H}_d^H(\mathbf{Q}+\mathbf{V})\mathbf{H}_d+I| - \mathrm{Tr}(\mathbf{S}_d(\mathbf{H}_d^H\mathbf{V}\mathbf{H}_d+\mathbf{I})) + \ln|\mathbf{S}_d| + N_d \geq t, \\
&\qquad \mathrm{Tr}(\mathbf{S}_m(\mathbf{H}_m^H(\mathbf{Q}+\mathbf{V})\mathbf{H}_m+\mathbf{I})) - \ln|\mathbf{S}_m| - N_e - \log|\mathbf{H}_m^H\mathbf{V}\mathbf{H}_m+\mathbf{I}| \leq v, \; \forall_m, \\
&\qquad \mathrm{Tr}(\mathbf{G}_k^H(\mathbf{Q}+\mathbf{V})\mathbf{G}_k) \leq \Gamma_k, \; \forall_k, \\
&\qquad \mathrm{Tr}(\mathbf{Q}+\mathbf{V}) \leq P, \mathbf{Q} \succeq \mathbf{0}, \mathbf{V} \succeq \mathbf{0}, t \geq 0, v \geq 0. \qquad (5.33)
\end{aligned}$$

Through solving problem (5.33), the optimal $\mathbf{Q}$ and $\mathbf{V}$ for the non-robust design can be obtained. Then, the channels included error can be randomly generated based on their distribution

$$\begin{aligned}
&\mathrm{vec}(\mathbf{H}_m) \sim \mathrm{CN}(\mathrm{vec}(\widehat{\mathbf{H}}_m), \mathbf{C}_m), \; \forall_m, \\
&\mathrm{vec}(\mathbf{G}_k) \sim \mathrm{CN}(\mathrm{vec}(\widehat{\mathbf{G}}_k), \mathbf{D}_k), \; \forall_k. \qquad (5.34)
\end{aligned}$$

The secrecy rate based non-robust design can be calculated by substituting the generated channels $\mathbf{H}_m$ and $\mathbf{G}_k$ as well as the optimal solution $\mathbf{Q}$ and $\mathbf{V}$ into (5.4).

5.4.2 Worst-Case Design

The distinct difference between the worst-case design and the proposed outage design is that the former design is based on the bounded CSI error model and the latter is based on the

stochastic CSI error model. In the bounded CSI error model, the channel can be expressed as

$$\begin{aligned}
\ddot{H} &= \{\mathbf{H}_d | \mathbf{H}_d = \widehat{\mathbf{H}}_d + \triangle\mathbf{E}_d, \triangle\mathbf{H}_d^H \mathbf{Z}_d \triangle\mathbf{H}_d \leq 1\}, \\
H &= \{\mathbf{H}_m | \mathbf{H}_m = \widehat{\mathbf{H}}_m + \triangle\mathbf{H}_m, \triangle\mathbf{H}_m^H \mathbf{C}_m \triangle\mathbf{H}_m \leq 1, \forall_m\}, \\
G &= \{\mathbf{G}_k | \mathbf{G}_k = \widehat{\mathbf{G}}_k + \triangle\mathbf{G}_k, \triangle\mathbf{G}_k^H \mathbf{D}_k \triangle\mathbf{G}_k \leq 1, \forall_k\}.
\end{aligned} \tag{5.35}$$

Without loss of generality, it sets $\mathbf{Z}_d = (1/\varepsilon_d^2)\mathbf{I}$, $\mathbf{C}_m = (1/\varepsilon_m^2)\mathbf{I}$ and $\mathbf{D}_k = (1/\varepsilon_k^2)\mathbf{I}$, where ε_m and ε_k represent the size of the bounded error region. In order to have a fair comparison between the proposed outage design and the worst case design, the error bound used in the worst case design can be calculated by $\varepsilon = \sqrt{\frac{\sigma^2 F_{2M}^{-1}(1-\rho)}{2}}$ based on the theory in [119, 120], where $F_{2M}^{-1}(\cdot)$ denotes the inverse cumulative distribution function (CDF) of the Chi-square distribution with $2M$ degrees of freedom. The original problem of the worst-case design is similar to problem (5.32). Based on the Lemma 4 and *S-procedure* lemma [101], the convex problem of the worst-case design under the PCU model can be expressed as

$$\max_{\mathbf{Q},\mathbf{V},\mathbf{S}_d,\mathbf{S}_m,t,v,a_m,b_m,\mu_m,\lambda_m,\omega_k} \quad t - v$$

$$s.t. \quad \log|\mathbf{H}_d^H(\mathbf{Q}+\mathbf{V})\mathbf{H}_d + I| - \mathrm{Tr}(\mathbf{S}_d(\mathbf{H}_d^H\mathbf{V}\mathbf{H}_d + \mathbf{I})) + \ln|\mathbf{S}_d| + N_d \geq t, \tag{5.36a}$$

$$a_m - \log b_m \leq v, \tag{5.36b}$$

$$\begin{bmatrix} \mu_m\mathbf{I} - \mathbf{S}_m^T \otimes (\mathbf{Q}+\mathbf{V}) & -\mathbf{S}_m^T \otimes (\mathbf{Q}+\mathbf{V})\widehat{\mathbf{h}}_m \\ -\widehat{\mathbf{h}}_m^H \mathbf{S}_m^T \otimes (\mathbf{Q}+\mathbf{V}) & -\mu_m\varepsilon_m^2 - s_m \end{bmatrix} \succeq \mathbf{0}, \forall_m, \tag{5.36c}$$

$$\begin{bmatrix} \lambda_m\mathbf{I} + \mathbf{I} \otimes \mathbf{V} & \mathbf{I} \otimes \mathbf{V}\widehat{\mathbf{h}}_m \\ \widehat{\mathbf{h}}_m^H \mathbf{I} \otimes \mathbf{V} & -\lambda_m\varepsilon_m^2 + \widehat{\mathbf{h}}_m^H(\mathbf{I} \otimes \mathbf{V})\widehat{\mathbf{h}}_m - b_m + 1 \end{bmatrix} \succeq \mathbf{0}, \forall_m, \tag{5.36d}$$

$$\begin{bmatrix} \omega_k\mathbf{I} + \mathbf{I} \otimes (\mathbf{Q}+\mathbf{V}) & \mathbf{I} \otimes (\mathbf{Q}+\mathbf{V})\widehat{\mathbf{g}}_k \\ \widehat{\mathbf{g}}_k^H \mathbf{I} \otimes (\mathbf{Q}+\mathbf{V}) & -\omega_k\varepsilon_k^2 + \widehat{\mathbf{g}}_k^H(\mathbf{I} \otimes (\mathbf{Q}+\mathbf{V}))\widehat{\mathbf{g}}_k - \Gamma_k \end{bmatrix} \succeq \mathbf{0}, \forall_k, \tag{5.36e}$$

$$\mathrm{Tr}(\mathbf{Q}+\mathbf{V}) \leq P, \mathbf{Q} \succeq \mathbf{0}, \mathbf{V} \succeq \mathbf{0}, t \geq 0, v \geq 0, \mu_m \geq 0, \lambda_m \geq 0, \omega_k \geq 0. \tag{5.36f}$$

where $\widehat{\mathbf{h}}_m = \text{vec}(\widehat{\mathbf{H}}_m)$, $\widehat{\mathbf{g}}_k = \text{vec}(\widehat{\mathbf{G}}_k)$, and $s_m = \widehat{\mathbf{h}}_m^H(\mathbf{S}_m^T \otimes (\mathbf{Q}+\mathbf{V}))\widehat{\mathbf{h}}_m - \ln|\mathbf{S}_m| + \text{Tr}(\mathbf{S}_m) - N_e - a_m$. Similarly, the worst-case design problem under the FCU model can be expressed as

$$
\begin{aligned}
\max_{\mathbf{Q},\mathbf{V},\mathbf{S}_d,\mathbf{S}_m,t,v,a_m,b_m,q_d,p_d,\nu_d,\phi_d} \quad & t - v \\
s.t. \quad & \log q_d - p_d \geq t, \\
& \begin{bmatrix} \nu_d\mathbf{I} + \mathbf{S}_d^T \otimes (\mathbf{Q}+\mathbf{V}) & (\mathbf{I}^T \otimes (\mathbf{Q}+\mathbf{V}))\widehat{\mathbf{h}}_d \\ \widehat{\mathbf{h}}_d^H(\mathbf{I}^T \otimes (\mathbf{Q}+\mathbf{V})) & -\nu_d\varepsilon_d^2 + \widehat{\mathbf{h}}_d^H(\mathbf{I}^T \otimes (\mathbf{Q}+\mathbf{V}))\widehat{\mathbf{h}}_d - q_d + 1 \end{bmatrix} \succeq \mathbf{0}, \\
& \begin{bmatrix} \phi_d\mathbf{I} - \mathbf{S}_D^T \otimes \mathbf{V} & -(\mathbf{S}_d^T \otimes \mathbf{V})\widehat{\mathbf{h}}_d \\ -\widehat{\mathbf{h}}_d^H(\mathbf{S}_d^T \otimes \mathbf{V}) & -\phi_d\varepsilon_d^2 - y_d \end{bmatrix} \succeq \mathbf{0}, \\
& \nu_d \geq 0, \phi_d \geq 0, (5.36\text{b}) - (5.36\text{f}).
\end{aligned} \tag{5.37}
$$

where $\widehat{\mathbf{h}}_d = \text{vec}(\widehat{\mathbf{H}}_d)$ and $y_d = \widehat{\mathbf{h}}_d^H(\mathbf{S}_d^T \otimes \mathbf{V})\widehat{\mathbf{h}}_d - \ln|\mathbf{S}_d| + \text{Tr}(\mathbf{S}_d) - N_d - p_d$. The results of the non-robust and worst-case design can be simulated by using the problems in this section.

5.5 Numerical Results

In this section, numerical results are provided to illustrate the secrecy performance of the proposed algorithm based on the two channel uncertainty models in a MIMO-CR system. To accomplish the simulation, it is considering the following parameter settings: $N_t = 6$, $N_d = N_e = N_p = 2$, EH receiver $M = 2$, PU receiver $K = 2$, outage probability $\rho_s = \rho_m = \rho_k = \rho, \forall_m, \forall_k$, harvested energy target $\eta_m = -4\,dB, \forall_m$, energy conversion efficiency $\xi_m = 0.8, \forall_m$, accuracy tolerance of the proposed algorithm $\varepsilon = 0.001, \mathbf{C}_m = \mathbf{D}_k = \mathbf{U}_d = \sigma^2\mathbf{I}, \forall_m, \forall_k$; the distribution of all randomly generated channels satisfies $\text{CN}(0,1)$. Over 500 estimated channel realizations are randomly generated to achieve the average accurate results. The remaining parameters are specifically given in each figure.

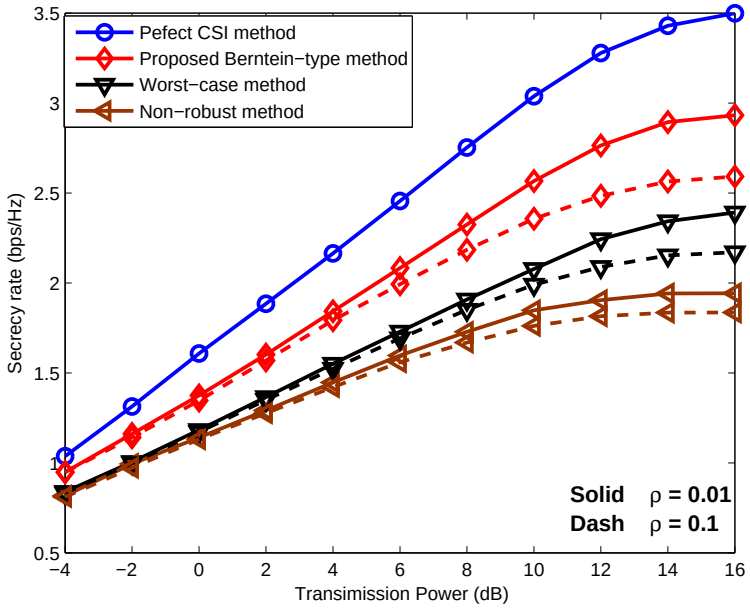

Fig. 5.2 The secrecy rate of the different methods versus the transmit power for different outage probability ρ based on the PCU model with $I = -2$ dB, $\sigma^2 = 0.005$.

Figure 5.2 represents the secrecy rate performance of the various schemes versus the transmit power with the different outage tolerance ρ of 1% and 10%. The secrecy rates of all methods increase with the increase of the transmit power. Moreover, Figure 5.2 indicates that there is remarkable enhancement in the system secrecy rate using the proposed Berntein-type method compared with those methods of the worst-case and the non-robust. The non-robust method performs the worst, due to its inconsideration of the channel uncertainties. The secrecy rate of the stricter outage tolerance $(\rho = 0.01)$ is higher than that of the relaxed outage tolerance $(\rho = 0.1)$. Figure 5.3 shows the secrecy rate performance of the three methods versus different error variance σ^2 based on the PCU model. The secrecy rates of all methods decrease along with the increase of the error variance. It can be observed that the proposed design method has the higher secrecy rate than other two methods. Also, the performance gap between the proposed design method and the worst-case method as well as the non-robust method becomes larger when the error variance σ^2 is bigger. Moreover, this

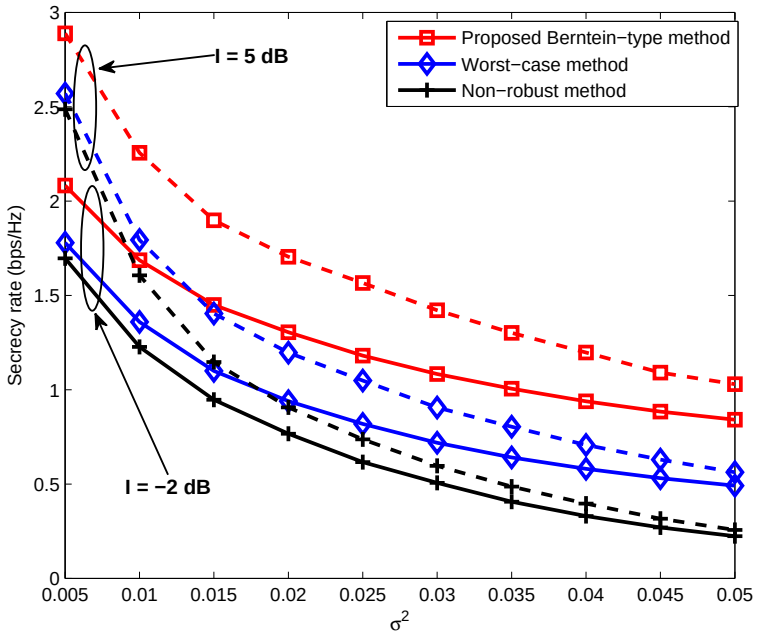

Fig. 5.3 The secrecy rate versus error variance σ^2 for the different interference power based on the PCU model with $\rho = 0.01$, $P = 6$ dB.

figure indicates that when the interference power tolerance of primary user is increased from $I = -2$ dB to $I = 5$ dB, all design methods can lead to high secrecy rate.

The results in Figure 5.4 indicate that the secrecy rate levels of all design methods increase as the transmit power becomes large, meanwhile the proposed Berntein-type method is also better than other two methods based on the PCU model. The performance gap between the perfect CSI method and the proposed method based on the PCU model (see Figure 5.2) is larger than the two methods based on the FCU model (see Figure 5.4) under the same simulation setting. This is because that system needs more power to overcome channel estimation and quantization errors for all channels. The results in Figure 5.5 indicate that the degradation trend of the secrecy rate of all methods based on the FCU model is similar with that of the PCU model. The proposed Berntein-type method based on the FCU model also outperforms the other two methods under any interference power tolerance.

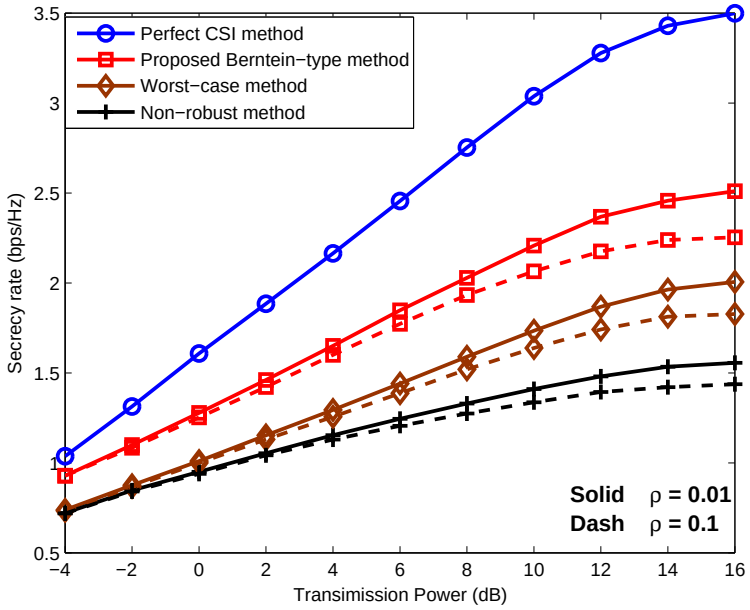

Fig. 5.4 The secrecy rate of the different methods versus the transmit power for different outage probability ρ based on the FCU model with $I = -2$ dB, $\sigma^2 = 0.005$.

5.6 Summary

This chapter investigates an OC-SRM problem for a MIMO-CR downlink network with SWIPT based on the two channel uncertainty models. In order to handle this non-convex problem, a safe approximation method is resorted to deal with the log det function and employ Berntein-type inequality approach to convert the outage constraints into the deterministic forms. After the conservative approximation, the original problem has been transformed to a tractable problem, which can be computed alternately by solving two convex subproblems. Simulation results show that the proposed safe design scheme outperforms worst-case scheme and non-robust scheme.

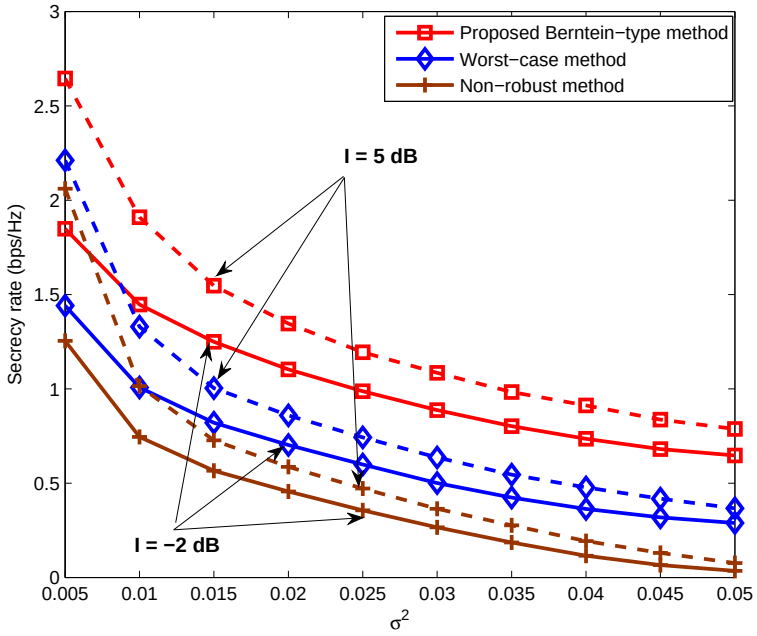

Fig. 5.5 The secrecy rate versus error variance σ^2 for the different interference power based on the FCU model with $\rho = 0.01$, $P = 6dB$.

Chapter 6

Robust Secrecy Design in MIMO Systems Based on a Non-linear EH Model

This chapter is organized as follows. The main contributions are first introduced in Section 6.1. The system model is presented in Section 6.2. The OC-SRM problem based on the PCU model is solved in Section 6.3. In Section 6.4, the OC-SRM problem is extended into the FCU model. Section 6.5 provides the computational complexity of the proposed approaches in the both channel uncertainty models. The performance of the proposed approaches is validated in Section 6.6. Conclusions are drawn in Section 6.7.

6.1 Introduction

In this chapter, a secure optimization issue is considered in a downlink MIMO-SWIPT scenario where non-linear ERs are considered as the potential eavesdroppers. Our main objective is to design the transmit signal covariance matrix based on a proposed OC-SRM problem while satisfying the secrecy rate outage constraints and the harvested energy outage constraints. In contrast to the deterministic design, the outage design provides the successful

transmission in the delay-critical scenario. The novel contributions of this chapter are summarized in the following:

- *Partial channel uncertainty (PCU) model.* In this model, the OC-SRM problem is formulated based on the assumption of Gaussian CSI errors for the ERs' channels. However, the formulated problem is non-convex due to the non-smooth secrecy rate function and complicated probabilistic constraints. The main difficulties stem from the probabilistic constraints that lack closed-form expressions in general. In order to tackle the challenges arising from probabilistic constraints, the date rate expressions between the transmitter and the ERs is transferred to the trace functions by using Fenchel conjugate arguments [116]. Then, the probabilistic constraints are solved without explicitly calculation. Specifically, three approaches proposed by [120] are adopted to convert the original problem to the safe approximation problem whose conservative solutions automatically satisfy the outage requirements of the original OC-SRM problem. Furthermore, an AO algorithm is proposed to alternately solve two convex conic optimization problems

- *Full channel uncertainty (FCU) model.* In this model, the OC-SRM problem is formulated under the assumption of Gaussian CSI errors for the information receiver's channel and the ERs' channels. Similar to the above model, the non-convexity of the formulated problem is caused by the probabilistic constraints, but with more complicated forms. Hence, the introduced three approaches in the above model still can be used to tackle the difficulty caused by the probabilistic constraints, but Fenchel conjugate arguments cannot be used to solve the rate terms since $\log|\cdot|$ functions are included in both data rate expressions. To surmount this difficulty, the inequality function in [117] is employed to approximate the determinant function to the trace function. In addition, the original OC-SRM problem can be transformed to the easily

handled problem, which only consists of LMI and SOC constraints. The bisection method [101] is used to efficiently solve the reformulated problem.

- The complexity order of the proposed AO algorithm and bisection method based on three approximation methods for the PCU model and the FCU model is analyzed, respectively.

6.2 Network Model

In this section, the system model and the problem formulation are introduced in the following parts.

6.2.1 Channel Model

In this chapter, a MIMO wiretap channel with SWIPT consisting of a transmitter, a IR and K ERs is considered in 6.1. The transmitter is equipped with $N_t \geq 1$ antennas. The IR and ERs

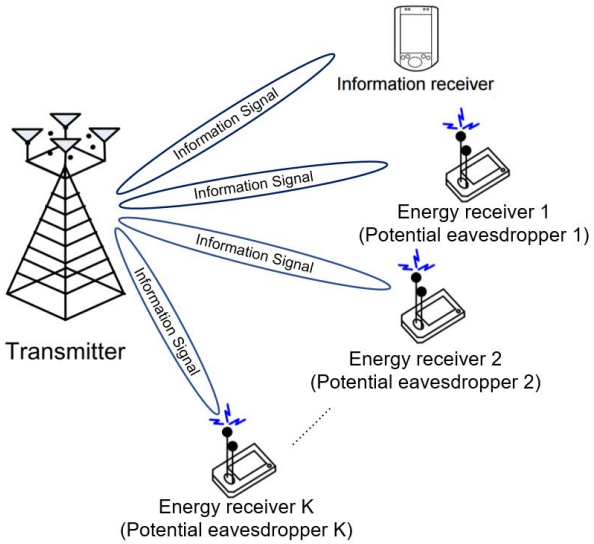

Fig. 6.1 An illustration for the considered secure SWIPT scenario.

are equipped with $N_d \geq 1$ and $N_e \geq 1$ antennas, respectively. Since multi-antenna techniques can significantly improve the system throughput without additional bandwidth and transmit power through spatial multiplexing, more antennas should be installed at the transmitters and receivers theoretically. In practical, the large number of antennas consumes high energy and makes signal processing complex. Using the advanced technologies and sustained energy supply can deal with these issues at the transmitter (base station), but they are difficult to be applied at the receivers, especially at the mobile terminal. Hence, in order to improve the system performance, it assumes that $N_t > N_d$ and $N_t > N_e$ in this chapter. The quasi-static frequency-flat fading channels from the transmitter to the IR and the k-th ER are denoted by $\mathbf{H}_d \in \mathbb{C}^{N_t \times N_d}$ and $\mathbf{G}_k \in \mathbb{C}^{N_t \times N_e}$. Then, the received signals at the IR and the k-th ER can be expressed as follows:

$$\mathbf{y}_d = \mathbf{H}_d \mathbf{x} + \mathbf{n}_d, \tag{6.1}$$

$$\mathbf{y}_k = \mathbf{G}_k \mathbf{x} + \mathbf{n}_k, \text{ for } k = 1, \ldots, K, \tag{6.2}$$

where $\mathbf{x}$ is the transmit signal vector following the distribution $\mathrm{CN}(0, \mathbf{Q})$; $\mathbf{Q} \in \mathbb{H}_+^{N_t}$ is the covariance of $\mathbf{x}$; $\mathbf{n}_d \sim \mathrm{CN}(0, \sigma_d^2 \mathbf{I}_{N_d})$ and $\mathbf{n}_k \sim \mathrm{CN}(0, \sigma_k^2 \mathbf{I}_{N_e})$ denote the additive Gaussian noises at the IR and the k-th ER, respectively. The security issue of the system should be taken into account since the transmitted information signal from the transmitter to the IR may be intercepted by the ERs, which are treated as potential eavesdroppers. Under the aforementioned system, the achievable secrecy rate for the considered scenario can be characterized as [30]

$$C_s = \left[\log \left| \mathbf{I}_d + \frac{1}{\sigma_d^2} \mathbf{H}_d \mathbf{Q} \mathbf{H}_d^H \right| - \max_k \log \left| \mathbf{I}_k + \frac{1}{\sigma_k^2} \mathbf{G}_k \mathbf{Q} \mathbf{G}_k^H \right| \right]^+ . \tag{6.3}$$

6.2.2 Energy Harvesting Model

According to the traditional SWIPT scenario, the ERs in the proposed system can resort the following linear model for EH:

$$E_k^{Linear} = \xi_k E_k, \;\; E_k = \mathrm{Tr}(\mathbf{G}_k \mathbf{Q} \mathbf{G}_k^H) + \sigma_k^2 N_e, \tag{6.4}$$

where E_k is the total received RF power at the k-th ER, and ξ_k is the energy conversion efficiency. From (6.4), it notes that the harvested energy is linearly proportional to the received RF power due to the independent relationship between the energy conversion efficiency and the input power level. However, there exist various non-linear characteristics in the end-to-end WPT in the practical RF-based EH circuits [122, 123]. In order to avoid the resource allocation mismatches caused by the linear EH model, the researchers designed a non-linear EH model in [124, 125]. Consequently, the total harvested energy based on the non-linear EH model at the k-th ER can be modeled as follows:

$$\begin{aligned} E_k^{Practical} &= \frac{\left[\frac{M_k}{1+\exp(-a_k(E_k-b_k))} - M_k\Omega_k\right]}{1-\Omega_k}, \\ \Omega_k &= \frac{1}{1+\exp(a_k b_k)} \end{aligned} \tag{6.5}$$

where M_k denotes the maximum harvested power as the EH circuit saturates, a_k and b_k are the constant values which are determined by the physical hardware phenomena [122–125].

6.2.3 Imperfect CSI Models

In practical wireless communication scenarios, perfect CSI of all receivers might not be practically obtained by the transmitter due to the system overhead and the channel estimation errors. In this chapter, the Gaussian channel error model is adopted to formulate the problem.

Two kinds of the Gaussian error models based on the different assumption are described in the following.

- **Partial Channel Uncertainty** : It assumes that the transmitter has imperfect CSI of ERs, as well as perfect CSI of ID. According to this assumption, the actual channel between the transmitter and the k-th ER can be modeled as follows:

$$\mathbf{G}_k = \widehat{\mathbf{G}}_k + \Delta\mathbf{G}_k, \forall_k, \tag{6.6}$$

  where $\widehat{\mathbf{G}}_k$ is estimated CSI of the k-th ER; $\Delta\mathbf{G}_k$ is the corresponding channel error, which follows the CSCG distribution, i.e., $\text{vec}(\Delta\mathbf{G}_k) \sim \text{CN}(0, \mathbf{C}_k)$, in which $\mathbf{C}_k$ is the positive semidefinite matrix.

- **Full Channel Uncertainty**: It assumes that the transmitter has imperfect CSI of both the IR and the ERs. The actual channel of the IR is modeled as

$$\mathbf{H}_d = \widehat{\mathbf{H}}_d + \Delta\mathbf{H}_d, \tag{6.7}$$

  where $\widehat{\mathbf{H}}_d$ is estimated CSI of the IR; $\Delta\mathbf{H}_d$ is the corresponding channel error, i.e., $\text{vec}(\Delta\mathbf{H}_d) \sim \text{CN}(0, \mathbf{E}_d)$, in which $\mathbf{E}_d$ is the positive semidefinite matrix.

6.2.4 Optimization Problem Formulation

Under the aforementioned system assumptions and setups, the OC-SRM problem can be formulated as follows:

$$\max_{\mathbf{Q},R} R \tag{6.8a}$$

$$s.t.\ \Pr\left\{C_s \geq R\right\} \geq 1-p, \tag{6.8b}$$

$$\Pr\left\{\frac{\left[\frac{M_k}{1+\exp(-a_k(E_k-b_k))}-M_k\Omega_k\right]}{1-\Omega_k} \geq \eta_k\right\} \geq 1-l_k, \forall_k, \tag{6.8c}$$

$$\mathrm{Tr}(\mathbf{Q}) \leq P, \quad \mathbf{Q} \succeq \mathbf{0}, \tag{6.8d}$$

where p and l_k denote the maximal outage probability of the secrecy rate and the harvested energy of the k-th ER, respectively. Probability constraint (6.8b) ensures that the probability for successfully transmitted signal to the IR needs to be keep above $(1-p)$. The similar interpretation also can be applied to describe (6.8c) with the minimum required EH target η_k. The main difficulty of solving problem (6.8) lies in the probability operator, which has no close-form expression. Even if it has, it seems computationally intractable. In the following two sections, the problem (6.8) will be solved based on the two Gaussian error models.

6.3 Robust Design in PCU Model

In this section, the OC-SRM problem (6.8) is designed and solved under the PCU model. Since the main difficulty of solving the problem (6.8) is the probabilistic constraints in (6.8b) and (6.8c), our task is to find out the safe approximation of the problem (6.8). The meaning of the safe approximation is to develop the computationally tractable upper bounds on the

probabilistic constraints. According to the technical challenge proposed in [120], it knows that if there exists a function $f(\mathbf{Q},\mathbf{r},s)$, satisfies

$$\Pr\{\mathbf{e}^H\mathbf{Q}\mathbf{e}+2\Re\{\mathbf{e}^H\mathbf{r}\}+s<0\}\leq f(\mathbf{Q},\mathbf{r},s), \tag{6.9}$$

It has the following implication

$$f(\mathbf{Q},\mathbf{r},s)\leq\rho\Longrightarrow\Pr\{\mathbf{e}^H\mathbf{Q}\mathbf{e}+2\Re\{\mathbf{e}^H\mathbf{r}\}+s\geq 0\}\geq 1-\rho. \tag{6.10}$$

The probability function in (6.10) is the probability of a complex Gaussian quadratic form. $f(\mathbf{Q},\mathbf{r},s)$ is the upper bound of the probability function in (6.10). Based on (6.9) and (6.10), the secrecy rate probabilistic constraint in (6.8b) and the EH probabilistic constraint in (6.8c) can be solved by solving their upper bound. However, the probability function in (6.8b) is still not the the probability of a complex Gaussian quadratic form due to the $\log|\cdot|$ function and the max function. Hence, the max function and the $\log|\cdot|$ function in (6.8b) need to be solved firstly. Since the channels of the ERs are independent from each other, the secrecy probabilistic constraint (6.8b) can be decoupled to the following constraint

$$\text{(6.8b)}\Longleftrightarrow\Pi_{k=1}^{K}Pr\{C_s\geq R\}\geq 1-p\Longleftarrow Pr\{C_s\geq R\}\geq 1-\bar{p}, \tag{6.11}$$

where $\bar{p}=1-(1-p)^{1/K}$. It notes that the last inequality in (6.11) can be considered as a per-ER secrecy probability. The next endeavour is to convert the $\log|\cdot|$ function into the easily handled function by using Fenchel conjugate arguments lemma [116], which has introduced in the Lemma 4 of chapter 4. Based on Lemma 4, the data rate between the

transmitter and the k-th ER can be reformulated as follows:

$$
\begin{aligned}
-\log\left|\left(\mathbf{I}_{N_e}+\frac{1}{\sigma_k^2}\mathbf{G}_k\mathbf{Q}\mathbf{G}_k^H\right)^{-1}\right| &= \min_{\mathbf{S}_k\succeq 0}\left(\mathrm{Tr}\left(\mathbf{S}_k(\mathbf{I}_{N_e}+\frac{1}{\sigma_k^2}\mathbf{G}_k\mathbf{Q}\mathbf{G}_k^H)\right)-\ln|\mathbf{S}_k|-N_e\right), \\
&= \min_{\mathbf{S}_k\succeq 0} g(\mathbf{S}_k,\mathbf{Q}) \qquad (6.12)
\end{aligned}
$$

where $\mathbf{S}_k$ is the auxiliary variable. The merit of this transformation is that the channel error part is transferred from the $\log|\cdot|$ function to the trace function, which is easily handled. Substituting (6.12) into the secrecy rate probabilistic constraint in (6.8b), it has

$$
\begin{aligned}
&\Pr\{C_s\geq R\}\geq 1-\bar{p} \\
&\overset{(a)}{\Longleftrightarrow}\Pr\left\{\min_{\mathbf{S}_k\succeq 0} g(\mathbf{S}_k,\mathbf{Q})\leq \log\left|\mathbf{I}_d+\frac{1}{\sigma_d^2}\mathbf{H}_d\mathbf{Q}\mathbf{H}_d^H\right|-R\right\}\geq 1-\bar{p}, \\
&\overset{(b)}{\Longleftarrow}\Pr\left\{g(\mathbf{S}_k,\mathbf{Q})\leq \log\left|\mathbf{I}_d+\frac{1}{\sigma_d^2}\mathbf{H}_d\mathbf{Q}\mathbf{H}_d^H\right|-R\right\}\geq 1-\bar{p} \\
&\Longleftrightarrow\Pr\left\{\frac{1}{\sigma_k^2}\mathrm{Tr}(\mathbf{S}_k\mathbf{G}_k\mathbf{Q}\mathbf{G}_k^H)\leq ss_k\right\}\geq 1-\bar{p}, \qquad (6.13)
\end{aligned}
$$

where $ss_k=\log\left|\mathbf{I}_d+\frac{1}{\sigma_d^2}\mathbf{H}_d\mathbf{Q}\mathbf{H}_d^H\right|-R+\log|\mathbf{S}_k|+N_e-\mathrm{Tr}(\mathbf{S}_k)$. Note that (a) is due to the equation (6.12); (b) indicates that if $g(\mathbf{S}_k,\mathbf{Q})$ satisfies the condition then $\min_{\mathbf{S}_k\succeq 0} g(\mathbf{S}_k,\mathbf{Q})$ certainly satisfies the condition. By substituting the actual channel in (6.6) into (6.13), it has

$$
\Pr\left\{\frac{1}{\sigma_k^2}\mathrm{Tr}(\mathbf{S}_k(\widehat{\mathbf{G}}_k+\Delta\mathbf{G}_k)\mathbf{Q}(\widehat{\mathbf{G}}_k+\Delta\mathbf{G}_k)^H)\leq ss_k\right\}\geq 1-\bar{p},\forall_k. \qquad (6.14)
$$

The expression in (6.14) is still different from the probability function in (6.10). Thus, the following matrix identities are considered

$$
\begin{aligned}
\mathrm{vec}(\mathbf{AXB}) &= (\mathbf{B}^T\otimes\mathbf{A})\mathrm{vec}(\mathbf{X}), \\
\mathrm{tr}(\mathbf{A}^T\mathbf{B}) &= \mathrm{vec}(\mathbf{A})^T\mathrm{vec}(\mathbf{B}), \\
(\mathbf{A}\otimes\mathbf{B})^T &= \mathbf{A}^T\otimes\mathbf{B}^T. \qquad (6.15)
\end{aligned}
$$

Based on the above identities, (6.14) can be reformulated as follow:

$$\Pr\left\{\mathbf{e}_k^H(\mathbf{Q}^T\otimes\mathbf{S}_k)\mathbf{e}_k+2\Re\{\mathbf{e}_k^H(\mathbf{Q}^T\otimes\mathbf{S}_k)\widehat{\mathbf{g}}_k\}+s_k\leq 0\right\}\geq 1-\bar{p}, \tag{6.16}$$

where $s_k=\widehat{\mathbf{g}}_k^H(\mathbf{Q}^T\otimes\mathbf{S}_k)\widehat{\mathbf{g}}_k-\sigma_k^2\Big(\ln|\mathbf{S}_k|-\mathrm{Tr}(\mathbf{S}_k)+N_e-R+\log|\mathbf{I}_d+\frac{1}{\sigma_d^2}\mathbf{H}_d\mathbf{Q}\mathbf{H}_d^H|\Big)$; $\mathbf{e}_k=\mathrm{vec}(\Delta G_k)$; $\widehat{\mathbf{g}}_k=\mathrm{vec}(\widehat{\mathbf{G}}_k)$. Since $\mathbf{e}_k\sim\mathrm{CN}(0,\mathbf{C}_k)$, $\mathbf{e}_k$ can be expressed by the Gaussian random vector $\mathbf{v}_k\sim\mathrm{CN}(0,\mathbf{I}_{N_t\times N_e})$, such that $\mathbf{e}_k=\mathbf{C}_k^{\frac{1}{2}}\mathbf{v}_k$. Thus, the probability constraint in (6.16) can be equivalently reformulated as follows:

$$\Pr\left\{-\mathbf{v}_k^H\mathbf{C}_k^{\frac{1}{2}}(\mathbf{Q}^T\otimes\mathbf{S}_k)\mathbf{C}_k^{\frac{1}{2}}\mathbf{v}_k-2\Re\{\mathbf{v}_k^H\mathbf{C}_k^{\frac{1}{2}}(\mathbf{Q}^T\otimes\mathbf{S}_k)\widehat{\mathbf{g}}_k\}-s_k\geq 0\right\}\geq 1-\bar{p},\ \ \forall_k. \tag{6.17}$$

Similarly, the EH outage constraint of the k-th ER in (6.8c) can be expressed as follows:

$$\Pr\left\{\mathbf{v}_k^H\mathbf{C}_k^{\frac{1}{2}}(\mathbf{Q}^T\otimes\mathbf{I})\mathbf{C}_k^{\frac{1}{2}}\mathbf{v}_k+2\Re\{\mathbf{v}_k^H\mathbf{C}_k^{\frac{1}{2}}(\mathbf{Q}^T\otimes\mathbf{I})\widehat{\mathbf{g}}_k\}+d_k\geq 0\right\}\geq 1-l_k,\ \ \forall_k, \tag{6.18}$$

where $d_k=\widehat{\mathbf{g}}_k^H(\mathbf{Q}^T\otimes\mathbf{I})\widehat{\mathbf{g}}_k+\sigma_k^2N_e+\frac{1}{a_k}\log\left(\frac{(M_k-\eta_k)\exp(a_kb_k)}{\eta_k\exp(a_k)+M_k}\right)-b_k$. It is interesting to point out that probability function in (6.17) and (6.18) is the probability of a complex Gaussian quadratic term $\mathbf{v}_k$. Hence, the probability function in (6.17) and (6.18) can be tackled by solving their upper bound. In the sequel, three approaches are derived to find out the safe approximation of the probabilistic constraints.

6.3.1 Bernstein-Type Inequality Safe Approximation

In this subsection, BTI approach is adopted to find out the safe approximation on the probabilistic constraints. The merit of BTI approach is that the computationally intractable probabilistic constraint can be equivalently expressed by its safe approximation constraint, which only contains the SOC constraint and LMI constraint.

Based on BTI approach derived in Lemma 5, the safe approximation of the probabilistic constraint in (6.17) can be expressed by

$$\begin{cases} \mathrm{Tr}(\mathbf{C}_k^{\frac{1}{2}}(\mathbf{Q}^T\otimes\mathbf{S}_k)\mathbf{C}_k^{\frac{1}{2}})+\sqrt{-2\ln(\bar{p})}\lambda_k-\ln(\bar{p})\mu_k+s_k\leq 0, \\ \left\| \begin{bmatrix} \mathrm{vec}(\mathbf{C}_k^{\frac{1}{2}}(\mathbf{Q}^T\otimes\mathbf{S}_k)\mathbf{C}_k^{\frac{1}{2}}) \\ \sqrt{2}\mathbf{C}_k^{\frac{1}{2}}(\mathbf{Q}^T\otimes\mathbf{S}_k)\widehat{\mathbf{g}}_k \end{bmatrix} \right\| \leq \lambda_k, \\ \mu_k\mathbf{I}_{N_t\times N_e}-\mathbf{C}_k^{\frac{1}{2}}(\mathbf{Q}^T\otimes\mathbf{S}_k)\mathbf{C}_k^{\frac{1}{2}}\succeq 0, \quad \mu_k\geq 0, \quad \forall_k. \end{cases} . \tag{6.19}$$

Similarly, the safe approximation of the EH probabilistic constraint in (6.18) can be transformed into the following form:

$$\begin{cases} \mathrm{Tr}(\mathbf{C}_k^{\frac{1}{2}}(\mathbf{Q}^T\otimes\mathbf{I})\mathbf{C}_k^{\frac{1}{2}})-\sqrt{-2\ln(l_k)}\alpha_k+\ln(l_k)\beta_k+d_k\geq 0, \\ \left\| \begin{bmatrix} \mathrm{vec}(\mathbf{C}_k^{\frac{1}{2}}(\mathbf{Q}^T\otimes\mathbf{I})\mathbf{C}_k^{\frac{1}{2}}) \\ \sqrt{2}\mathbf{C}_k^{\frac{1}{2}}(\mathbf{Q}^T\otimes\mathbf{I})\widehat{\mathbf{g}}_k \end{bmatrix} \right\| \leq \alpha_k, \\ \beta_k\mathbf{I}_{N_t\times N_e}+\mathbf{C}_k^{\frac{1}{2}}(\mathbf{Q}^T\otimes\mathbf{I})\mathbf{C}_k^{\frac{1}{2}}\succeq \mathbf{0}, \ \beta_k\geq 0, \ \forall_k. \end{cases} . \tag{6.20}$$

Replacing the constraint in (6.8b) and (6.8c) by the constraints in (6.19) and (6.20), the original problem in (6.8) can be reformulated by

$$\begin{aligned} \max_{\mathbf{Q},\mathbf{S}_k,R,\lambda_k,\mu_k,\alpha_k,\beta_k} \quad & R \\ s.t. \quad & (6.19),(6.20),\mu_k\geq 0,\beta_k\geq 0,\mathrm{tr}(\mathbf{Q})\leq P,\mathbf{Q}\succeq\mathbf{0},\mathbf{S}_k\succeq\mathbf{0}. \end{aligned} \tag{6.21}$$

Note that problem in (6.21) is the safe approximation of the original problem (6.8). Based on the condition in (6.10), it can be verified that any feasible solution to problem (6.21) satisfies the probabilistic constraints in problem (6.8). Note that problem in (6.21) is nonconvex w.r.t. all the variables jointly [101]. However, problem in (6.21) becomes convex when fixing either $\mathbf{Q}$ or $\mathbf{S}_k$. Hence, an AO algorithm is proposed to optimize all variables in (6.21) [126]. Specifically, the problem in (6.21) becomes a convex SDP problem by fixing $\mathbf{S}_k$. Then, the

Algorithm 6.1 Proposed AO algorithm for OC-SRM problem by using BTI safe approximation under the PCU model

1. **Initialize:** Set $n = 1$, $\varepsilon > 0$ and $\mathbf{S}_k^0 = \mathbf{I}$, $k = 1, \ldots, K$;
2. **Repeat**
   (a) Given fixed $\mathbf{S}_k^{n-1}$, solve (6.21) to obtain $(\mathbf{Q}^{n-1},\ \mathbf{R}^{n-1})$;
   (b) Given fixed $\mathbf{Q}^{n-1}$ solve (6.21) to obtain $(\mathbf{S}_k^n,\ \mathbf{R}^n)$;
   (c) n = n+1;
3. **Until** $|\mathbf{R}^n - \mathbf{R}^{n-1}| < \varepsilon$.
4. Output the solution.

same operation can be considered to optimize $\mathbf{S}_k$. The summarization of the proposed AO algorithm is presented in Algorithm 6.1.

It notes that the convex problems in step $a)$ and $b)$ can be efficiently solved by using off-the-shelf solver, e.g., CVX [105]. Moveover, the solutions obtained at the $n-1$st iteration are the feasible solutions at the nth iteration in Algorithm 6.1, which yields a nondecreasing objective value of (6.21). Hence, the proposed AO algorithm stop when the returned value achieves the predefined accuracy ε.

6.3.2 S-Procedure Safe Approximation

In this subsection, an alternative approach, which is based on robust optimization techniques, is derived to obtain the safe approximation on the probabilistic constraints. This main idea of this approach is to choose the channel uncertainty region satisfying the probability of the secrecy rate. The following lemma can be used to find out the safe approximation of the probabilistic constraints (6.17) and (6.18).

Lemma 6. *[120] Consider a set $S \subset \mathbb{C}^{N_T \times 1}$ always satisfying $\Pr\{\mathbf{e} \in S\} \geq 1-\rho$, where $e \sim \mathscr{CN}(0, \mathbf{I})$. The following implication holds true:*

$$\mathbf{e}^H\mathbf{A}\mathbf{e} + 2\mathfrak{R}\{\mathbf{e}^H\mathbf{r}\} + \theta \geq 0, \text{for all } \mathbf{e} \in S \Longrightarrow \Pr\{\mathbf{e}^H\mathbf{A}\mathbf{e} + 2\mathfrak{R}\{\mathbf{e}^H\mathbf{r}\} + \theta \geq 0\} \geq 1-\rho. \quad (6.22)$$

The left hand side of (6.22) is the safe approximation of the probabilistic function on the right hand side. The merit of Lemma 6 is using the deterministic model to represent the probabilistic model and freedom choosing the set S. Based on Lemma 6, the secrecy probabilistic constraint (6.17) can be converted into the following deterministic quadratic form

$$-\mathbf{v}_k^H \mathbf{C}_k^{\frac{1}{2}} (\mathbf{Q}^T \otimes \mathbf{S}_k) \mathbf{C}_k^{\frac{1}{2}} \mathbf{v}_k - 2\Re\{\mathbf{v}_k^H \mathbf{C}_k^{\frac{1}{2}} (\mathbf{Q}^T \otimes \mathbf{S}_k) \widehat{\mathbf{g}}_k\} - s_k \geq 0, \forall_k. \tag{6.23}$$

The Gaussian random vector $\mathbf{v}_k$ belongs to the following set

$$S = \{\mathbf{v}_k | \Pr\{\mathbf{v}_k^H \mathbf{v}_k \leq \gamma_k^2\} \geq 1 - l_k\}, \tag{6.24}$$

where the channel uncertainty region γ_k can be expressed by the inverse CDF of the Chi-square random variable with $2N_tN_e$ degrees of freedom (DoF) $F^{-1}_{2N_tN_e}(a)$, such as $\gamma_k = \sqrt{\frac{F^{-1}_{2N_eN_t}(1-l_k)}{2}}$. By employing Lemma 6, the probabilistic constraint of vector $\mathbf{v}_k$ in (6.24) can be expressed by its deterministic constraint

$$-\mathbf{v}_k^H \mathbf{v}_k + \gamma_k^2 \geq 0, \quad \forall_k. \tag{6.25}$$

According to the inequality (6.23) and (6.25), the secrecy probabilistic constraint (6.17) can be equivalently reformulated into the following set of inequalities:

$$\begin{cases} -\mathbf{v}_k^H \mathbf{C}_k^{\frac{1}{2}} (\mathbf{Q}^T \otimes \mathbf{S}_k) \mathbf{C}_k^{\frac{1}{2}} \mathbf{v}_k - 2\Re\{\mathbf{v}_k^H \mathbf{C}_k^{\frac{1}{2}} (\mathbf{Q}^T \otimes \mathbf{S}_k) \widehat{\mathbf{g}}_k\} - s_k \geq 0, \\ -\mathbf{v}_k^H \mathbf{v}_k + \gamma_k^2 \geq 0. \end{cases} \tag{6.26}$$

The above set can be transformed into a more tractable LMI form by using the following *S-procedure* lemma, which has been introduced in the Lemma 3 of chapter 3. By exploiting the *S-Procedure* lemma, the secrecy probabilistic constraint (6.17) can be reformulated as

the following LMIs with any positive μ_k,

$$\begin{bmatrix} \mu_k \mathbf{I}_{N_e \times N_t} - \mathbf{C}_k^{\frac{1}{2}} (\mathbf{Q}^T \otimes \mathbf{S}_k) \mathbf{C}_k^{\frac{1}{2}} & -\mathbf{C}_k^{\frac{1}{2}} (\mathbf{Q}^T \otimes \mathbf{S}_k) \widehat{\mathbf{g}}_k \\ -\widehat{\mathbf{g}}_k^H (\mathbf{Q}^T \otimes \mathbf{S}_k) \mathbf{C}_k^{\frac{1}{2}} & -s_k - \mu_k \gamma_k^2 \end{bmatrix} \succeq \mathbf{0}, \forall_k, \tag{6.27}$$

Similarly, the EH probabilistic constraint of the k-th ER in (6.18) can be transformed to the following LMIs,

$$\begin{bmatrix} \lambda_k \mathbf{I}_{N_e \times N_t} + \mathbf{C}_k^{\frac{1}{2}} (\mathbf{Q}^T \otimes \mathbf{I}) \mathbf{C}_k^{\frac{1}{2}} & \mathbf{C}_k^{\frac{1}{2}} (\mathbf{Q}^T \otimes \mathbf{I}) \widehat{\mathbf{g}}_k \\ \widehat{\mathbf{g}}_k^H \mathbf{C}_k^{\frac{1}{2}} (\mathbf{Q}^T \otimes \mathbf{I}) & d_k - \lambda_k \gamma_k^2 \end{bmatrix} \succeq \mathbf{0}, \forall_k. \tag{6.28}$$

After transformation and approximation, the original problem (6.8) can be reformulated by

$$\begin{aligned} &\max_{\mathbf{Q}, \mathbf{S}_k, R, \mu_k, \lambda_k} \quad R \\ &s.t. \quad (6.27), (6.28), \mu_k \geq 0, \lambda_k \geq 0, \mathrm{tr}(\mathbf{Q}) \leq P, \mathbf{Q} \succeq \mathbf{0}, \mathbf{S}_k \succeq \mathbf{0}. \end{aligned} \tag{6.29}$$

However, problem (6.29) is still not jointly convex for all variables [101]. The AO algorithm proposed in the above subsection can also be employed to solve problem (6.29). The processing of solving (6.29) by using the AO algorithm is similar to Algorithm 6.1. Hence, the summarization and convergence analysis for the application of the AO algorithm are omitted here due to the space limitation.

6.3.3 Large Deviation Inequality Safe Approximation

Although *S-Procedure* approach has the lower complexity compared with *BTI* approach, both approaches need to convert the original problem to the SDP problem, which are polynomial-time solvable [101]. The processing time for solving the SDP problem depends on the size of the LMI constraints. Hence, a simpler approach, which can transfer the problem only

including SOC constraints, is derived. This approach is designed based on the theory of the decomposition-based Large Deviation Inequality (LDI), which decomposes a sum of dependent random variables into sums of independent random variables [127, 128]. The specific approach is shown in the following lemma.

Lemma 7. *[120] Fixing the Gaussian random vector* $\mathbf{x} \sim \mathrm{CN}(0, \mathbf{I})$*, a matrix* $\mathbf{A} \in \mathbb{H}^{n \times n}$ *and a vector* $\mathbf{r} \in \mathbb{C}^n$*, if exist any* $v > \frac{1}{\sqrt{2}}$ *and* $\zeta > 0$*, it has*

$$Pr\{\mathbf{x}^H\mathbf{A}\mathbf{x} + 2\Re\{\mathbf{x}^H\mathbf{r}\} \leq \mathrm{tr}(\mathbf{A}) - \zeta\} \leq \begin{cases} \exp\left(-\dfrac{\zeta^2}{4T^2}\right) & 0 < \zeta \leq 2\bar{v}vT \\ \exp\left(-\dfrac{\bar{v}v\zeta}{T} + (\bar{v}v)^2\right) & \zeta > 2\bar{v}vT \end{cases}, \tag{6.30}$$

where $\bar{v} = 1 - \frac{1}{2v^2}$ *and* $T = v\|\mathbf{A}\| + \frac{1}{\sqrt{2}}\|\mathbf{r}\|$.

In order to employ the *LDI* approach in Lemma 7 to the secrecy outage constraint (6.17), it obtains the following sets

$$\zeta_k = \mathrm{tr}\left(-\mathbf{C}_k^{\frac{1}{2}}(\mathbf{Q}^T \otimes \mathbf{S}_k)\mathbf{C}_k^{\frac{1}{2}}\right) - s_k, \tag{6.31}$$

$$T_k = v\|-\mathbf{C}_k^{\frac{1}{2}}(\mathbf{Q}^T \otimes \mathbf{S}_k)\mathbf{C}_k^{\frac{1}{2}}\|_F + \frac{1}{\sqrt{2}}\|-\mathbf{C}_k^{\frac{1}{2}}(\mathbf{Q}^T \otimes \mathbf{S}_k)\widehat{\mathbf{g}}_k\|, \tag{6.32}$$

where v is the solution of the quadratic equation $(1 - 1/(2v^2))v = \sqrt{\ln(1/\bar{p})}$. Since the value of $(1 - 1/(2v^2))v$ is greater than zero and $(1 - 1/(2v^2))v$ is a monotonically increasing function of v within the domain, thus $v > \frac{1}{\sqrt{2}}$ is satisfied. By defining $\bar{v} = (1 - 1/(2v^2))$, It concludes that $\bar{p} = \exp(-(\bar{v}v)^2)$. By utilizing Lemma 5, the secrecy probability function

(6.17) can be expressed as the following two probability functions

$$\Pr\left\{-\mathbf{v}_k^H\mathbf{C}_k^{\frac{1}{2}}(\mathbf{Q}^T\otimes\mathbf{S}_k)\mathbf{C}_k^{\frac{1}{2}}\mathbf{v}_k-2\Re\left\{\mathbf{v}_k^H\mathbf{C}_k^{\frac{1}{2}}(\mathbf{Q}^T\otimes\mathbf{S}_k)\widehat{\mathbf{g}}_k\right\}-s_k\leq 0\right\}\leq\exp\left(-\frac{\zeta_k^2}{4T_k^2}\right)$$
$$=\exp(\ln(\bar{p}))=\bar{p},\forall_k, \quad (6.33a)$$
$$\Pr\left\{-\mathbf{v}_k^H\mathbf{C}_k^{\frac{1}{2}}(\mathbf{Q}^T\otimes\mathbf{S}_k)\mathbf{C}_k^{\frac{1}{2}}\mathbf{v}_k-2\Re\{\mathbf{v}_k^H\mathbf{C}_k^{\frac{1}{2}}(\mathbf{Q}^T\otimes\mathbf{S}_k)\widehat{\mathbf{g}}_k\}-s_k\leq 0\right\}\leq\exp\left(-\frac{\bar{v}v\zeta_k}{T}+(\bar{v}v)^2\right)$$
$$<\exp\left(-(\bar{v}v)^2\right)=\bar{p},\forall_k. \quad (6.33b)$$

Notice that (6.33a) and (6.17) are equivalent when $\zeta_k=2\sqrt{-\ln(\bar{p})}T_k$ within the interval $(0,2\bar{v}vT_k]$ is chosen. Similarly, if $\zeta_k>2\sqrt{-\ln(\bar{p})}T_k$ from $(2\bar{v}vT_k,+\infty)$ is chosen, the probabilistic constraint (6.17) is still satisfied. Combining these two conditions, the safe function $f(\mathbf{Q},\mathbf{r},s)$ of (6.17) can be found when $\zeta_k\geq 2\sqrt{-\ln(\bar{p})}T_k$ is chosen. Substituting ζ_k into (6.31), it gets the following restriction function

$$\mathrm{tr}(-\mathbf{C}_k^{\frac{1}{2}}(\mathbf{Q}^T\otimes\mathbf{S}_k)\mathbf{C}_k^{\frac{1}{2}})+c_k\geq 2\sqrt{-\ln(\bar{p})}T_k,\forall_k. \quad (6.34)$$

According to equation in (6.32), T_k consists of two SOC functions. Hence, the above convex restriction of (6.17) can be decomposed into the following three constraints

$$\begin{cases}\mathrm{Tr}\left(-\mathbf{C}_k^{\frac{1}{2}}(\mathbf{Q}^T\otimes\mathbf{S}_k)\mathbf{C}_k^{\frac{1}{2}}\right)+c_k\geq 2\sqrt{-\ln(\bar{p})}(\mu_k+\lambda_k),\forall_k,\\ v\left\|\mathrm{vec}(-\mathbf{C}_k^{\frac{1}{2}}(\mathbf{Q}^T\otimes\mathbf{S}_k)\mathbf{C}_k^{\frac{1}{2}})\right\|\leq\mu_k,\forall_k,\\ \frac{1}{\sqrt{2}}\left\|-\mathbf{C}_k^{\frac{1}{2}}(\mathbf{Q}^T\otimes\mathbf{S}_k)\widehat{\mathbf{g}}_k\right\|\leq\lambda_k,\forall_k,\end{cases} \quad (6.35)$$

where $\mu_k,\lambda_k\in\mathbb{R},\forall_k$ are slack variables. With the setting $\zeta_k=\mathrm{Tr}(\mathbf{C}_k^{\frac{1}{2}}(\mathbf{Q}^T\otimes\mathbf{I})\mathbf{C}_k^{\frac{1}{2}})+d_k$ and $T_k=v\left\|\mathbf{C}_k^{\frac{1}{2}}(\mathbf{Q}^T\otimes\mathbf{I})\mathbf{C}_k^{\frac{1}{2}}\right\|_F+\frac{1}{\sqrt{2}}\|\mathbf{C}_k^{\frac{1}{2}}(\mathbf{Q}^T\otimes\mathbf{I})\widehat{\mathbf{g}}_k\|$, the safe approximations of the EH probabilistic

constraint (6.18) can be expressed as follows by using Lemma5

$$\begin{cases} \mathrm{Tr}\left(\mathbf{C}_k^{\frac{1}{2}}(\mathbf{Q}^T\otimes\mathbf{I})\mathbf{C}_k^{\frac{1}{2}}\right)+d_k\geq 2\sqrt{-\ln(l_k)}(\alpha_k+\beta_k),\forall_k, \\ a\left\|\mathbf{C}_k^{\frac{1}{2}}(\mathbf{Q}^T\otimes\mathbf{I})\mathbf{C}_k^{\frac{1}{2}}\right\|_F\leq\alpha_k,\forall_k, \\ \frac{1}{\sqrt{2}}\left\|\mathbf{C}_k^{\frac{1}{2}}(\mathbf{Q}^T\otimes\mathbf{I})\widehat{\mathbf{g}}_k\right\|\leq\beta_k,\forall_k, \end{cases} \tag{6.36}$$

where α_k and β_k are slack variables; a is the solution of the quadratic equation $(1-1/(2a^2))a=\sqrt{\ln(1/l_k)}$.

Replacing the probabilistic constraints (6.8b) and (6.8c) by the determinant constraints (6.35) and (6.36), the original OC-SRM problem (6.8) can be reformulated as follows:

$$\begin{aligned} &\max_{\mathbf{Q},\mathbf{S}_k,R,\mu,\lambda,\alpha,\beta} \quad R \\ &\quad s.t. \qquad (6.35),\ (6.36), \mathrm{tr}(\mathbf{Q})\leq P,\ \mathbf{Q}\succeq\mathbf{0},\ \mathbf{S}_k\succeq\mathbf{0}. \end{aligned} \tag{6.37}$$

Similar to the problem (6.21) and (6.29), problem (6.37) can be alternately solved by using AO the algorithm. The processing of the AO algorithm of the *LDI* approach is similar with Algorithm 6.1.

6.4 Robust Design in FCU Model

In this section, a more challenging case is investigated where the transmitter has the knowledge about the distribution of errors at all the receivers only. Comparing with the PCU model, the FCU model is more difficult to be handled since the channel estimation errors exist in the both rate terms in the secrecy rate function. The probabilistic constraint needs to be transferred to the standard ones (6.10) in order to find out the safe approximation of the probabilistic constraint. However, Fenchel conjugate arguments introduced in the

above section cannot be used to tackle the rate terms in (6.8b). Hence, the approximation of determinant function in [117] is adopted to solve this issue.

According to [117], if there exists a nonnegative matrix $\mathbf{A} \in \mathbb{C}^{m\times m}$, the determinant of matrix $\mathbf{A}$ satisfies the following inequality

$$\det(\mathbf{I}+\mathbf{A}) \geq 1+\lambda_{max}(\mathbf{A}) \geq 1+\frac{1}{m}\mathrm{Tr}(\mathbf{A}). \tag{6.38}$$

Based on (6.38), the both date terms in (6.8) can be approximated to the following functions

$$\begin{aligned}
\log\left|\mathbf{I}_d+\frac{1}{\sigma_d^2}\mathbf{H}_d\mathbf{Q}\mathbf{H}_d^H\right| &\approx \log\left(1+\frac{1}{N_d\sigma_d^2}\mathrm{Tr}(\mathbf{H}_d\mathbf{Q}\mathbf{H}_d^H)\right),\\
\log\left|\mathbf{I}_k+\frac{1}{\sigma_k^2}\mathbf{G}_k\mathbf{Q}\mathbf{G}_k^H\right| &\approx \log\left(1+\frac{1}{\sigma_k^2 N_e}\mathrm{Tr}(\mathbf{G}_k\mathbf{Q}\mathbf{G}_k^H)\right),\forall_k.
\end{aligned} \tag{6.39}$$

By replacing the secrecy function in (6.8b) with (6.39) and substituting the actual channels, the secrecy rate probabilistic constraint (6.8b) can be reformulated as follows:

$$\begin{aligned}
\Pr\Bigg\{&\frac{\mathbf{e}_d^H(\mathbf{Q}^T\otimes\mathbf{I})\mathbf{e}_d+2\Re\left\{\mathbf{e}_d^H(\mathbf{Q}^T\otimes\mathbf{I})\mathbf{h}_d\right\}+\mathbf{h}_d^H(\mathbf{Q}^T\otimes\mathbf{I})\mathbf{h}_d}{N_d\sigma_d^2}\\
&-\frac{e^R\left(\mathbf{e}_k^H(\mathbf{Q}^T\otimes\mathbf{I})\mathbf{e}_k+2\Re\left\{\mathbf{e}_k^H(\mathbf{Q}^T\otimes\mathbf{I})\widehat{\mathbf{g}}_k\right\}+\widehat{\mathbf{g}}_k^H(\mathbf{Q}^T\otimes\mathbf{I})\widehat{\mathbf{g}}_k\right)}{N_e\sigma_k^2} \geq e^R-1\Bigg\} \geq 1-\bar{p},\ \ \forall_k.
\end{aligned} \tag{6.40}$$

With the error definitions $\mathbf{e}_k = \mathbf{C}_k^{\frac{1}{2}}\mathbf{v}_k$, $\mathbf{v}_k \sim \mathrm{CN}(0, \mathbf{I}_{N_t \times N_e})$ and $\mathbf{e}_d = \mathbf{E}_d^{\frac{1}{2}}\mathbf{v}_d$, $\mathbf{v}_d \sim \mathscr{CN}(0, \mathbf{I}_{N_t \times N_d})$, the above probability constraint can be expressed in a matrix form as follows:

$$\begin{aligned}
\Pr\Bigg\{ & \begin{bmatrix} \mathbf{v}_d^H, \mathbf{v}_k^H \end{bmatrix} \begin{bmatrix} \frac{\mathbf{E}_d^{\frac{1}{2}}(\mathbf{Q}^T \otimes \mathbf{I})\mathbf{E}_d^{\frac{1}{2}}}{N_d \sigma_d^2} & \mathbf{0} \\ \mathbf{0} & -\frac{e^R \mathbf{C}_k^{\frac{1}{2}}(\mathbf{Q}^T \otimes \mathbf{I})\mathbf{C}_k^{\frac{1}{2}}}{\sigma_k^2 N_e} \end{bmatrix} \begin{bmatrix} \mathbf{v}_d \\ \mathbf{v}_k \end{bmatrix} \\
& + 2\Re\Bigg\{ \begin{bmatrix} \mathbf{v}_d^H, \mathbf{v}_k^H \end{bmatrix} \begin{bmatrix} \frac{\mathbf{E}_d^{\frac{1}{2}}(\mathbf{Q}^T \otimes \mathbf{I})}{N_d \sigma_d^2} & \mathbf{0} \\ \mathbf{0} & -\frac{e^R \mathbf{C}_k^{\frac{1}{2}}(\mathbf{Q}^T \otimes \mathbf{I})}{\sigma_k^2 N_e} \end{bmatrix} \begin{bmatrix} \widehat{\mathbf{h}}_d \\ \widehat{\mathbf{g}}_k \end{bmatrix} \Bigg\} \\
& + \begin{bmatrix} \widehat{\mathbf{h}}_d^H, \widehat{\mathbf{g}}_k^H \end{bmatrix} \begin{bmatrix} \frac{(\mathbf{Q}^T \otimes \mathbf{I})}{N_d \sigma_d^2} & \mathbf{0} \\ \mathbf{0} & -\frac{e^R (\mathbf{Q}^T \otimes \mathbf{I})}{\sigma_k^2 N_e} \end{bmatrix} \begin{bmatrix} \widehat{\mathbf{h}}_d \\ \widehat{\mathbf{g}}_k \end{bmatrix} \geq e^R - 1 \Bigg\} \geq 1 - \bar{p}, \forall_k. \qquad (6.41)
\end{aligned}$$

Furthermore, constraint (6.41) can be equivalently reformulated as follows:

$$\Pr\left\{ \widetilde{\mathbf{v}}_{d,k}^H \Theta_{d,k} \widetilde{\mathbf{v}}_{d,k} + 2\Re\{\widetilde{\mathbf{v}}_{d,k}^H \mathbf{u}_{d,k}\} + s_{d,k} \geq 0 \right\} \geq 1 - \bar{p}, \forall_k, \qquad (6.42)$$

where

$$\begin{aligned}
\widetilde{\mathbf{v}}_{d,k} &= \begin{bmatrix} \mathbf{v}_d^H, \mathbf{v}_k^H \end{bmatrix}^H, \\
\Theta_{d,k} &= \begin{bmatrix} \frac{\mathbf{E}_d^{\frac{1}{2}}(\mathbf{Q}^T \otimes \mathbf{I})\mathbf{E}_d^{\frac{1}{2}}}{N_d \sigma_d^2} & \mathbf{0} \\ \mathbf{0} & -\frac{e^R \mathbf{C}_k^{\frac{1}{2}}(\mathbf{Q}^T \otimes \mathbf{I})\mathbf{C}_k^{\frac{1}{2}}}{\sigma_k^2 N_e} \end{bmatrix}, \\
\mathbf{u}_{d,k} &= \begin{bmatrix} \frac{\mathbf{E}_d^{\frac{1}{2}}(\mathbf{Q}^T \otimes \mathbf{I})}{N_d \sigma_d^2} & \mathbf{0} \\ \mathbf{0} & -\frac{e^R \mathbf{C}_k^{\frac{1}{2}}(\mathbf{Q}^T \otimes \mathbf{I})}{\sigma_k^2 N_e} \end{bmatrix} \begin{bmatrix} \widehat{\mathbf{h}}_d \\ \widehat{\mathbf{g}}_k \end{bmatrix}, \\
s_{d,k} &= \begin{bmatrix} \widehat{\mathbf{h}}_d^H, \widehat{\mathbf{g}}_k^H \end{bmatrix} \begin{bmatrix} \frac{(\mathbf{Q}^T \otimes \mathbf{I})}{N_d \sigma_d^2} & \mathbf{0} \\ \mathbf{0} & -\frac{e^R (\mathbf{Q}^T \otimes \mathbf{I})}{\sigma_k^2 N_e} \end{bmatrix} \begin{bmatrix} \widehat{\mathbf{h}}_d \\ \widehat{\mathbf{g}}_k \end{bmatrix} - e^R + 1.
\end{aligned}$$

It notes that the form of the probabilistic constraint in (6.42) is similar to the form in (6.10). Thus, the derived the three approaches in the above section can be used to approximate the probabilistic constraint (6.42).

6.4.1 Bernstein-Type Inequalit Safe Approximation

In this subsection, the *BTI* approach is adopted to transform the probabilistic constraints into the deterministic constraints. Based on the *BTI* theory in Lemma 5, the secrecy probabilistic constraint (6.42) can be transformed into the following inequalities:

$$\begin{cases} \mathrm{Tr}(\Theta_{d,k}) - \sqrt{-2\ln(p)}\omega_k + \ln(p)\nu_k + s_{d,k} \geq 0, \\ \left\| \begin{bmatrix} \mathrm{vec}(\Theta_{d,k}) \\ \sqrt{2}\mathbf{u}_{d,k} \end{bmatrix} \right\| \leq \omega_k, \\ \nu_k \mathbf{I}_{N_d \times N_t + N_e \times N_t} + \Theta_{d,k} \succeq 0, \quad \nu_k \geq 0, \forall_k. \end{cases} \tag{6.43}$$

Note that the probabilistic constraints of EH (6.8c) has been solved in the PCU model.

Now, the desired safe approximation of OC-SRM under the FCU model is shown in (6.44) by replacing the difficult probabilistic constraints (6.8b) and (6.8c) with the easy-handled constraints (6.43) and (6.20).

$$\begin{aligned} &\max_{\mathbf{Q},R,\omega,\nu,\alpha,\beta} \quad R \\ &\quad s.t. \quad (6.20), (6.43), \nu_k \geq 0, \beta_k \geq 0, \mathrm{tr}(\mathbf{Q}) \leq P, \mathbf{Q} \succeq \mathbf{0}. \end{aligned} \tag{6.44}$$

However, the desired safe approximation problem (6.44) is still non-convex due to the coupled variables. It considers to solve the following power minimization problem for each

Algorithm 6.2 Bisection method for problem (6.45)

1. **Initialize:** ρ_d, $R_{LB}=0$, $R_{UB}=\log(1+\frac{P\|H_d\|_F^2}{\sigma_d^2})$, ε;
2. **Repeat**
3. $R=(R_{LB}+R_{UB})/2$;
4. Solve problem (6.45) to obtain the optimal $\mathbf{Q}$;
5. **if** $\mathrm{Tr}(\mathbf{Q})\leq P$ **then**
6. $R_{LB}=R$
7. **else**
8. $R_{UB}=R$
9. **end**
10. **Until** $|R_{UB}-R_{LB}|<\varepsilon$.
11. Output the optimal solution.

target rate $R>0$ instead of solving problem (6.44)

$$\begin{aligned}&\min_{\mathbf{Q},R,\omega,\nu,\alpha,\beta}\quad \mathrm{Tr}(\mathbf{Q})\\ &s.t.\quad (6.20),\ (6.43),\ \nu_k\geq 0,\ \beta_k\geq 0,\ \mathbf{Q}\succeq\mathbf{0}.\end{aligned}\tag{6.45}$$

It is easily verified that the feasible solutions to (6.45) are also the feasible solutions to (6.44). Problem (6.45) can be efficiently solved by utilizing the bisection method [101], which is summarized in Algorithm 6.2.

6.4.2 S-Procedure Based Safe Approximation

In this subsection, the conservative approach is used to tackle the probabilistic constraint in (6.8). By applying Lemma 6, the secrecy probabilistic constraint (6.42) can be solved by tackling the following deterministic constraint

$$\widetilde{\mathbf{v}}_{d,k}^H\Theta_{d,k}\widetilde{\mathbf{v}}_{d,k}+2\Re\{\widetilde{\mathbf{v}}_{d,k}^H\mathbf{u}_{d,k}\}+s_{d,k}\geq 0,\forall_k.\tag{6.46}$$

The Gaussian random vector $\mathbf{v}_d$ satisfies the following channel uncertainty region set

$$R = \{\mathbf{v}_d | \Pr\{\mathbf{v}_d^H \mathbf{v}_d \leq \gamma_d^2\} \geq 1 - \bar{p}\}, \tag{6.47}$$

where $\gamma_d = \sqrt{\frac{\mathscr{F}^{-1}_{2N_dN_t}(1-\bar{p})}{2}}$. By exploiting the approximation approach in Lemma 6 and *S-Procedure* in Lemma 3, the deterministic constraint (6.46) can be transformed into the following one linear inequality and two LMIs

$$t_d - t_{e,k} \geq e^R - 1, \tag{6.48}$$

$$\begin{bmatrix} \alpha\mathbf{I} + \frac{\mathbf{E}_d^{\frac{1}{2}}(\mathbf{Q}^T \otimes \mathbf{I})\mathbf{E}_d^{\frac{1}{2}}}{N_d\sigma_d^2} & \frac{\mathbf{E}_d^{\frac{1}{2}}(\mathbf{Q}^T \otimes \mathbf{I})\widehat{\mathbf{h}}_d}{N_d\sigma_d^2} \\ \frac{\widehat{\mathbf{h}}_d^H(\mathbf{Q}^T \otimes \mathbf{I})\mathbf{E}_d^{\frac{1}{2}}}{N_d\sigma_d^2} & \frac{\widehat{\mathbf{h}}_d^H(\mathbf{Q}^T \otimes \mathbf{I})\widehat{\mathbf{h}}_d}{N_d\sigma_d^2} - t_d - \alpha\gamma_d^2 \end{bmatrix} \succeq \mathbf{0}, \tag{6.49}$$

$$\begin{bmatrix} \beta_k\mathbf{I} - \frac{e^R\mathbf{C}_k^{\frac{1}{2}}(\mathbf{Q}^T \otimes \mathbf{I})\mathbf{C}_k^{\frac{1}{2}}}{\sigma_k^2 N_e} & -\frac{e^R\mathbf{C}_k^{\frac{1}{2}}(\mathbf{Q}^T \otimes \mathbf{I})\widehat{\mathbf{g}}_k}{\sigma_k^2 N_e} \\ -\frac{e^R\widehat{\mathbf{g}}_k^H(\mathbf{Q}^T \otimes \mathbf{I})\mathbf{C}_k^{\frac{1}{2}}}{\sigma_k^2 N_e} & t_{e,k} - \frac{e^R\widehat{\mathbf{g}}_k^H(\mathbf{Q}^T \otimes \mathbf{I})\widehat{\mathbf{g}}_k}{\sigma_k^2 N_e} - \beta_k\gamma_k^2 \end{bmatrix} \succeq \mathbf{0}, \forall_k, \tag{6.50}$$

where $\alpha \geq 0$ and $\beta_k \geq 0$ are slack variables. Then, the safe approximation problem of the OC-SRM problem can be reformulated as follows:

$$\begin{aligned} &\max_{\mathbf{Q},R,\alpha,\beta,\lambda} \quad R \\ &s.t. \quad (6.28),\ (6.48)-(6.50),\ \alpha \geq 0,\ \beta_k \geq 0,\ \lambda_k \geq 0,\ \mathrm{tr}(\mathbf{Q}) \leq P, \mathbf{Q} \succeq \mathbf{0}. \end{aligned} \tag{6.51}$$

Although problem (6.51) is non-convex, it can be solved by using the bisection method to deal with its corresponding power minimization.

6.4.3 Large Deviation Inequality Safe Approximation

Similar to the PCU model, a low complexity approach is proposed to approximate the secrecy rate probabilistic constraint in this subsection. According to the large deviation inequality for complex Gaussian quadratic forms in Lemma 7, it sets

$$\zeta_{d,k} = \mathrm{tr}(\Theta_{d,k}) + s_{d,k}, \forall_k, \tag{6.52}$$

$$T_{d,k} = v\|\Theta_{d,k}\|_F + \frac{1}{\sqrt{2}}\|\mathbf{u}_{d,k}\|, \forall_k, \tag{6.53}$$

where v is the solution of the quadratic equation $(1-1/(2v^2))v = \sqrt{\ln(1/\bar{p})}$. It demonstrates that $\zeta_{d,k} \geq 2\sqrt{-\ln(\bar{p})}T_{d,k}$ in IV-C. Thus, the following three deterministic constraints can be used to present the probabilistic constraint (6.42)

$$\begin{cases} \mathrm{Tr}(\Theta_{d,k}) + s_k \geq 2\sqrt{-\ln(p)}(\lambda_k + \mu_k), \forall_k, \\ v\|\Theta_{d,k}\|_F \leq \lambda_k, \forall_k, \\ \dfrac{1}{\sqrt{2}}\|\mathbf{u}_{d,k}\| \leq \mu_k, \forall_k, \end{cases} \tag{6.54}$$

where $\mu_k, \lambda_k \in \mathbb{R}, \forall_k$ are slack variables. Then, the safe approximation problem under the FCU model can be reformulated as follows:

$$\begin{aligned} \max_{\mathbf{Q},R,\mu,\lambda,\alpha,\beta} \quad & R \\ s.t. \quad & (6.36),\ (6.54),\ \mathrm{tr}(\mathbf{Q}) \leq P,\ \mathbf{Q} \succeq \mathbf{0}. \end{aligned} \tag{6.55}$$

Similar to (6.45) and (6.51), the non-convex problem in (6.55) can be tackled through the bisection method proposed in Algorithm 6.2. The details of the proposed algorithm is omitted due to the space limitation.

6.5 Computational Complexity Analysis

In the previous two sections, three approaches are derived to solve the OC-SRM problem under the PCU model and the FCU model. Hence, it is presenting the computational complexity of the proposed three approaches for different channel models in the following two subsections.

6.5.1 Partial Channel Uncertainty Model

In this subsection, the complexity of the three approaches under the PCU model is analyzed. The computational complexity of solving the safe approximation problems in (6.21), (6.29) and (6.37) mainly comes from the AO algorithm and the interior point method [129]. In addition, these problems are not the standard SDP due to the existing log-det function [108]. Hence, the CVX solver resorts an embedded successive approximation method to solve the above problems in each iterative procedure. L_A, L_S and L_Q are defined as the iterative number of the AO algorithm, the number of the successive approximation with fixed $\mathbf{S}_k$ and with fixed $\mathbf{Q}$, respectively. Note that the number of decision variables n is on the order of N_t^2+1 (ignoring the slack variables) with fixed $\mathbf{S}_k$ and the number of decision variables n_1 is on the order of KN_e^2+1 (ignoring the slack variables) with fixed $\mathbf{Q}$.

- In the iteration with the fixed $\mathbf{S}_k$, the safe approximation problem in (6.21) obtained by using the *BTI* approach has $2K$ SOC constraints of size $(N_tN_e)^2+N_tN_e+1$, $2K+1$ LMI constraints of size 1, $2K$ LMI constraints of size N_tN_e, 1 LMI constraints of size N_t. In the iteration with the fixed $\mathbf{Q}$, the problem in (6.21) has K SOCs of size $(N_tN_e)^2+N_tN_e+1$, $2K$ LMI constraints of size 1, K LMI constraints of size N_tN_e, K LMI constraints of size N_e. Thus, the complexity of the AO algorithm based on the *BTI* approach is shown in the first row of Table 6.1.

Table 6.1 Complexity analysis of the AO algorithm based on proposed approaches under PCU model

Algorithms	Complexity Order ($n=\mathcal{O}(N_t^2+1)$, $n_1=\mathcal{O}(KN_e^2+1)$)
AO-BTI	$L_A\ln(\frac{1}{\varepsilon})\Big(nL_S\sqrt{8K+2KN_tN_e+N_t+1}(2K((N_tN_e)^3+n(N_tN_e)^2))+N_t^3+nN_t^2$ $+2K((N_tN_e)^2+N_tN_e+1)^2+n(2K+1)+2K+1+n^2)+n_1L_Q\sqrt{KN_tN_e+KN_e+4K}$ $(K((N_tN_e)^3+N_t^3+n_1((N_tN_e)^2+N_e^2))+K((N_tN_e)^2+N_tN_e+1)^2+2n_1K+2K+n_1^2)\Big)$
AO-S-procedure	$L_A\ln(\frac{1}{\varepsilon})\Big(nL_S\sqrt{2KN_tN_e+N_t+4K+1}(2K((N_tN_e+1)^3+n(N_tN_e+1)^2)+N_t^3+nN_t^2$ $+n(2K+1)+2K+1+n^2)+n_1L_Q\sqrt{K(N_tN_e+1)+KN_e+K}(K((N_tN_e+1)^3$ $+n_1(N_tN_e+1)^2)+K(N_e^3+n_1N_e^2)+n_1K+K+n_1^2)\Big)$
AO-LDI	$L_A\ln(\frac{1}{\varepsilon})\Big(nL_S\sqrt{N_t+10K+1}\big(N_t^3+nN_t^2+2K(((N_tN_e)^2+1)^2+(N_tN_e+1)^2)$ $+(2K+1)(n+1)+n^2\big)+n_1L_Q\sqrt{KN_e+5K}\big(K(N_e^3+1)+n_1K(N_e^2+1)$ $+2K((N_tN_e)^2+1)^2+n_1^2)\big)\Big)$

- In the iteration with the fixed $\mathbf{S}_k$, the safe approximation problem in (6.29) obtained by using the *S-procedure* approach has $2K+1$ LMI constraints of size 1, $2K$ LMI constraints of size N_tN_e+1, 1 LMI constraints of size N_t. In the iteration with the fixed $\mathbf{Q}$, the problem in (6.29) has K LMI constraints of size 1, K LMI constraints of size N_tN_e+1, K LMI constraints of size N_e. Thus the complexity of the AO algorithm based on the *S-procedure* approach is shown in the second row of Table 6.1.

- In the iteration with the fixed $\mathbf{S}_k$, the safe approximation problem in (6.37) obtained by using the *LDI* approach has $2K+1$ LMI constraints of size 1, $2K$ SOCs of size $(N_tN_e)^2+1$, $2K$ SOCs of size N_tN_e+1, 1 LMI constraints of size N_t. In the iteration with the fixed $\mathbf{Q}$, the problem in (6.37) has K LMI constraints of size 1, $2K$ SOCs of size $(N_tN_e)^2+1$, K LMI constraints of size N_e. Thus the complexity of the *LDI* approach is shown in the third row of Table 6.1.

Table 6.2 Complexity analysis of bisection method based on proposed approaches under FCU model

Algorithms	Complexity Order ($n = \mathcal{O}(N_t^2+1)$)
Bisection-BTI	$nM_s \ln(\frac{1}{\varepsilon})\sqrt{K(2N_tN_e+N_tN_d+6)+Nt+2}(K((N_tN_e)^3+(N_tN_d+N_tN_e)^3$ $+n((N_tN_e)^2+(N_tN_d+N_tN_e)^2))+N_t^3+nN_t^2+K(((N_tN_e)^2+N_tN_e+1)^2$ $+((N_tN_d+N_tN_e)^2+(N_tN_d+N_tN_e)+1)^2)+n2(K+1)+2(K+1)+n^2)$
Bisection-S-procedure	$nM_s\sqrt{2KN_tN_e+N_tN_d+5K+N_t+2}(2K((N_tN_e+1)^3+n(N_tN_e+1)^2)$ $+(N_tN_d+1)^3+n(N_tN_d+1)^2+N_t^3+nN_t^2+n(3K+1)+3K+1+n^2)\ln(\frac{1}{\varepsilon})$
Bisection-LDI	$nM_s\sqrt{N_t+10K}(N_t^3+nN_t^2+K(((N_tN_e)^2+1)^2+(N_tN_e+1)^2$ $+((N_tN_d+N_tN_e)^2+1)^2+(N_tN_d+N_tN_e+1)^2)+n(2K+1)+n^2)\ln(\frac{1}{\varepsilon})$

6.5.2 Full Channel Uncertainty Model

The complexity of the three approaches based on the FCU model is investigated in this subsection. From (6.44), (6.51) and (6.55), it knows that the complexity is arising from the bisection search over R and the IPM. Based on [129, 108], the complexities of the three approaches are shown below with defining M_s as the searching time of the bisection search. The number of decision variables n is on the order of N_t^2+1 (ignoring the slack variables).

- The safe approximation problem in (6.44) has $2(K+1)$ LMI constraints of size 1, K SOCs of size $(N_tN_e)^2+N_tN_e+1$, K SOCs of size $(N_tN_d+N_tN_e)^2+(N_tN_d+N_tN_e)+1$, K LMI constraints of size N_tN_e, K LMI constraints of size $N_tN_d+N_tN_e$, 1 LMI constraints of size N_t. Thus, the complexity of the bisection method based on the *BTI* approach is shown in the first row of Table 6.2.

- The safe approximation problem in (6.51) has $3K+1$ LMI constraints of size 1, $2K$ LMI constraints of size N_tN_e+1, 1 LMI constraints of size N_tN_d+1, 1 LMI constraints of size N_t. Thus, the complexity of the bisection method based on the *S-procedure* approach is shown in the seconde row of Table 6.2.

- The safe approximation problem in (6.55) has $2K$ LMI constraints of size 1, K SOCs of size $(N_tN_e)^2+1$, K SOCs of size N_tN_e+1, K SOCs of size $(N_tN_d+N_tN_e)^2+1$, K SOCs of size $N_tN_d+N_tN_e+1$, 1 LMI constraints of size N_t. Thus, the complexity of the bisection method based on the *LDI* approach is shown in the third row of Table 6.2.

6.5.3 Complexity Example

In this subsection, an example about the complexity of the proposed approaches under two uncertainty models is provided to show the exactly difference between them. The results shown in Table 6.3 are based on the setting $N_t = 5$, $K = 2$, and $N_d = N_e = 2$.

Table 6.3 Complexity analysis of the proposed approaches under PCU and FCU

Complexity and Performance				
	PCU based AO		FCU based Bisection	
	Rate (bits/Hz)	Time (s)	Rate (bits/Hz)	Time (s)
BTI	7.956336508921782	58.089347	7.00312535278684	65.01264
S-procedure	7.58411124756454	53.204832	6.202126634575	62.674252
LDI	7.886580201305601	46.525381	6.9256725321078	51.982231

6.6 Numerical Results

In this section, numerical results are presented to illustrate the performance of the proposed algorithms based on the two statistical channel uncertainty models in the MIMO-SWIPT system. All simulation results are averaged over 1,000 independent channel trials. Particularly, it assumes that all the channel coefficients are randomly generated following an i.i.d. complex Gaussian distribution with zero mean and unit variance in each simulation trial. Specifically, it considers that the transmitter is equipped with $N_t = 5$ and all the receivers are equipped with $N_d = N_e = 2$ antennas. It assumes that the number of ERs is 2, unless indicated otherwise.

According to the parameters setting of the non-linear EH model in [123], it assumes $M_k = 24$ mW, $a_k = 1500$, and $b_k = 0.0022$, $\eta_k = -5$ dBm, $\forall_k$. The variances of the channel estimation errors are set as $\mathbf{E}_d = \mathbf{C}_k = \sigma^2\mathbf{I}$, $\forall_k$, unless indicated otherwise. The outage probability requirements of the secrecy rate and EHs are set to the same, $p = l_k = \rho = 0.01$. It supposes that the noise variances of all users are same, $\sigma_d^2 = \sigma_k^2 = 0$ dBm. The linear EH model is considered as a baseline model. The power conversion efficiency of the linear model is set as $\xi_k = 0.6$. Furthermore, all the considered convex optimization problems are efficiently solved by utilizing CVX [105].

6.6.1 Robust OC-SRM in PCU model

It is illustrating the outage secrecy rate performance of OC-SRM problem based on the PCU model in Figure 6.2-6.5. Figure 6.2 shows the convergence performance of the proposed three approaches. As can be seen from Figure 6.2, the proposed three approaches converge after several iterations. The *BTI* approach has the best performance compared with the *LDI* and *S-procedure* approach. It shows that the convergence speed of the non-linear EH model is slightly faster than that of the linear EH model. Notice that the convergence speed of the AO algorithm depends on the initial values. If the initial value is relatively closer to the optimal solution, the algorithm converges faster [130].

Figure 6.3 depicts the outage secrecy rate performance versus the maximum transmit power allowance P for the different proposed approaches. As can be seen in the figure, the secrecy rates of all the considered schemes increase with respect to the transmit power budget P and finally become saturate. This is due to the fact that ERs can use the additional harvested energy to intercept the information after the task of harvested energy is accomplished. Furthermore, the performance gaps between the three approaches are gradually increased when the maximum transmit power allowance becomes greater than 15 dBm. The *BTI*

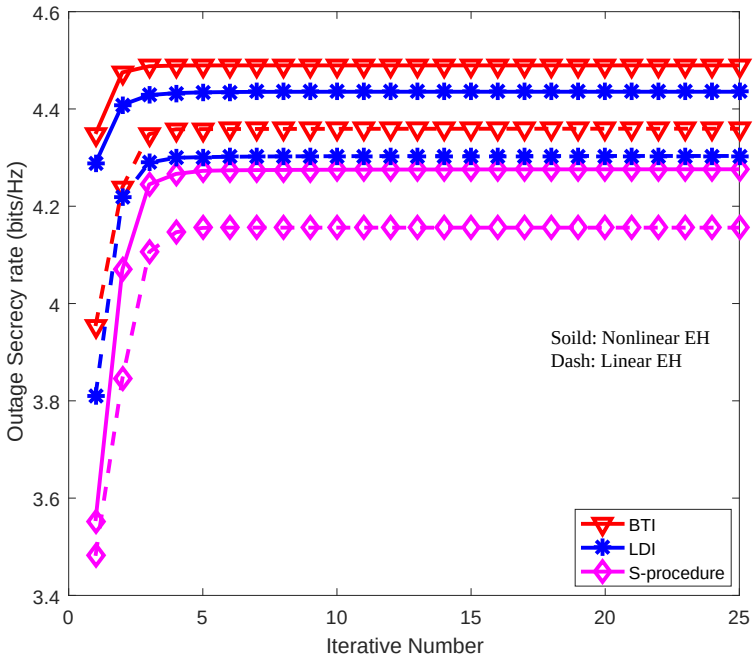

Fig. 6.2 Convergence rate of the AO algorithm for the three safe approximation approaches, $P = 15$ dBm. $\sigma^2 = 0.001$

approach exhibits the best performance followed by the *LDI* and *S-procedure* approach when the transmit power is greater than 15 dBm. In addition, the secrecy rate performance of the linear EH model is considered as a baseline to compare with the proposed non-linear EH model. As can be observed, the linear model performs a severe degradation compared with the non-linear model when the transmit power is quite smaller, however, the performance gap becomes gradually small with the increased transmit power. The reason is that the linear EH model has less power to intercept information in the low input transmit power due to the independent relationship between the energy conversion efficiency and the input power.

Figure 6.4 shows the outage secrecy rate versus channel error variance σ^2 for the different proposed approaches. It observes that the outage secrecy rates of all robust approaches degrade as the quality of the CSI decreases. The performance gaps between the three approaches significantly increase as the error variance is increased. The *BTI* approach has the best performance compared with the other two approaches over the whole error variance

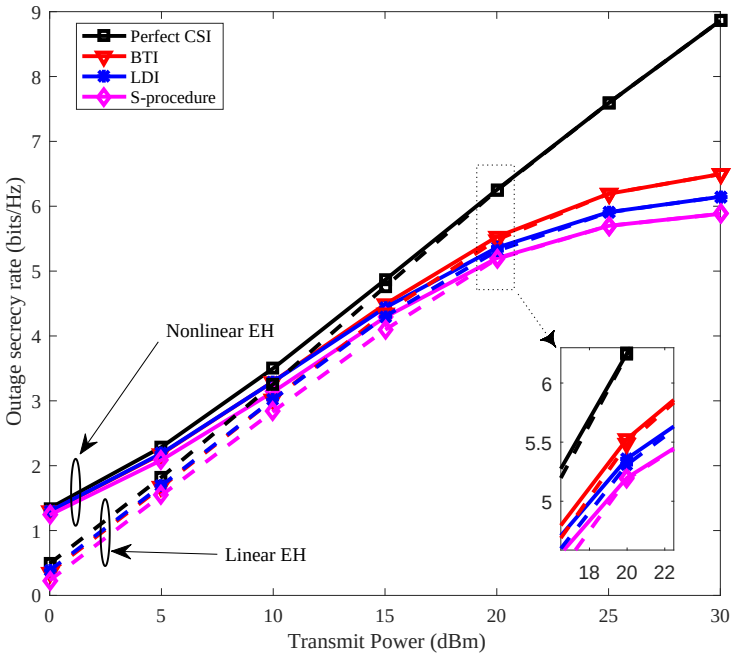

Fig. 6.3 The outage secrecy rate versus the transmission power for the PCU.

range. Additionally, the performance gap between the proposed non-linear EH model and the linear EH model gradually shrinks when the error variance becomes larger. Lastly, there is no performance degradation for the perfect CSI model since this scheme can fully utilize the spatial degrees of freedom provided by the multiple antennas.

Figure 6.5 presents the outage secrecy rate versus the number of ERs K for different approaches. The outage secrecy rates of all the schemes decrease as the number of ERs increases since the ER with the stronger channel has a higher probability to eavesdrop. Although the *BTI* approach outperforms the other two approaches, the performance gap between them is obviously reduced when the number of ER increases. In addition, the non-linear EH model can achieve a higher secrecy rate compared with the linear EH model.

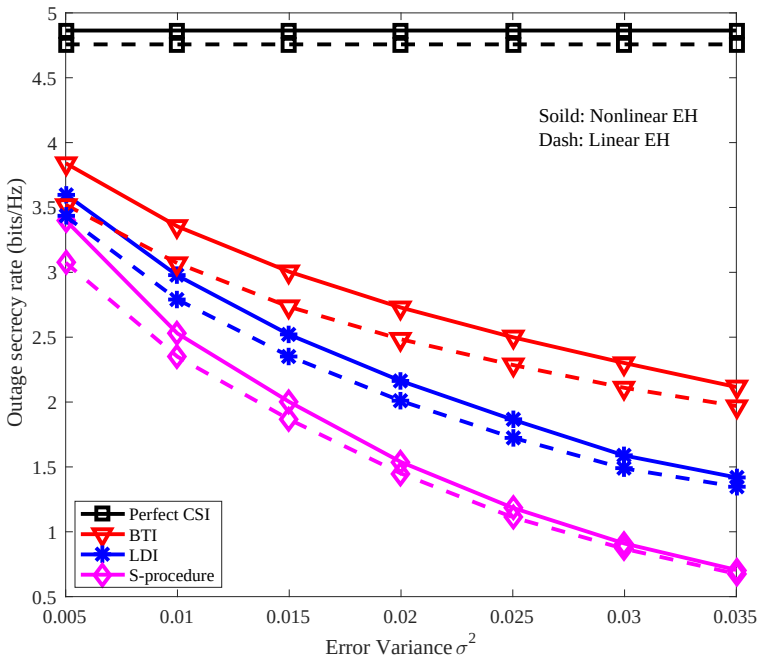

Fig. 6.4 The outage secrecy rate versus error variance σ^2 for the PCU, $P = 15$ dBm.

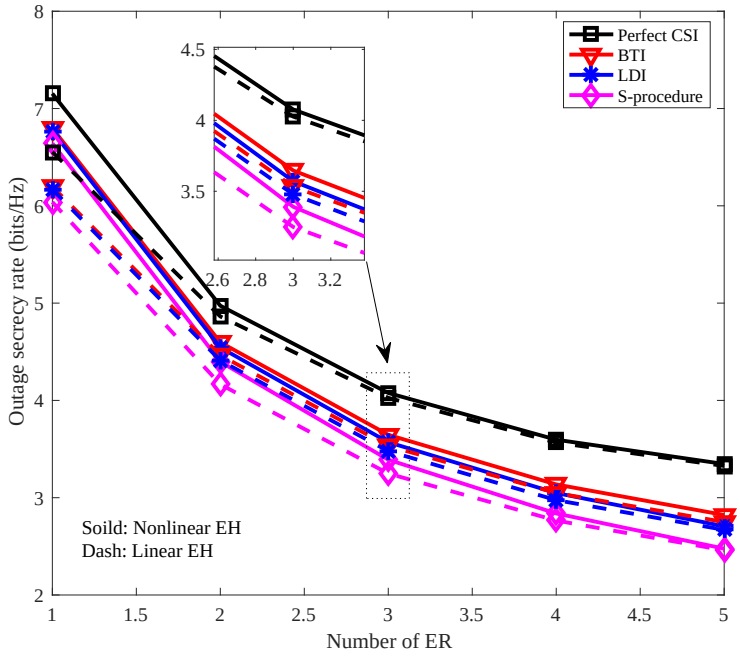

Fig. 6.5 The outage secrecy rate for different numbers of ER for the PCU, $P = 15$ dBm.

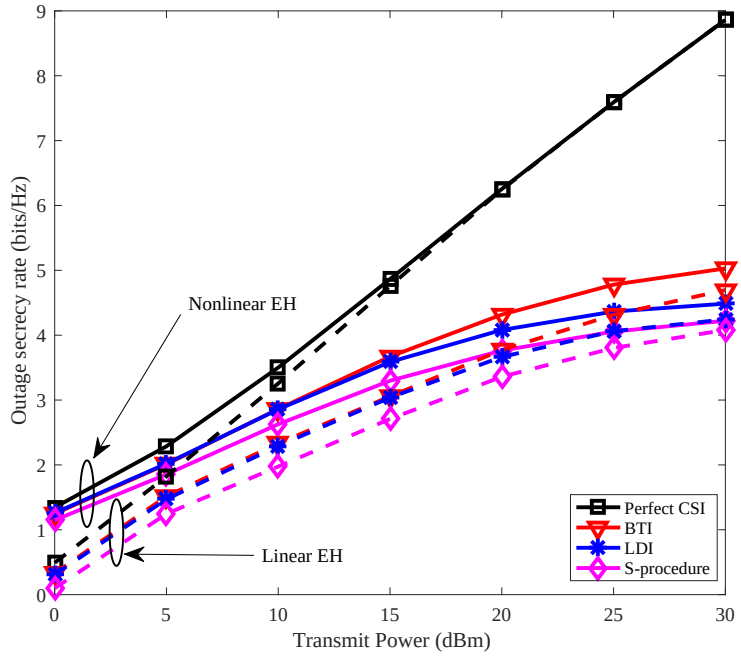

Fig. 6.6 The outage secrecy rate versus the transmission power for the FCU.

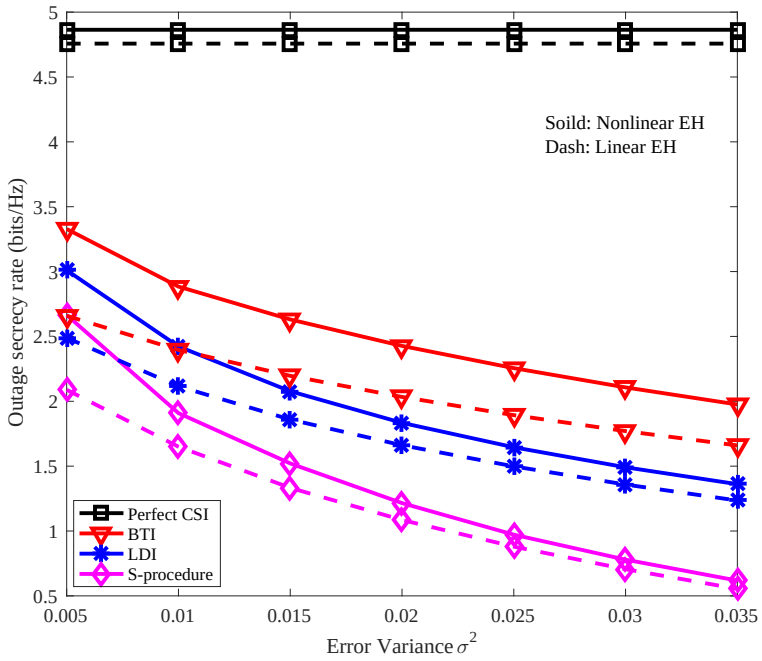

Fig. 6.7 The outage secrecy rate versus error variance σ^2 for the FCU, $P = 15$ dBm.

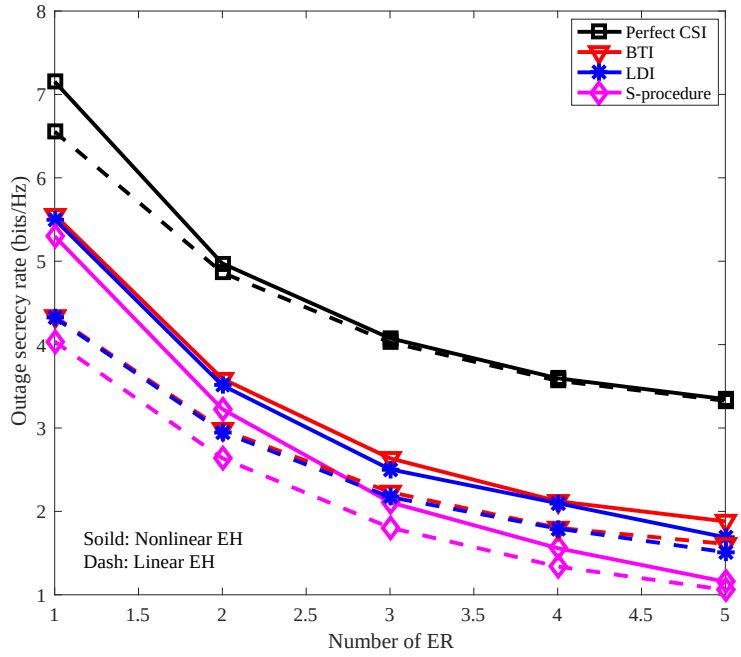

Fig. 6.8 The outage secrecy rate for different numbers of ER for the FCU, $P = 15$ dBm.

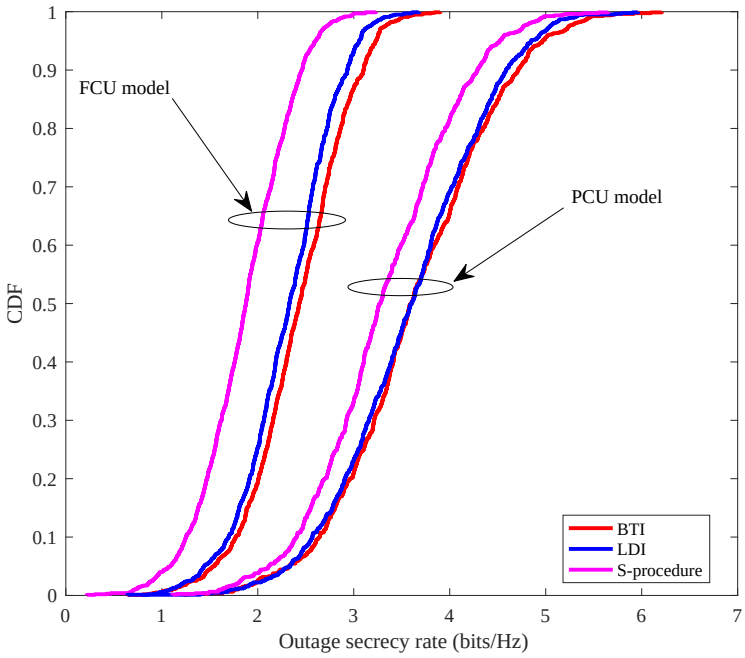

Fig. 6.9 The CDF of the outage secrecy rate for the PCU and the FCU, $P = 10$ dBm.

6.6.2 Robust OC-SRM in FCU model

The outage secrecy rate performance of the OC-SRM problem based on the FCU model is shown in Figure 6.6-6.9. It depicts the outage secrecy rate performance versus the maximum transmit power based on the FCU model in Figure 6.6. As expected, the outage secrecy rates of all the schemes obviously grow with a larger transmit power. As can be observed in the figure, the outage secrecy rate performance of the *BTI* approach still has the best performance compared with the other two approaches. More interestingly, the outage secrecy rates of the three approaches in the FCU model are obviously lower than that of the PCU model, since the system has to overcome all the channel uncertainties. As can be observed in the figure, the performance gap between the linear and the non-linear EH model in the FCU is greater than that of the PCU. Figure 6.7 presents the outage secrecy rate against the channel error variance σ^2 in the FCU model. The outage secrecy rates of the three approaches degrade when the channel error variance grows. The *BTI* approach still yields the best performance compared with the other two approaches. The outage secrecy rate of the non-linear EH model is better than that of the linear model over the whole error variance range. The difference between them becomes smaller when the quality level of the channel becomes worse. The impact of the number of ERs on the outage secrecy rate is investigated in Figure 6.8. There exists a huge gap between the perfect design and the robust design due to the channel uncertainties in both the type of users. One can observe that the *BTI* and *LDI* approaches can provide higher security compared with the *S-procedure* approach, especially when the number of ER is larger. Although the performance of the non-linear model is better than that of the line model, the gap between them becomes gradually smaller with a larger number of ER. Figure 6.9 shows the cumulative density function (CDF) of the outage secrecy rate under the PCU and the FCU model. When the target outage secrecy rate equals to 3.5, $R = 3.5$, the information transmission in the FCU model is always outage, and around 55% of the outage secrecy rates are below the target in the PCU model. There exists approximate 10% gap

between the *S-procedure* approach and the other two approaches in the PCU model. When the target outage secrecy rate equal to 2, $R = 2$, around 20% of the outage secrecy rates are below the target with BTI and LDI approaches; while approximate 55% of the outage secrecy rates are below the target rate with S-porcedure approach in the FCU model. As expected, the *BTI* and *LDI* approaches outperform the *S-procedure* approach.

6.7 Summary

In this chapter, a robust OC-SRM problem is proposed to design the covariance matrix of the transmit signal by taking into account both the statistical channel uncertainty models and a practical non-linear EH model in the MIMO-SWIPT system. The formulated OC-SRM problem is non-convex for both the PCU and FCU models due to the probabilistic constrains. The three approaches are derived to find the safe approximation of the probabilistic constrains. In addition, an AO algorithm and a bisection method are introduced to address the non-convexity of the proposed OC-SRM problem in both the uncertainty models. Furthermore, the computational complexity of the proposed approaches is also provided. Simulation results demonstrate that the proposed non-linear EH model significantly outperforms in the outage secrecy rate than the linear EH model in the lower range scalar, i.e., transmit power, error variance, number of ER. The *BTI* approach yields the best outage secrecy rate performance compared with the *LDI* and *S-procedure* approaches.

Chapter 7

Conclusion and Future Work

7.1 Conclusion

This thesis has provided a comprehensive and in depth investigation on the resource allocation and PHY security in SWIPT systems by applying assorted optimization techniques. The non-convex optimization problems can be reformulated into convex problems by using the state-of-art methods and algorithms. The conclusions of this thesis are summarized as follows.

In Chapter 3, the application of SWIPT technique in AF cooperative networks was investigated. Each receiver adopted power splitter to enable simultaneously ID and EH. The robust optimization problems were proposed to jointly design relay beamforming and PS ratio by incorporating two deterministic uncertainty models. For both channel models, SDP relaxation approach was utilized to convert the non-convex problem into SDP problem. The Cauchy-Schwarz inequality was adopted to handle the infinite constraints caused by channel coefficient model, and the Lagrange dual was adopted to address the infinite constraints caused by channel covariance model. Furthermore, the proof was proposed to show that the optimal solution for the relaxed problem was rank-one. Numerical results indicated that

the channel covariance uncertainty model consumed less power compared to the channel coefficient uncertainty model.

In Chapter 4, a security issue was studied in a AF cooperative network with the presence of multiple idle receivers (potential eavesdropper). A relay transmit power minimization problem was proposed to investigate the impact of security on the energy consumption of the SWIPT system. The beamforming at the relay and the PS ratio at the DR were jointly optimized in order to reduce the system energy consumption while guaranteeing security and energy harvest requirements. The proposed two-layer algorithm, which was designed based on SDR and one-dimensional line search, solved the non-convex problem. In addition, a rank reduction algorithm was proposed to achieve the global optimality of the original problem. A low-complexity iterative algorithm was proposed to achieve the suboptimal solution of the non-convex problem. Besides, the beamforming and PS ratio design was extended to the imperfect CSI case. It was demonstrated that the proposed iterative algorithm using an acceptable growth energy consumption could provide lower complexity compared to the global search algorithm. It was also worth pointing out that the quality of channels, required security and EH target might impact the system power consumption.

In Chapter 5, a novel security problem was investigated in underlay CR networks by considering SWIPT at the secondary transmitter. Building upon the celebrated AN approach, a transmission scheme was proposed by utilizing the AN signal to enhance the secondary system security while satisfying the tolerable interference requirement at the primary system. The information signal covariance and AN signal covariance were jointly designed by incorporating the statistical channel uncertainty model for SERs and PUs. A decomposition approach was adopted to decompose the original problem to two subproblems. The BTI approximation approach was employed to convert the probabilistic constraints into deterministic constraints in each subproblem. Then, the suboptimal solution was obtained by alternately solving the two convex conic optimization subproblems. In addition, the proposed

transmission scheme was extended to full statistical channel uncertainty model. Simulation results indicated that the proposed transmission scheme outperformed the worst-case scheme and the non-robust scheme. It also demonstrated that the security performance could be enhanced by invoking AN signals.

In Chapter 6, PHY security was examined in downlinke MIMO networks with invoking the non-linear EH model at the potential eavesdroppers. An OC-SRM problem subject to the secrecy rate and the EH outage probability requirements was designed by incorporating statistical channel uncertainty model for ERs. The decomposition and approximation approaches were employed to convert the original problem into two conservative convex subproblems. Then, an AO algorithm was proposed to alternately solve the two convex conic optimization subproblems. Furthermore, the proposed outage optimization problem was extended to full statistical channel uncertainty model to investigate the impact of the non-linear EH model on the system security. The bisection method was adopted to achieve the solutions of the conservative problem, which had been reformulated by the proposed approximation approaches. The analysis and simulations indicated that the approximation approach based BTI presented the best secrecy performance but with the highest computational complexity compared to other two approximation approaches. One interesting conclusion was that the non-linear energy receiver intercept less message compared to the linear energy receiver when the transmit power was small and channel condition was good.

7.2 Future Work

In this section, the potential extensions of the current works in this thesis and promising future work directions are discussed in the following.

7.2.1 Extensions of Current Works

The system performance in this thesis is achieved based on the assumption that the HD model is adopted at the BS and at the relay, it will be interesting to extend the work in this thesis to the full duplex (FD) scenario. In this context, the FD-BS is capable to simultaneously transmit information to users and receive feedback or message from users. Besides, self-interference can be harvested as energy by the FD-BS based on the practical receiver architecture design. FD-BS will guarantee the uplink and downlink secure communication by using the harvested energy to disturb eavesdroppers. Thus, the FD system with SWIPT may enhance not only efficiency but also security.

Current work in this thesis investigates the security problem for one information receiver (e.g., in Chapter 3, 4, 5) in order to expose the impact of the security on SWIPT systems. The designed algorithms extending to the more general case with multiple information receivers is thus worth pursing in future work. Furthermore, only PHY security techniques are applied in this thesis. Combining this approach with cryptography techniques in the higher communication protocol layers to further improve the secrecy communication performance in SWIPT systems is thus another interesting problem to investigate in the future.

Current works in Chapter 4 and 5 only focus on the security improvement in SWIPT systems. The considered system may cause high energy consumption since energy saving and wireless security are not aligned with each other in general. According to the state-of-the-art design in wireless communications, the secrecy energy efficiency (SEE) is regarded as a proper scalar to reflect the balance between security and energy consumption. Therefore, it is imperative to study the tradeoff between the secrecy spectral efficiency (SSE) and the SEE in the future work.

7.2.2 Future Work Directions

In this subsection, we introduce the potential application of SWIPT for some promising future directions.

7.2.2.1 Device-to-device Communications

D2D communication has been recognized as a emerging technology, which enables direct communications between mobile devices rather than through the BS, for next generation communication system since it is capable to satisfy rapid growth in the demand of local area services in cellular networks [131]. This technology improves not only the energy efficiency by low-power transmission of proximity services but also the spectral efficiency by reusing the frequency of the cellular networks. Similar to traditional communication systems, wireless devices with capacity-constrained battery still limit the performance of D2D communication systems. On the other hand, the harmful noise and interference, which can be considered as energy source, are managed to enhance the spectral efficiency. Motivated by this, it naturally consider to apply SWIPT in D2D communication systems to address the energy-constrained and resource allocation issues.

7.2.2.2 Millimetre Wave Communications

Millimetre Wave (mmWave) communications has been considered as a key candidate technology for future 5G communications due to the availability of large spectrum resources at higher frequencies. In general, mmWave systems are also attractive for WPT since mmWave systems have the following features: very high frequencies, narrow beam, large array gains, and dense network with mmWave base stations. However, mmWave communications, which have poor penetration and diffraction, are more sensitive to blockage by buildings. Therefore,

there exists research challenges to use mmWave for SWIPT assisted wireless networks. Also, it is unclear whether mmWave networks with SWIPT will provide better system performance compared to the conventional frequency networks with SWIPT. Motivated by this, it is important to study energy harvesting in a mmWave cellular network.

References

[1] J. A. Paradiso and T. Starner, "Energy scavenging for mobile and wireless electronics," *IEEE Pervasive Computing*, vol. 4, no. 1, pp. 18–27, Jan 2005.

[2] V. Raghunathan, S. Ganeriwal, and M. Srivastava, "Emerging techniques for long lived wireless sensor networks," *IEEE Communications Magazine*, vol. 44, no. 4, pp. 108–114, April 2006.

[3] S. L. Ho, J. Wang, W. N. Fu, and M. Sun, "A comparative study between novel witricity and traditional inductive magnetic coupling in wireless charging," *IEEE Transactions on Magnetics*, vol. 47, no. 5, pp. 1522–1525, May 2011.

[4] A. Kurs, A. Karalis, R. Moffatt, J. D. Joannopoulos, P. Fisher, and M. Soljacic, "Wireless power transfer via strongly coupled magnetic resonances," *Science*, vol. 317, no. 5834, pp. 83–86, 2007. [Online]. Available: http://science.sciencemag.org/content/317/5834/83

[5] Z. Popovic, "Cut the cord: Low-power far-field wireless powering," *IEEE Microwave Magazine*, vol. 14, no. 2, pp. 55–62, March 2013.

[6] H. J. Visser and R. J. M. Vullers, "Rf energy harvesting and transport for wireless sensor network applications: Principles and requirements," *Proceedings of the IEEE*, vol. 101, no. 6, pp. 1410–1423, June 2013.

[7] L. Xie, Y. Shi, Y. T. Hou, and A. Lou, "Wireless power transfer and applications to sensor networks," *IEEE Wireless Communications*, vol. 20, no. 4, pp. 140–145, August 2013.

[8] H. Jiang, J. Zhang, D. Lan, K. K. Chao, S. Liou, H. Shahnasser, R. Fechter, S. Hirose, M. Harrison, and S. Roy, "A low-frequency versatile wireless power transfer technology for biomedical implants," *IEEE Transactions on Biomedical Circuits and Systems*, vol. 7, no. 4, pp. 526–535, Aug 2013.

[9] S. Rao and J. C. Chiao, "Body electric: Wireless power transfer for implant applications," *IEEE Microwave Magazine*, vol. 16, no. 2, pp. 54–64, March 2015.

[10] Y. K. Chen, "Challenges and opportunities of internet of things," in *17th Asia and South Pacific Design Automation Conference*, Jan 2012, pp. 383–388.

[11] S. Gollakota, M. S. Reynolds, J. R. Smith, and D. J. Wetherall, "The emergence of rf-powered computing," *Computer*, vol. 47, no. 1, pp. 32–39, Jan 2014.

[12] D. W. K. Ng and R. Schober, "Energy-efficient power allocation for m2m communications with energy harvesting transmitter," in *2012 IEEE Globecom Workshops*, Dec 2012, pp. 1644–1649.

[13] M. Erol-Kantarci and H. T. Mouftah, "Suresense: sustainable wireless rechargeable sensor networks for the smart grid," *IEEE Wireless Communications*, vol. 19, no. 3, pp. 30–36, June 2012.

[14] G. Papotto, F. Carrara, A. Finocchiaro, and G. Palmisano, "A 90-nm cmos 5-mbps crystal-less rf-powered transceiver for wireless sensor network nodes," *IEEE Journal of Solid-State Circuits*, vol. 49, no. 2, pp. 335–346, Feb 2014.

[15] X. Lu, P. Wang, D. Niyato, D. I. Kim, and Z. Han, "Wireless networks with rf energy harvesting: A contemporary survey," *IEEE Communications Surveys Tutorials*, vol. 17, no. 2, pp. 757–789, Secondquarter 2015.

[16] Z. Xun, "Wireless information and power transfer: System modeling, performance analysis and resource allocation optimization," Ph.D. dissertation, 2015.

[17] S. Ladan, N. Ghassemi, A. Ghiotto, and K. Wu, "Highly efficient compact rectenna for wireless energy harvesting application," *IEEE Microwave Magazine*, vol. 14, no. 1, pp. 117–122, Jan 2013.

[18] I. Krikidis, S. Timotheou, S. Nikolaou, G. Zheng, D. W. K. Ng, and R. Schober, "Simultaneous wireless information and power transfer in modern communication systems," *IEEE Communications Magazine*, vol. 52, no. 11, pp. 104–110, Nov 2014.

[19] C. A. Balanis, *Antenna theory: analysis and design*. Wiley-Interscience, 2005.

[20] T. Rappaport, *Wireless Communications: Principles and Practice*, 2nd ed. Upper Saddle River, NJ, USA: Prentice Hall PTR, 2001.

[21] L. R. Varshney, "Transporting information and energy simultaneously," in *2008 IEEE International Symposium on Information Theory*, July 2008, pp. 1612–1616.

[22] P. Grover and A. Sahai, "Shannon meets tesla: Wireless information and power transfer," in *2010 IEEE International Symposium on Information Theory*, June 2010, pp. 2363–2367.

[23] R. Zhang and C. K. Ho, "Mimo broadcasting for simultaneous wireless information and power transfer," *IEEE Transactions on Wireless Communications*, vol. 12, no. 5, pp. 1989–2001, May 2013.

[24] X. Zhou, R. Zhang, and C. K. Ho, "Wireless information and power transfer: Architecture design and rate-energy tradeoff," *IEEE Transactions on Communications*, vol. 61, no. 11, pp. 4754–4767, November 2013.

[25] A. J. Menezes, P. C. Van Oorschot, and S. A. Vanstone, *Handbook of applied cryptography*. CRC press, 1996.

[26] R. Liu and W. Trappe, *Securing Wireless Communications at the Physical Layer*, 1st ed. Springer Publishing Company, Incorporated, 2009.

[27] M. Bloch and J. Barros, *Physical-Layer Security: From Information Theory to Security Engineering*, 1st ed. New York, NY, USA: Cambridge University Press, 2011.

[28] Y. Liang, H. V. Poor, and S. Shamai (Shitz), "Information theoretic security," *Found. Trends Commun. Inf. Theory*, vol. 5, no. 4, pp. 355–580, Apr. 2009. [Online]. Available: http://dx.doi.org/10.1561/0100000036

[29] A. D. Wyner, "The wire-tap channel," *The Bell System Technical Journal*, vol. 54, no. 8, pp. 1355–1387, Oct 1975.

[30] M. Bloch, J. Barros, M. R. D. Rodrigues, and S. W. McLaughlin, "Wireless information-theoretic security," *IEEE Transactions on Information Theory*, vol. 54, no. 6, pp. 2515–2534, June 2008.

[31] E. Tekin and A. Yener, "The general gaussian multiple-access and two-way wire-tap channels: Achievable rates and cooperative jamming," *IEEE Transactions on Information Theory*, vol. 54, no. 6, pp. 2735–2751, June 2008.

[32] S. Goel and R. Negi, "Guaranteeing secrecy using artificial noise," *IEEE Transactions on Wireless Communications*, vol. 7, no. 6, pp. 2180–2189, June 2008.

[33] T. Cover and A. E. Gamal, "Capacity theorems for the relay channel," *IEEE Transactions on Information Theory*, vol. 25, no. 5, pp. 572–584, September 1979.

[34] A. Nosratinia, T. E. Hunter, and A. Hedayat, "Cooperative communication in wireless networks," *IEEE Communications Magazine*, vol. 42, no. 10, pp. 74–80, Oct 2004.

[35] A. Scaglione, D. L. Goeckel, and J. N. Laneman, "Cooperative communications in mobile ad hoc networks," *IEEE Signal Processing Magazine*, vol. 23, no. 5, pp. 18–29, Sept 2006.

[36] Q. Zhang, J. Jia, and J. Zhang, "Cooperative relay to improve diversity in cognitive radio networks," *IEEE Communications Magazine*, vol. 47, no. 2, pp. 111–117, February 2009.

[37] Z. Sheng, K. K. Leung, and Z. Ding, "Cooperative wireless networks: from radio to network protocol designs," *IEEE Communications Magazine*, vol. 49, no. 5, pp. 64–69, May 2011.

[38] J. N. Laneman, G. W. Wornell, and D. N. C. Tse, "An efficient protocol for realizing cooperative diversity in wireless networks," in *Proceedings. 2001 IEEE International Symposium on Information Theory (IEEE Cat. No.01CH37252)*, 2001, pp. 294–.

[39] A. Sendonaris, E. Erkip, and B. Aazhang, "User cooperation diversity. part i. system description," *IEEE Transactions on Communications*, vol. 51, no. 11, pp. 1927–1938, Nov 2003.

[40] ——, "User cooperation diversity. part ii. implementation aspects and performance analysis," *IEEE Transactions on Communications*, vol. 51, no. 11, pp. 1939–1948, Nov 2003.

[41] J. Mitola, "Cognitive radio—an integrated agent architecture for software defined radio," 2000.

[42] U. S. F. C. C. S. P. T. Force, *Spectrum Policy Task Force Report*. Federal Communications Commission, Spectrum Policy Task Force, 2002. [Online]. Available: https://books.google.co.uk/books?id=p9MQtwAACAAJ

[43] A. Goldsmith, S. A. Jafar, I. Maric, and S. Srinivasa, "Breaking spectrum gridlock with cognitive radios: An information theoretic perspective," *Proceedings of the IEEE*, vol. 97, no. 5, pp. 894–914, May 2009.

[44] S. Haykin, "Cognitive radio: brain-empowered wireless communications," *IEEE Journal on Selected Areas in Communications*, vol. 23, no. 2, pp. 201–220, Feb 2005.

[45] Y. C. Liang, Y. Zeng, E. C. Y. Peh, and A. T. Hoang, "Sensing-throughput tradeoff for cognitive radio networks," *IEEE Transactions on Wireless Communications*, vol. 7, no. 4, pp. 1326–1337, April 2008.

[46] Q. Zhao and B. M. Sadler, "A survey of dynamic spectrum access," *IEEE Signal Processing Magazine*, vol. 24, no. 3, pp. 79–89, May 2007.

[47] L. Liu, R. Zhang, and K. C. Chua, "Wireless information transfer with opportunistic energy harvesting," *IEEE Transactions on Wireless Communications*, vol. 12, no. 1, pp. 288–300, January 2013.

[48] ——, "Wireless information and power transfer: A dynamic power splitting approach," *IEEE Transactions on Communications*, vol. 61, no. 9, pp. 3990–4001, September 2013.

[49] D. W. K. Ng, E. S. Lo, and R. Schober, "Wireless information and power transfer: Energy efficiency optimization in ofdma systems," *IEEE Transactions on Wireless Communications*, vol. 12, no. 12, pp. 6352–6370, December 2013.

[50] X. Zhou, R. Zhang, and C. K. Ho, "Wireless information and power transfer in multiuser ofdm systems," *IEEE Transactions on Wireless Communications*, vol. 13, no. 4, pp. 2282–2294, April 2014.

[51] Z. Xiang and M. Tao, "Robust beamforming for wireless information and power transmission," *IEEE Wireless Communications Letters*, vol. 1, no. 4, pp. 372–375, August 2012.

[52] J. Park and B. Clerckx, "Joint wireless information and energy transfer in a two-user mimo interference channel," *IEEE Transactions on Wireless Communications*, vol. 12, no. 8, pp. 4210–4221, August 2013.

[53] ——, "Joint wireless information and energy transfer in a *k*-user mimo interference channel," *IEEE Transactions on Wireless Communications*, vol. 13, no. 10, pp. 5781–5796, Oct 2014.

[54] J. Xu, L. Liu, and R. Zhang, "Multiuser miso beamforming for simultaneous wireless information and power transfer," *IEEE Transactions on Signal Processing*, vol. 62, no. 18, pp. 4798–4810, Sept 2014.

[55] H. Zhang, K. Song, Y. Huang, and L. Yang, "Energy harvesting balancing technique for robust beamforming in multiuser miso swipt system," in *2013 International Conference on Wireless Communications and Signal Processing*, Oct 2013, pp. 1–5.

[56] S. Timotheou, I. Krikidis, G. Zheng, and B. Ottersten, "Beamforming for miso interference channels with qos and rf energy transfer," *IEEE Transactions on Wireless Communications*, vol. 13, no. 5, pp. 2646–2658, May 2014.

[57] Q. Shi, L. Liu, W. Xu, and R. Zhang, "Joint transmit beamforming and receive power splitting for miso swipt systems," *IEEE Transactions on Wireless Communications*, vol. 13, no. 6, pp. 3269–3280, June 2014.

[58] Q. Shi, W. Xu, T. H. Chang, Y. Wang, and E. Song, "Joint beamforming and power splitting for miso interference channel with swipt: An socp relaxation and decentralized algorithm," *IEEE Transactions on Signal Processing*, vol. 62, no. 23, pp. 6194–6208, Dec 2014.

[59] M. R. A. Khandaker and K. K. Wong, "Swipt in miso multicasting systems," *IEEE Wireless Communications Letters*, vol. 3, no. 3, pp. 277–280, June 2014.

[60] B. Medepally and N. B. Mehta, "Voluntary energy harvesting relays and selection in cooperative wireless networks," *IEEE Transactions on Wireless Communications*, vol. 9, no. 11, pp. 3543–3553, November 2010.

[61] P. T. Venkata, S. N. A. U. Nambi, R. V. Prasad, and I. Niemegeers, "Bond graph modeling for energy-harvesting wireless sensor networks," *Computer*, vol. 45, no. 9, pp. 31–38, Sept 2012.

[62] B. K. Chalise, Y. D. Zhang, and M. G. Amin, "Energy harvesting in an ostbc based amplify-and-forward mimo relay system," in *2012 IEEE International Conference on Acoustics, Speech and Signal Processing (ICASSP)*, March 2012, pp. 3201–3204.

[63] I. Krikidis, S. Timotheou, and S. Sasaki, "Rf energy transfer for cooperative networks: Data relaying or energy harvesting?" *IEEE Communications Letters*, vol. 16, no. 11, pp. 1772–1775, November 2012.

[64] I. Krikidis, S. Sasaki, S. Timotheou, and Z. Ding, "A low complexity antenna switching for joint wireless information and energy transfer in mimo relay channels," *IEEE Transactions on Communications*, vol. 62, no. 5, pp. 1577–1587, May 2014.

[65] A. A. Nasir, X. Zhou, S. Durrani, and R. A. Kennedy, "Relaying protocols for wireless energy harvesting and information processing," *IEEE Transactions on Wireless Communications*, vol. 12, no. 7, pp. 3622–3636, July 2013.

[66] ——, "Wireless-powered relays in cooperative communications: Time-switching relaying protocols and throughput analysis," *IEEE Transactions on Communications*, vol. 63, no. 5, pp. 1607–1622, May 2015.

[67] Z. Ding, S. M. Perlaza, I. Esnaola, and H. V. Poor, "Power allocation strategies in energy harvesting wireless cooperative networks," *IEEE Transactions on Wireless Communications*, vol. 13, no. 2, pp. 846–860, February 2014.

[68] M. Ju, K. M. Kang, K. S. Hwang, and C. Jeong, "Maximum transmission rate of psr/tsr protocols in wireless energy harvesting df-based relay networks," *IEEE Journal on Selected Areas in Communications*, vol. 33, no. 12, pp. 2701–2717, Dec 2015.

[69] K. Xiong, P. Fan, C. Zhang, and K. B. Letaief, "Wireless information and energy transfer for two-hop non-regenerative mimo-ofdm relay networks," *IEEE Journal on Selected Areas in Communications*, vol. 33, no. 8, pp. 1595–1611, Aug 2015.

[70] I. Krikidis, "Simultaneous information and energy transfer in large-scale networks with/without relaying," *IEEE Transactions on Communications*, vol. 62, no. 3, pp. 900–912, March 2014.

[71] Z. Ding, I. Krikidis, B. Sharif, and H. V. Poor, "Wireless information and power transfer in cooperative networks with spatially random relays," *IEEE Transactions on Wireless Communications*, vol. 13, no. 8, pp. 4440–4453, Aug 2014.

[72] D. S. Michalopoulos, H. A. Suraweera, and R. Schober, "Relay selection for simultaneous information transmission and wireless energy transfer: A tradeoff perspective," *IEEE Journal on Selected Areas in Communications*, vol. 33, no. 8, pp. 1578–1594, Aug 2015.

[73] I. Krikidis, "Relay selection in wireless powered cooperative networks with energy storage," *IEEE Journal on Selected Areas in Communications*, vol. 33, no. 12, pp. 2596–2610, Dec 2015.

[74] K. H. Liu, "Performance analysis of relay selection for cooperative relays based on wireless power transfer with finite energy storage," *IEEE Transactions on Vehicular Technology*, vol. 65, no. 7, pp. 5110–5121, July 2016.

[75] S. Lee, R. Zhang, and K. Huang, "Opportunistic wireless energy harvesting in cognitive radio networks," *IEEE Transactions on Wireless Communications*, vol. 12, no. 9, pp. 4788–4799, September 2013.

[76] X. Lu, P. Wang, D. Niyato, and E. Hossain, "Dynamic spectrum access in cognitive radio networks with rf energy harvesting," *IEEE Wireless Communications*, vol. 21, no. 3, pp. 102–110, June 2014.

[77] D. T. Hoang, D. Niyato, P. Wang, and D. I. Kim, "Opportunistic channel access and rf energy harvesting in cognitive radio networks," *IEEE Journal on Selected Areas in Communications*, vol. 32, no. 11, pp. 2039–2052, November 2014.

[78] C. Xu, Q. Zhang, Q. Li, Y. Tan, and J. Qin, "Robust transceiver design for wireless information and power transmission in underlay mimo cognitive radio networks," *IEEE Communications Letters*, vol. 18, no. 9, pp. 1665–1668, Sept 2014.

[79] A. H. Sakr and E. Hossain, "Cognitive and energy harvesting-based d2d communication in cellular networks: Stochastic geometry modeling and analysis," *IEEE Transactions on Communications*, vol. 63, no. 5, pp. 1867–1880, May 2015.

[80] G. Zheng, Z. Ho, E. A. Jorswieck, and B. Ottersten, "Information and energy cooperation in cognitive radio networks," *IEEE Transactions on Signal Processing*, vol. 62, no. 9, pp. 2290–2303, May 2014.

[81] L. Liu, R. Zhang, and K. C. Chua, "Secrecy wireless information and power transfer with miso beamforming," *IEEE Transactions on Signal Processing*, vol. 62, no. 7, pp. 1850–1863, April 2014.

[82] Q. Shi, W. Xu, J. Wu, E. Song, and Y. Wang, "Secure beamforming for mimo broadcasting with wireless information and power transfer," *IEEE Transactions on Wireless Communications*, vol. 14, no. 5, pp. 2841–2853, May 2015.

[83] D. W. K. Ng, E. S. Lo, and R. Schober, "Robust beamforming for secure communication in systems with wireless information and power transfer," *IEEE Transactions on Wireless Communications*, vol. 13, no. 8, pp. 4599–4615, Aug 2014.

[84] R. Feng, Q. Li, Q. Zhang, and J. Qin, "Robust secure transmission in miso simultaneous wireless information and power transfer system," *IEEE Transactions on Vehicular Technology*, vol. 64, no. 1, pp. 400–405, Jan 2015.

[85] S. Wang and B. Wang, "Robust secure transmit design in mimo channels with simultaneous wireless information and power transfer," *IEEE Signal Processing Letters*, vol. 22, no. 11, pp. 2147–2151, Nov 2015.

[86] Z. Chu, Z. Zhu, M. Johnston, and S. Y. L. Goff, "Simultaneous wireless information power transfer for miso secrecy channel," *IEEE Transactions on Vehicular Technology*, vol. 65, no. 9, pp. 6913–6925, Sept 2016.

[87] M. R. A. Khandaker, K. K. Wong, Y. Zhang, and Z. Zheng, "Probabilistically robust swipt for secrecy misome systems," *IEEE Transactions on Information Forensics and Security*, vol. 12, no. 1, pp. 211–226, Jan 2017.

[88] M. R. A. Khandaker and K. K. Wong, "Robust secrecy beamforming for mimo swipt with probabilistic constraints," in *2016 IEEE Globecom Workshops (GC Wkshps)*, Dec 2016, pp. 1–6.

[89] X. Chen, Z. Zhang, H. h. Chen, and H. Zhang, "Enhancing wireless information and power transfer by exploiting multi-antenna techniques," *IEEE Communications Magazine*, vol. 53, no. 4, pp. 133–141, April 2015.

[90] Z. Ding, C. Zhong, D. W. K. Ng, M. Peng, H. A. Suraweera, R. Schober, and H. V. Poor, "Application of smart antenna technologies in simultaneous wireless information and power transfer," *IEEE Communications Magazine*, vol. 53, no. 4, pp. 86–93, April 2015.

[91] Q. Li, Q. Zhang, and J. Qin, "Secure relay beamforming for simultaneous wireless information and power transfer in nonregenerative relay networks," *IEEE Transactions on Vehicular Technology*, vol. 63, no. 5, pp. 2462–2467, Jun 2014.

[92] H. Xing, K. K. Wong, Z. Chu, and A. Nallanathan, "To harvest and jam: A paradigm of self-sustaining friendly jammers for secure af relaying," *IEEE Transactions on Signal Processing*, vol. 63, no. 24, pp. 6616–6631, Dec 2015.

[93] A. Salem, K. A. Hamdi, and K. M. Rabie, "Physical layer security with rf energy harvesting in af multi-antenna relaying networks," *IEEE Transactions on Communications*, vol. 64, no. 7, pp. 3025–3038, July 2016.

[94] X. Chen, J. Chen, and T. Liu, "Secure transmission in wireless powered massive mimo relaying systems: Performance analysis and optimization," *IEEE Transactions on Vehicular Technology*, vol. 65, no. 10, pp. 8025–8035, Oct 2016.

[95] Y. Feng, Z. Yang, W. P. Zhu, Q. Li, and B. Lv, "Robust cooperative secure beamforming for simultaneous wireless information and power transfer in amplify-and-forward relay networks," *IEEE Transactions on Vehicular Technology*, vol. 66, no. 3, pp. 2354–2366, March 2017.

[96] Q. Li and J. Qin, "Joint source and relay secure beamforming for nonregenerative mimo relay systems with wireless information and power transfer," *IEEE Transactions on Vehicular Technology*, vol. 66, no. 7, pp. 5853–5865, July 2017.

[97] B. Fang, Z. Qian, W. Zhong, and W. Shao, "An-aided secrecy precoding for swipt in cognitive mimo broadcast channels," *IEEE Communications Letters*, vol. 19, no. 9, pp. 1632–1635, Sept 2015.

[98] D. W. K. Ng, E. S. Lo, and R. Schober, "Multiobjective resource allocation for secure communication in cognitive radio networks with wireless information and power transfer," *IEEE Transactions on Vehicular Technology*, vol. 65, no. 5, pp. 3166–3184, May 2016.

[99] A. Singh, M. R. Bhatnagar, and R. K. Mallik, "Secrecy outage of a simultaneous wireless information and power transfer cognitive radio system," *IEEE Wireless Communications Letters*, vol. 5, no. 3, pp. 288–291, June 2016.

[100] F. Zhou, Z. Li, J. Cheng, Q. Li, and J. Si, "Robust an-aided beamforming and power splitting design for secure miso cognitive radio with swipt," *IEEE Transactions on Wireless Communications*, vol. 16, no. 4, pp. 2450–2464, April 2017.

[101] S. Boyd and L. Vandenberghe, *Convex Optimization*. New York, NY, USA: Cambridge University Press, 2004.

[102] Z.-Q. Luo and W. Yu, "An introduction to convex optimization for communications and signal processing," *IEEE Journal on Selected Areas in Communications*, vol. 24, no. 8, pp. 1426–1438, Aug 2006.

[103] J. F. Sturm, "Using sedumi 1.02, a matlab toolbox for optimization over symmetric cones," *Optimization Methods and Software*, vol. 11, no. 1-4, pp. 625–653, 1999. [Online]. Available: http://dx.doi.org/10.1080/10556789908805766

[104] J. Lofberg, "Yalmip : a toolbox for modeling and optimization in matlab," in *2004 IEEE International Conference on Robotics and Automation (IEEE Cat. No.04CH37508)*, Sept 2004, pp. 284–289.

[105] M. Grant and S. Boyd, "CVX: Matlab software for disciplined convex programming, version 2.1," http://cvxr.com/cvx, Mar. 2014.

[106] A. J. Laub, *Matrix Analysis For Scientists And Engineers*. Philadelphia, PA, USA: Society for Industrial and Applied Mathematics, 2004.

[107] D. Mitrinovi, J. Peari, and A. Fink, "Cauchys and related inequalities," in *Classical and New Inequalities in Analysis*. Springer, 1993, pp. 83–98.

[108] Z. q. Luo, W. k. Ma, A. M. c. So, Y. Ye, and S. Zhang, "Semidefinite relaxation of quadratic optimization problems," *IEEE Signal Processing Magazine*, vol. 27, no. 3, pp. 20–34, May 2010.

[109] S. Zhang, "Quadratic maximization and semidefinite relaxation," *Mathematical Programming*, vol. 87, no. 3, pp. 453–465, 5 2000.

[110] A. Beck, A. Ben-Tal, and L. Tetruashvili, "A sequential parametric convex approximation method with applications to nonconvex truss topology design problems," *Journal of Global Optimization*, vol. 47, no. 1, pp. 29–51, May 2010. [Online]. Available: https://doi.org/10.1007/s10898-009-9456-5

[111] Y. Huang and D. P. Palomar, "Rank-constrained separable semidefinite programming with applications to optimal beamforming," *IEEE Transactions on Signal Processing*, vol. 58, no. 2, pp. 664–678, Feb 2010.

[112] M. S. Lobo, L. Vandenberghe, S. Boyd, and H. Lebret, "Applications of second-order cone programming," *Linear algebra and its applications*, vol. 284, no. 1-3, pp. 193–228, 1998.

[113] Q. Li and W. K. Ma, "Optimal and robust transmit designs for miso channel secrecy by semidefinite programming," *IEEE Transactions on Signal Processing*, vol. 59, no. 8, pp. 3799–3812, Aug 2011.

[114] G. Zheng, K. K. Wong, and B. Ottersten, "Robust cognitive beamforming with bounded channel uncertainties," *IEEE Transactions on Signal Processing*, vol. 57, no. 12, pp. 4871–4881, Dec 2009.

[115] M. Bengtsson and B. Ottersten, "Optimal and suboptimal transmit beamforming," *Handbook of Antennas in Wireless Communications*, 2001.

[116] J. Jose, N. Prasad, M. Khojastepour, and S. Rangarajan, "On robust weighted-sum rate maximization in mimo interference networks," in *2011 IEEE International Conference on Communications (ICC)*, June 2011, pp. 1–6.

[117] S. Verdu, "Spectral efficiency in the wideband regime," *IEEE Transactions on Information Theory*, vol. 48, no. 6, pp. 1319–1343, Jun 2002.

[118] J. Wang and D. P. Palomar, "Worst-case robust mimo transmission with imperfect channel knowledge," *IEEE Transactions on Signal Processing*, vol. 57, no. 8, pp. 3086–3100, Aug 2009.

[119] Z. Chu, H. Xing, M. Johnston, and S. L. Goff, "Secrecy rate optimizations for a miso secrecy channel with multiple multiantenna eavesdroppers," *IEEE Transactions on Wireless Communications*, vol. 15, no. 1, pp. 283–297, Jan 2016.

[120] K. Y. Wang, A. M. C. So, T. H. Chang, W. K. Ma, and C. Y. Chi, "Outage constrained robust transmit optimization for multiuser miso downlinks: Tractable approximations by conic optimization," *IEEE Transactions on Signal Processing*, vol. 62, no. 21, pp. 5690–5705, Nov 2014.

[121] I. Bechar, "A bernstein-type inequality for stochastic processes of quadratic forms of gaussian variables," *arXiv preprint arXiv:0909.3595*, 2009.

[122] C. R. Valenta and G. D. Durgin, "Harvesting wireless power: Survey of energy-harvester conversion efficiency in far-field, wireless power transfer systems," *IEEE Microwave Magazine*, vol. 15, no. 4, pp. 108–120, June 2014.

[123] J. Guo and X. Zhu, "An improved analytical model for rf-dc conversion efficiency in microwave rectifiers," in *2012 IEEE/MTT-S International Microwave Symposium Digest*, June 2012, pp. 1–3.

[124] E. Boshkovska, D. W. K. Ng, N. Zlatanov, and R. Schober, "Practical non-linear energy harvesting model and resource allocation for swipt systems," *IEEE Communications Letters*, vol. 19, no. 12, pp. 2082–2085, Dec 2015.

[125] E. Boshkovska, D. W. K. Ng, N. Zlatanov, A. Koelpin, and R. Schober, "Robust resource allocation for mimo wireless powered communication networks based on a non-linear eh model," *IEEE Transactions on Communications*, vol. 65, no. 5, pp. 1984–1999, May 2017.

[126] M. Schubert and H. Boche, "Solution of the multiuser downlink beamforming problem with individual sinr constraints," *IEEE Transactions on Vehicular Technology*, vol. 53, no. 1, pp. 18–28, Jan 2004.

[127] S. Janson, "Large deviations for sums of partly dependent random variables," *Random Struct. Algorithms*, vol. 24, no. 3, pp. 234–248, May 2004. [Online]. Available: http://dx.doi.org/10.1002/rsa.v24:3

[128] S.-S. Cheung, A. M.-C. So, and K. Wang, "Linear matrix inequalities with stochastically dependent perturbations and applications to chance-constrained semidefinite optimization," *SIAM Journal on Optimization*, vol. 22, no. 4, pp. 1394–1430, 2012. [Online]. Available: https://doi.org/10.1137/110822906

[129] A. Ben-Tal and A. S. Nemirovskiaei, *Lectures on Modern Convex Optimization: Analysis, Algorithms, and Engineering Applications*. Philadelphia, PA, USA: Society for Industrial and Applied Mathematics, 2001.

[130] J. C. Bezdek and R. J. Hathaway, "Convergence of alternating optimization," *Neural, Parallel Sci. Comput.*, vol. 11, no. 4, pp. 351–368, Dec. 2003. [Online]. Available: http://dl.acm.org/citation.cfm?id=964885.964886

[131] G. Fodor, E. Dahlman, G. Mildh, S. Parkvall, N. Reider, G. Miklos, and Z. Turanyi, "Design aspects of network assisted device-to-device communications," *IEEE Communications Magazine*, vol. 50, no. 3, pp. 170–177, March 2012.